

New approaches for ultrafast laser pulse characterization using enhanced Graphene-based materials

Tiago dos Santos Gomes
Dissertação de Mestrado apresentada à
Faculdade de Ciências da Universidade do Porto em
Engenharia Física
2020

MSc
2.º CICLO
FCUP
2020



New approaches for ultrafast laser pulse characterization using enhanced Graphene-based materials

Tiago dos Santos Gomes
FC



New approaches for ultrafast laser pulse characterization using enhanced Graphene-based materials

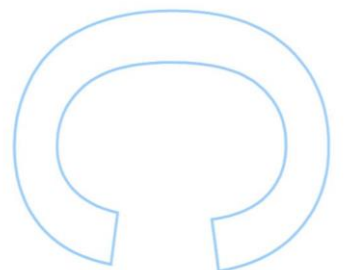
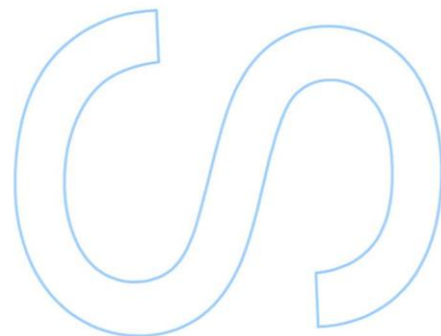
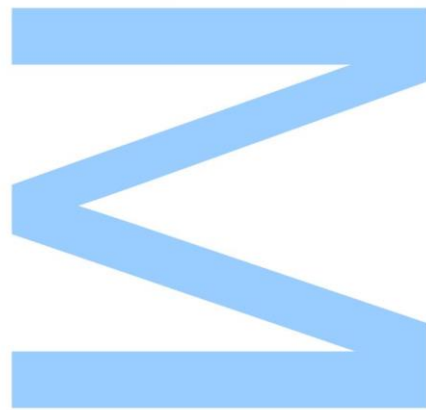
Tiago dos Santos Gomes
Mestrado Integrado em Engenharia Física
Departamento de Física e Astronomia
2020

Orientador

Prof. Dr. Helder Crespo, Docente, Departamento de Física e Astronomia da FCUP

Coorientador

Dr. Miguel Canhota, Investigador, Departamento de Física e Astronomia da FCUP



U. PORTO

FC FACULDADE DE CIÊNCIAS
UNIVERSIDADE DO PORTO

Todas as correções determinadas pelo júri, e só essas, foram efetuadas.

O Presidente do Júri,

Porto, ____/____/____

W

S

Q

UNIVERSIDADE DO PORTO

MASTERS THESIS

**New approaches for ultrafast laser pulse
characterization using enhanced
Graphene-based materials**

Author:

Tiago GOMES

Supervisor:

Helder CRESPO

Co-supervisor:

Miguel CANHOTA

*A thesis submitted in fulfilment of the requirements
for the degree of MSc. Engineering Physics*

at the

Faculdade de Ciências da Universidade do Porto
Departamento de Física e Astronomia

October 8, 2020

“ Time isn't the main thing. It's the only thing. ”

Miles Davis

Acknowledgements

This thesis is the result of many months of hard work, persistence, and above all, of a crucial learning line, which I wouldn't have followed if it weren't for some people. And to those, I would like to present my sincere acknowledgments.

To my supervisor, Prof. Dr. Helder Crespo, I would like to thank for his guidance, inspiration, and for teaching me that *one can only mess up if trying to succeed*. Without him, this work wouldn't have been possible, and for that I thank him the most.

I would like to thank to my co-supervisor, Dr. Miguel Canhota, for giving me all the help I needed in the lab, for being a great friend, and for teaching me that *two points make a straight line*.

To my friends from the University of Porto, I would like to thank, especially to José Miguel Mesquita for doing a *live concert* at every break, and to João Magalhães, Marco Ramos and Nuno Macedo for all the challenges that we've been through (WE MATTER: one team to rule them all!).

To my co-workers from the FEMTOLAB, namely Ana Vieira da Silva and Ana Silva (yes, there are two!), I would like to give my sincere thanks for all the special moments that happened since I've joined the group as a junior researcher, which I will forever treasure in my heart.

To my friends from my hometown, I would like to thank from the bottom of my heart and say that life is indeed beautiful with friends like you!

I would like to thank Dr. Miguel Miranda for the full-retrievals performed in some d-scans; to Bohdan Kulyk, Alexandre Carvalho, Prof. Dr. António José Fernandes and Prof. Dr. Florinda Costa from University of Aveiro for synthesizing all the studied graphene samples; to Dr. Bruno Jarrais and Prof. Dr. Cristina Freire from University of Porto for all the performed functionalizations and Raman and XPS analysis of the graphene samples; and to Prof. Dr. Agostinho Moreira from University of Porto for the 2D Raman analysis of some graphene samples.

I would also like to thank IFIMUP, namely D. Isabel Alves and Eng. Francisco Carpinheiro for all the given support.

To my father Alexandre, to my mother Gabriela and to my sister Mariana, I thank you from the bottom of my heart, for I have no words for all you have done for me. I hope that one day I can repay.

And, finally, I would like to give a special thanks to Rita. For being there when I needed the most. For making me laugh. **For everything.**

UNIVERSIDADE DO PORTO

Abstract

Faculdade de Ciências da Universidade do Porto

Departamento de Física e Astronomia

MSc. Engineering Physics

New approaches for ultrafast laser pulse characterization using enhanced Graphene-based materials

by [Tiago GOMES](#)

We have fully built and tested a setup that allows for broadband third-harmonic generation of femtosecond laser pulses. By measuring the third-harmonic signal of different graphene samples as a function of the dispersion applied to the ultrashort pulse, we get a d-scan trace that allows for the complete electric field retrieval of said pulse.

We were also able to study the influence of the synthesis conditions and the number of layers of the graphene samples on the third-harmonic generation properties, such as intensity, bandwidth and wavelength peak.

The process of altering the third order nonlinear response of graphene through chemical or morphological functionalization was also studied, as well as the samples' damage resilience and its dependence on the functionalization process.

The graphene samples were grown and transferred by Bohdan Kulyk, Alexandre Carvalho, Prof. Dr. António José Fernandes and Prof. Dr. Florinda Costa, at I3N - University of Aveiro. Graphene functionalization took place at REQUIMTE/LAQV, and was performed by Dr. Bruno Jarrais and Prof. Dr. Cristina Freire, who also performed Raman imaging and XPS. Prof. Dr. Agostinho Moreira also performed 2D Raman analysis in order to study graphene's topography.

This work was supported by Fundação para a Ciência e Tecnologia (FCT), through a junior research fellowship within the grant 'UltraGraf - Harnessing third-harmonic generation in graphene-coated optics - new devices for ultrafast pulse measurement and frequency up-conversion' (M-ERA-NET2/0002/2016), and through the plurianual funding of IFIMUP - Institute of Physics for Advanced Materials, Nanotechnology and Photonics (UIDB/04968/2020).

Ultimately, the work developed in this thesis will result in a THG d-scan prototype with optically improved graphene, which will allow for time domain characterization of ultra-short pulses with fundamental spectrum ranging from the visible/NIR (approx. 800 nm) to the MIR.

UNIVERSIDADE DO PORTO

Resumo

Faculdade de Ciências da Universidade do Porto

Departamento de Física e Astronomia

Mestrado Integrado em Engenharia Física

Novas abordagens para a caracterização de impulsos laser ultracurtos usando materiais baseados em grafeno funcionalizado

por [Tiago GOMES](#)

Foi construída e testada uma montagem experimental que permite a geração e medição de terceiro harmónico de banda larga em impulsos laser de femtossegundo. Ao medir o sinal de terceiro harmónico de diferentes amostras de grafeno em função da dispersão aplicada ao pulso ultracurto, obtemos um d-scan que permite a reconstrução completa do campo elétrico do impulso referido.

Também pudemos estudar a influência das condições de síntese e do número de camadas das amostras de grafeno nas propriedades de geração do terceiro harmónico, como a intensidade, a largura de banda e o pico de comprimento de onda.

O processo de alteração da resposta não linear de terceira ordem do grafeno através da funcionalização química ou morfológica também foi estudado, assim como a resiliência das amostras a dano e a sua dependência no processo de funcionalização.

As amostras de grafeno foram crescidas e transferidas por Bohdan Kulyk, Alexandre Carvalho, Prof. Dr. António José Fernandes e Prof. Dra. Florinda Costa, no I3N - Universidade de Aveiro. A funcionalização do grafeno ocorreu no REQUIMTE / LAQV, e foi realizada pelo Dr. Bruno Jarrais e pela Prof. Dra. Cristina Freire, que realizaram também imagens Raman e XPS. O Prof. Dr. Agostinho Moreira também realizou uma análise Raman 2D para estudar a topografia do grafeno.

Este trabalho teve o apoio da Fundacao para a Ciencia e a Tecnologia (FCT), através de uma bolsa de investigação no âmbito do projeto 'UltraGraf - Harnessing third-harmonic generation in graphene-coated optics - new devices for ultrafast pulse measurement and frequency upconversion' (M-ERA-NET2/0002/2016), e do financiamento plurianual do IFIMUP - Instituto de Física dos Materiais Avançados, Nanotecnologia e Fotónica (UIDB/04968/2020).

Em última análise, o trabalho desenvolvido nesta tese resultará num protótipo de d-scan de terceiro harmónico com grafeno funcionalizado, o que permitirá a caracterização no domínio temporal de pulsos ultracurtos com espectro fundamental do visível / NIR (aproximadamente 800 nm) ao MIR.

Contents

Acknowledgements	v
Abstract	vii
Resumo	ix
Contents	xi
List of Figures	xiii
Glossary	xvii
1 Introduction	1
1.1 Ultrashort Laser Pulses	1
1.1.1 Mathematical description	2
1.2 Dispersion	3
1.3 Dispersion compensation	5
1.4 Nonlinear Optics	6
1.4.1 Second-Harmonic Generation	7
1.4.2 Third-Harmonic Generation	7
1.4.3 Intensity-Dependent Refractive Index	8
1.5 Ultrashort pulse characterization	9
1.5.1 Autocorrelation	9
1.5.2 Frequency Resolved Optical Gating (FROG)	11
1.5.3 Spectral phase interferometry for direct electric field reconstruction (SPIDER)	11
1.5.4 Multiphoton Intrapulse Interference Phase Scan (MIIPS)	11
1.5.5 Dispersion-scan	12
1.5.5.1 Mathematical description	12
1.6 Ultrafast time-resolved spectroscopy	15
1.7 Purpose of this thesis	17
2 Graphene	19
2.1 Electronic structure	20
2.2 Optical properties	22
2.3 Hybridization in graphene	22

2.4	Ultrafast dynamics of charge carriers in graphene	23
2.4.1	Literature review	23
2.5	Raman Spectroscopy	26
2.5.1	Raman Scattering	26
2.5.2	Raman spectrum	26
2.6	Our graphene samples	27
2.6.1	TCVD graphene	27
2.6.2	MPCVD graphene	29
2.7	Functionalization	30
2.7.1	<i>In situ</i> diazonium reaction	30
2.7.2	Diels-Alder reaction	31
2.7.3	Photoassisted transfer hydrogenation reaction	31
2.7.4	Absorption spectra	33
2.7.5	Raman analysis	34
3	Experimental setup and Results	37
3.1	Experimental setup	37
3.2	Samples	41
3.3	MPCVD-grown graphene	41
3.3.1	Third-Harmonic Generation	41
3.3.2	Retrievals	45
3.3.3	Durability	47
3.4	TCVD-grown graphene	49
3.4.1	Third-Harmonic Generation	49
3.4.2	Durability	51
3.5	Graphene functionalization	51
3.5.1	Retrievals	53
3.5.2	Durability	53
3.6	TCVD-grown graphene with islands	55
3.6.1	Clarification	55
3.6.2	Comparison	55
3.6.3	d-scans	55
3.7	Simulation	60
4	Final remarks and future work	63
5	Related work and publications	65
5.1	Poster presentations	65
5.2	Oral presentations	66
A	Publications	67
	Bibliography	71

List of Figures

1.1	Relevance of the CEP for high peak power ultrashort pulses. The red lines represent the field envelope, the blue lines represent the electric field with CEP equal to zero (a - few-cycles and d - multi-cycles), $\pi/2$ (b - few-cycles and e - multi-cycles) and π (c - few-cycles and f - multi-cycles) radians, and the black dashed lines represent the electric field with CEP = 0. One can clearly see that the CEP affects mostly the peak intensity of few-cycle ultrashort pulses.	4
1.2	Effects of a flat (top), quadratic (middle) and cubic (bottom) phase in a gaussian spectrum. One clearly sees that a quadratic phase broadens the pulse in the time domain, and a cubic phase distorts the pulse, generating pre- or post- pulses (depending on the phase sign).	5
1.3	Chirped Mirror configuration. The dark grey areas correspond to layers with a higher refractive index and light grey areas to layers with a lower refractive index.	6
1.4	Third-Harmonic Generation in an ultrashort pulse.	8
1.5	Michelson interferometer setup.	10
1.6	Typical d-scan setup. DCM: Double Chirped Mirrors.	12
1.7	THG d-scan trace for a constant (a,b), quadratic (c,d) and cubic phase (e,f). One sees that, if the ultrashort pulse has a quadratic phase, its d-scan trace changes the optimum dispersion, and the trace gets slightly tilted, whereas if the phase is cubic, the d-scan trace is strongly tilted.	14
1.8	Typical pump-probe scheme.	15
1.9	Typical degenerate pump-probe setup in transmission geometry.	16
2.1	Graphene honeycomb lattice with 2 triangular sublattices (A and B, represented in red and blue dots, respectively). The distance between a carbon atom and its nearest neighbour is $a = 1.42\text{\AA}$	20
2.2	Graphene energy band structure with $t = 2.7eV$ and $t' = 0 eV$, for the π (yellow) and π^* (blue) bands.	21
2.3	Ultrafast carrier dynamics in graphene. A photon interacts with the material (a), and is absorbed, causing an electron to be promoted to the conduction band (b). Later, the electron will begin to lose energy due to electron-electron and electron-phonon scattering (c) and will eventually decay to its initial state (d).	24
2.4	Raman spectrum of graphene, for different number of layers (1-4) and of bulk graphene (graphite). Reproduced from [55].	27
2.5	Topography of an island grown in TCVD-grown graphene. Courtesy of Prof. Dr. Joaquim Agostinho Moreira from IFIMUP/IN - University of Porto.	28

2.6	SEM images of 5 layers TCVD-grown graphene multi-islands (left) and few-islands (right). Courtesy of Bohdan Kulyk from I3N - University of Aveiro.	29
2.7	SEM images for the MPCVD-grown graphene samples with higher (left) and lower (right) absorption in the DUV region. Courtesy of Bohdan Kulyk from I3N - University of Aveiro.	30
2.8	Preparation of functionalized 5 layers multi-islands TCVD-grown graphene, through <i>in situ</i> diazonium reaction. Courtesy of Dr. Bruno Jarrais from LAQV /REQUIMTE - University of Porto.	31
2.9	Preparation of functionalized 3 layers multi-islands 3 and 1 layers few-islands TCVD-grown graphene, through Diels-Alder reaction. Courtesy of Dr. Bruno Jarrais from LAQV/REQUIMTE - University of Porto.	32
2.10	Preparation of functionalized 5 layers few-islands TCVD-grown graphene, through hydrogenation. Courtesy of Dr. Bruno Jarrais from LAQV/REQUIMTE - University of Porto.	32
2.11	Absorption spectra for the non-functionalized (left) and the functionalized (right) multi-islands TCVD-grown samples. Courtesy of Dr. Bruno Jarrais from LAQV/REQUIMTE - University of Porto.	33
2.12	Absorption spectra for the non-functionalized (left) and the functionalized (right) few-islands TCVD-grown samples. Courtesy of Dr. Bruno Jarrais from LAQV/REQUIMTE - University of Porto.	33
2.13	Raman spectra of the pristine and functionalized CVD graphene materials. Courtesy of Dr. Bruno Jarrais from LAQV/REQUIMTE - University of Porto.	34
2.14	Optical micrographs (top), Raman IG/I2D (middle) and FWHM(2D) (down) maps of the 3 layers few-islands TCVD-grown graphene non-functionalized (left) and functionalized (right). Courtesy of Dr. Bruno Jarrais from LAQV/REQUIMTE - University of Porto.	35
3.1	Experimental setup for THG d-scan. DCM1 and DCM2: Double Chirped Mirrors; M1, M2, M3 and M4: mirrors.	38
3.2	Experimental setup for the wavelength separator alignment. L1 and L2: Focusing and Collimating Lens; M2, M3 and M4: mirrors.	38
3.3	Experimental setup for THG (red-labeled components) and wavelength separator aligner (blue-labeled components), described in Figure 3.1. 1 - Variable power filter. 2,6,10 - Mirrors. 3,5 - Focusing and collimating concave mirrors, respectively. 4 - Graphene sample. 7 - Periscope. 8,9 - Focusing and collimating lenses for THG in air plasma, respectively. 11 - Flip mirror, to switch between aligning the wavelength separator and measuring THG in graphene. Red circle - Wavelength separator. All the setup is mobile.	39
3.4	Experimental setup for the wavelength separator. 1,2 - Set of two prisms to separate the THG from the fundamental beam. The green paper blocks the fundamental beam. 3 - Back-reflecting mirror/periscope. 4,5 - Mirror. 6 - Focusing lens. 7 - Fiber mount.	40
3.5	Dispersion compensation setup. 1,2 - Glass wedges (wedge no. 1 is connected to the Zaber motor). 3,4 - Double Chirped Mirrors.	40
3.6	Transmission curves of the MPCVD-grown graphene samples	42
3.7	MPCVD-grown graphene sample's uniformity regarding THG	42
3.8	THG signal as a function of the laser's input average power.	43

3.9	THG signal vs. peak absorption for the MPCVD-grown graphene samples .	44
3.10	THG shape study vs peak absorption for the MPCVD-grown graphene samples.	44
3.11	THG d-scan for each MPCVD-grown graphene sample.	45
3.12	Phase retrieval for the MPCVD-grown 1C graphene sample.	46
3.13	Measured and retrieved THG d-scan for the MPCVD-grown 1C graphene sample, by using one of the 10 retrieved phases.	46
3.14	Retrieved temporal profile of the ultrashort pulses used for THG d-scan for each MPCVD-grown graphene sample.	47
3.15	THG decay rate study for the MPCVD-grown 1C graphene sample.	48
3.16	THG decay rate for the MPCVD-grown graphene samples.	49
3.17	THG spectra for the TCVD-grown graphene samples with no islands and the substrate.	49
3.18	THG spectra for the 5 layers TCVD-grown graphene with no islands and the MPCVD-grown 1C graphene.	50
3.19	THG d-scan for 5 layers TCVD-grown graphene with no islands.	50
3.20	Decay rate for the MPCVD-grown 1C and the 5 layers TCVD-grown graphene sample	51
3.21	THG spectra for the non-functionalized and the functionalized 5 layers TCVD-grown graphene sample with no islands.	52
3.22	THG d-scan for the non-functionalized (left) and the functionalized (right) TCVD-grown 5 layers graphene sample with no islands.	52
3.23	Temporal profile of the ultrashort pulses used to perform THG in TCVD-grown graphene with 5 layers (functionalized and non-functionalized).	53
3.24	THG signal overtime for the 5 layers TCVD-grown functionalized graphene sample with no islands.	54
3.25	THG decay rate for the MPCVD-grown 1C, 5 layers TCVD-grown and 5 layers TCVD-grown functionalized graphene sample.	54
3.26	Third Harmonic Generation in functionalized TCVD-grown graphene - multi-islands and few-islands.	56
3.27	Measured (left) and retrieved (right) d-scans for 5 layers multi-islands TCVD-grown functionalized graphene.	56
3.28	Measured (left) and retrieved (right) d-scans for 3 layers multi-islands TCVD-grown functionalized graphene.	57
3.29	Measured (left) and retrieved (right) d-scans for 5 layers few-islands TCVD-grown functionalized graphene.	57
3.30	Measured (left) and retrieved (right) d-scans for 3 layers few-islands TCVD-grown functionalized graphene.	58
3.31	Measured (left) and retrieved (right) d-scans for 1 layer few-islands TCVD-grown functionalized graphene.	58
3.32	Full retrieval for THG d-scan with functionalized TCVD-grown graphene with islands.	59
3.33	Comparison of the measured (orange) and retrieved (blue) spectra for THG d-scan with TCVD-grown functionalized graphene.	59
3.34	Simulated THG spectrum vs measured THG spectra for the representative graphene samples.	60

A.1	Poster presented at Ultrafast Optics (UFO 2019) in Bol, Croatia, from 6 th -11 th October 2019.	68
A.2	Poster presented at the online conference Graphene Industrial Forum & 2DM 2020, presented in May 27 th 2020.	69
A.3	Poster presented at the COST Action CA17126, at University of Porto, presented in March, 4 th 2019, and at the Condensed Matter Physics National Conference, at University of Porto, presented from May 8 th -10 th 2019.	70

Glossary

CVD	Chemical Vapour Deposition
CEP	Carrier-Envelope Phase
DCM	Double-Chirped Mirrors
d-scan	Dispersion Scan
DUV	Deep Ultraviolet
FBZ	First Brillouin Zone
FROG	Frequency Resolved Optical Gating
FWHM	Full Width at Half Maximum
MIIPS	Multiphoton Intrapulse Interference Phase Scan
MIR	Mid Infrared
MLG	Multi Layer Graphene
MPCVD	Microwave Plasma Chemical Vapour Deposition
NIR	Near Infrared
SEM	Scanning Electron Microscopy
SHG	Second Harmonic Generation
SLG	Single Layer Graphene
SNR	Signal to Noise Ratio
SPIDER	Spectral Phase Interferometry for Direct Electric field Reconstruction
TCVD	Thermal Chemical Vapour Deposition
THG	Third Harmonic Generation
XPS	X-ray Photoelectron Spectroscopy

This thesis is dedicated to my family, for their love and support.

Chapter 1

Introduction

1.1 Ultrashort Laser Pulses

It was with the discovery that electromagnetic energy is quantized (Max Planck, 1900) and the theoretical study of stimulated emission (Albert Einstein, 1917) that the world began to look at light as Nobel-inspiring. The first LASER (Light Amplification by Stimulated Emission of Radiation) was created in 1960, by T. Maiman [1], using a synthetic ruby cylinder with silver-coated ends as the Fabry-Perot resonator and photographic flash lamps as the pump source, leading to a worldwide optical revolution. With the invention of the Q-switch technique [2], the production of laser pulses in the nanosecond regime was achieved, being extended to the pico- and femtosecond with the invention of the mode-locking [3]. But what is, nowadays, the definition of ultrashort pulses?

Ultrashort pulses are laser pulses (electromagnetic wave packets) with time durations of a few picoseconds or less. In order to realize how short these pulses are, let's consider their spatial equivalent. If we could take a snapshot of a 1-s light pulse, its size would be 300 000 km. If we do the same but with a 1 ns-pulse, its size would be 30 cm (this time scale is the current high-speed electronic time scale). If we now have a 10-fs light pulse, its size would be 3 μm , much less than the diameter of a human hair [4]!

These ultrashort pulses have very unique properties, like high time resolution (allowing for the measurement of ultrafast physical processes in solid-state [5]), high spatial resolution (used for microscopy and imaging [6]), high bandwidth (used for optical communications [7]) and high intensities (peak intensities exceeding $10^{20} \text{W}/\text{cm}^2$). In order to

achieve these high intensities, a technique named Chirped Pulse Amplification was developed by Donna Strickland and Gérard Mourou, [8] which gave them the Nobel Prize in Physics in 2018 [9].

1.1.1 Mathematical description

In optics, it is useful to write the optical electric field as a complex quantity $\vec{E}(\vec{r}, t)$, which is related to the real electric field as:

$$\vec{E}_{real}(\vec{r}, t) = \frac{\vec{E}(\vec{r}, t) + \vec{E}^*(\vec{r}, t)}{2} \quad (1.1)$$

For the purpose of this thesis, we will only consider a linearly polarized electric field ($\vec{E}(\vec{r}, t) = E(\vec{r}, t)\hat{e}$), whose amplitude can be described as a function of the pulse intensity $I(\vec{r}, t)$ and temporal phase $\phi(\vec{r}, t)$:

$$E(\vec{r}, t) = \sqrt{I(\vec{r}, t)}e^{i[\omega_0 t - \phi(\vec{r}, t)]} \quad (1.2)$$

It can be useful to define the field envelope as:

$$E_{env}(\vec{r}, t) = \sqrt{I(\vec{r}, t)} \quad (1.3)$$

If we want to represent the electric field in the frequency domain for a specific point in space, we can simply take the Fourier transform [10]:

$$E(\omega) = \mathcal{F}\{E(t)\} = \int_{-\infty}^{+\infty} E(t)e^{-i\omega t} dt = |E(\omega)|e^{i\phi(\omega)} \quad (1.4)$$

which is defined by a spectral power $|E(\omega)|$ and a spectral phase $\phi(\omega)$. We can now define the central frequency as the center of gravity of the spectral power:

$$\omega_0 = \frac{\int \omega |E(\omega)| d\omega}{\int |E(\omega)| d\omega} \quad (1.5)$$

If we want to go back to the time domain, we simply take the inverse Fourier transform:

$$E(t) = \mathcal{F}^{-1}\{E(\omega)\} = \frac{1}{2\pi} \int_{-\infty}^{+\infty} E(\omega)e^{+i\omega t} d\omega \quad (1.6)$$

By making use of the properties of the Fourier transform, one can get a relation between the spectral bandwidth $\Delta\omega$ and time bandwidth Δt :

$$\Delta\omega\Delta t \geq 2\pi K \quad (1.7)$$

where K is a constant that depends on the pulse profile. One can see the similarities between the above equation and Heisenberg's uncertainty principle: if we have the pulse energy concentrated in time, it must be dispersed in frequency, and vice-versa. When the equality is obtained, we say that the pulse is transform-limited, which is equivalent to saying that the pulse has a flat or linear spectral phase.

1.2 Dispersion

When an ultrashort pulse propagates through a linear material, the spectral phase of the pulse $\phi(\omega)$ changes its shape. This effect is known as dispersion, and can be understood if we expand the spectral phase as a Taylor series:

$$\phi(\omega) = \phi_0 + \frac{d\phi}{d\omega}(\omega - \omega_0) + \frac{1}{2!} \frac{d^2\phi}{d\omega^2}(\omega - \omega_0)^2 + \frac{1}{3!} \frac{d^3\phi}{d\omega^3}(\omega - \omega_0)^3 + \dots = \sum_{n=0}^{\infty} \frac{1}{n!} \phi_n (\omega - \omega_0)^n \quad (1.8)$$

Where the terms ϕ_n represents the n^{th} order partial derivative of ϕ in respect to ω , at ω_0 . ϕ_0 is known as the absolute phase of the pulse, or the Carrier Envelope Phase (CEP), which is the relative phase between the carrier wave and the envelope wave. Therefore, a change in the CEP will shift the carrier peak relative to the envelope peak, and is therefore crucial knowing this variable when working with few-cycle laser pulses, as can be seen in [Figure 1.1](#).

ϕ_1 - the first order coefficient - is called the group delay and is responsible for a pulse delay in the time domain. In the scope of this project, the most important terms are the second and the third order, which are the ones that start to change the pulse shape by a process called dispersion.

The second order coefficient ϕ_2 is called Group Delay Dispersion, or GDD, and translates in a quadratic spectral phase, which broadens the pulse in the temporal domain by lagging shorter wavelengths in respect to longer ones if the GDD is positive. The GDD introduced by a certain material can be estimated by calculating the second derivative of its wavelength-dependent refraction index $n(\lambda)$, at a wavelength of choice, and can be used to crudely estimate the change in the pulse's width.

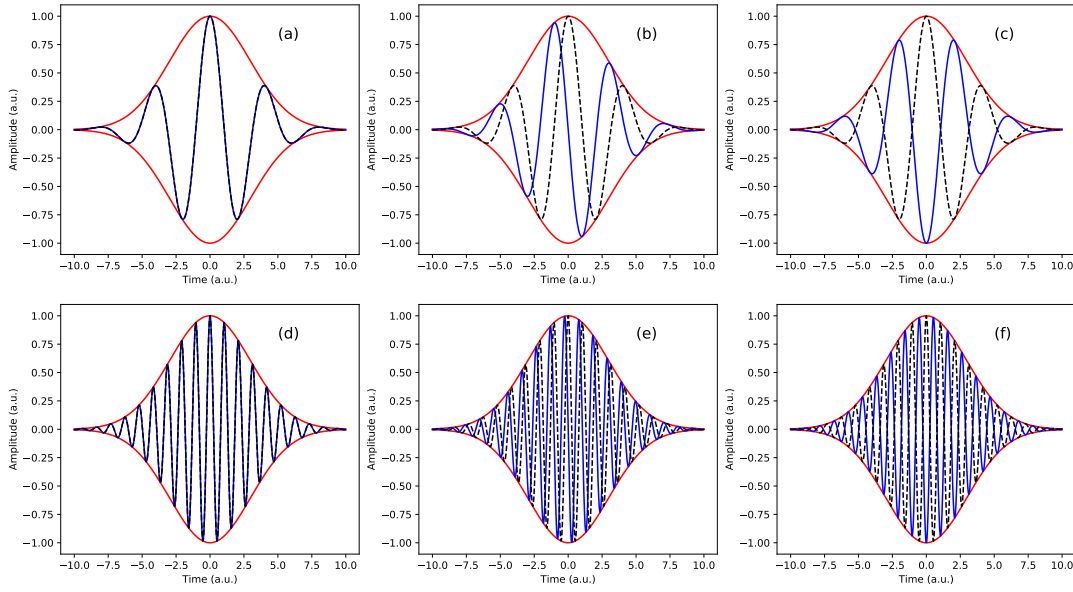


FIGURE 1.1: Relevance of the CEP for high peak power ultrashort pulses. The red lines represent the field envelope, the blue lines represent the electric field with CEP equal to zero (a - few-cycles and d - multi-cycles), $\pi/2$ (b - few-cycles and e - multi-cycles) and π (c - few-cycles and f - multi-cycles) radians, and the black dashed lines represent the electric field with CEP = 0. One can clearly see that the CEP affects mostly the peak intensity of few-cycle ultrashort pulses.

The third order coefficient ϕ_3 is called third order dispersion (TOD) and translates in a cubic phase, resulting from the frequency dependence of the GDD. Typically, TOD not only increases the pulse's width, but also distorts it, by creating pre- or post-pulses, depending on the TOD sign.

The effects of a quadratic and cubic phase on an ultrashort pulse can be seen in [Figure 1.2](#). The simulated spectrum is similar regarding center wavelength and bandwidth to the one obtained when using a typical Ti:Sa oscillator.

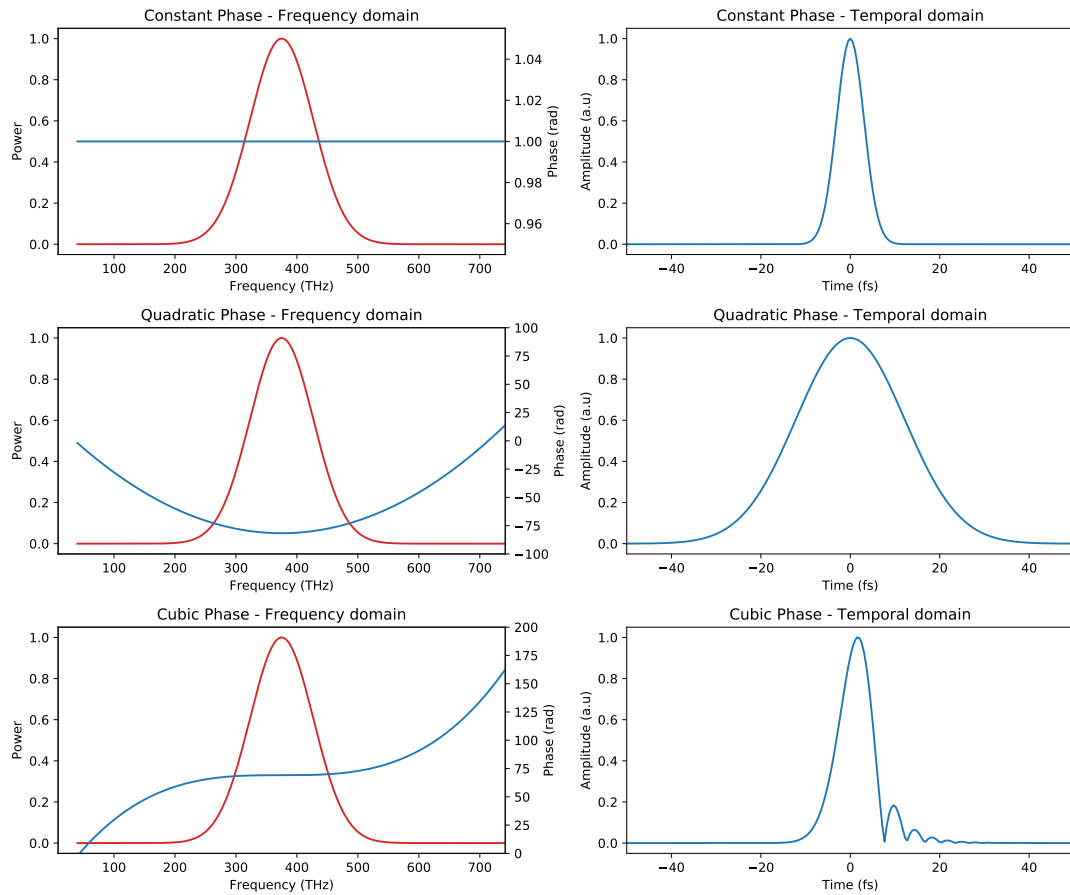


FIGURE 1.2: Effects of a flat (top), quadratic (middle) and cubic (bottom) phase in a gaussian spectrum. One clearly sees that a quadratic phase broadens the pulse in the time domain, and a cubic phase distorts the pulse, generating pre- or post- pulses (depending on the phase sign).

1.3 Dispersion compensation

Nowadays, we can easily cancel the travelling-induced chromatic dispersion using special mirrors called chirped mirrors, that introduce negative dispersion on the pulse.

A chirped mirror is a dielectric dispersive mirror composed of a superposition of alternate layers with a spatial modulation of the layer thickness values, where the multi-layer period is increased near the substrate and decreased near the air-coating interface. This effect produces a group delay that increases with the wavelength, i.e., a negative group delay dispersion [11], which means that faster frequencies travel a greater distance and slower frequencies travel a shorter distance, hence introducing negative dispersion. A scheme of a typical DCM mirror is presented in [Figure 1.3](#).

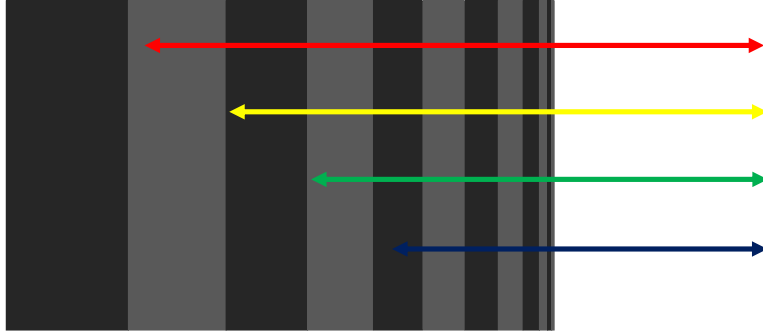


FIGURE 1.3: Chirped Mirror configuration. The dark grey areas correspond to layers with a higher refractive index and light grey areas to layers with a lower refractive index.

1.4 Nonlinear Optics

When light sources have an extremely high intensity (in the case of ultrashort pulses, due to their extremely short time duration) there is a need for a nonlinear model of light-matter interaction. In these cases, the polarization density \vec{P} responds nonlinearly with the electric field \vec{E} . If we start with the wave equation valid for both linear and nonlinear nonmagnetic materials without free carriers, one gets [12]:

$$\nabla \times \nabla \times \vec{E}(\vec{r}, t) - \frac{1}{c^2} \frac{\partial^2 \vec{E}(\vec{r}, t)}{\partial t^2} = \frac{1}{\epsilon_0 c^2} \frac{\partial^2 \vec{P}(\vec{r}, t)}{\partial t^2} \quad (1.9)$$

which can be written in the frequency domain as:

$$\nabla \times \nabla \times \vec{E}(\vec{r}, \omega) + \frac{\omega^2}{c^2} \vec{E}(\vec{r}, \omega) = -\frac{1}{\epsilon_0 c^2} \omega^2 \vec{P}(\vec{r}, \omega) \quad (1.10)$$

If there are only linear interactions with the medium, then a linear polarization $\vec{P}(\vec{r}, \omega) = \epsilon_0 \chi^{(1)} \vec{E}(\vec{r}, \omega)$ is created. However, there are also nonlinear terms arising in the polarization, which are responsible for the generation of new frequencies. In general, if we assume that the medium responds instantaneously, the scalar polarization can be written as:

$$P(t) = \epsilon_0 [\chi^{(1)} E(t) + \chi^{(2)} E^2(t) + \chi^{(3)} E^3(t) + \dots] \quad (1.11)$$

where the quantities $\chi^{(2)}$ and $\chi^{(3)}$ are the second- and third-order nonlinear optical susceptibilities, respectively.

1.4.1 Second-Harmonic Generation

We can assume that the material has a second-order response, given by (assuming that the response is instantaneous and scalar):

$$P^{(2)}(t) = \epsilon_0 \chi^{(2)} E^2(t) \quad (1.12)$$

Let's assume that the electric field in a certain point in space can be described by the superposition of two sinusoidal waves with different frequencies:

$$E(t) = E_1 e^{-i\omega_1 t} + E_2 e^{-i\omega_2 t} + c.c \quad (1.13)$$

Then, the second order polarization can be written as:

$$P^{(2)}(t) = \epsilon_0 \chi^{(2)} [E_1^2 e^{-2i\omega_1 t} + E_2^2 e^{-2i\omega_2 t} + 2E_1 E_2 e^{-i(\omega_1 + \omega_2)t} + 2E_1 E_2^* e^{-i(\omega_1 - \omega_2)t} + 2E_1 E_1^* + 2E_2 E_2^* + c.c] \quad (1.14)$$

The first and second terms inside brackets are called Second Harmonic Generation (SHG), which consists in the generation of radiation with double the frequency of the original wave, whereas the third and fourth terms are called sum-frequency and difference-frequency generation, respectively.

As we can see, the nonlinear polarization can be responsible for the generation of light at new frequencies.

1.4.2 Third-Harmonic Generation

If the material now has a third order instantaneous and scalar response:

$$P^{(3)}(t) = \epsilon_0 \chi^{(3)} E^3(t) \quad (1.15)$$

we can already determine that, if the electric field is given as in [Equation 1.13](#), the resulting polarization will have terms of the form $\epsilon_0 \chi^{(3)} [E_1^3 e^{-3i\omega_1 t} + E_2^3 e^{-3i\omega_2 t}]$, known as the Third Harmonic Generation, which is of particular interest for this thesis.

Since this process is nonlinear, to calculate the THG, we would need to solve the nonlinear coupled equations. However, there is a method that gives good results, with the condition that the conversion efficiency is low, which consists in taking the ultrashort pulse in the time domain, cubing it, and returning to the frequency domain to find the spectral amplitude of the THG pulse, as seen in [Equation 1.16](#).

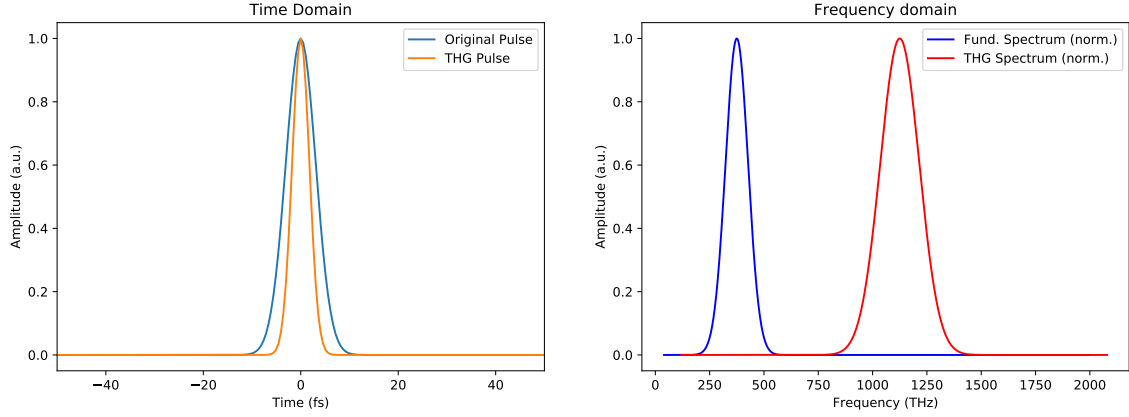


FIGURE 1.4: Third-Harmonic Generation in an ultrashort pulse.

$$E(\omega) \xrightarrow{F} E(t) \xrightarrow{\wedge^3} E^3(t) \xrightarrow{F^{-1}} E_{THG}(\omega) \quad (1.16)$$

A simulation of THG in an ultrashort pulse using Equation 1.16 can be seen in Figure 1.4. We can clearly see that the THG spectrum consists on a double auto-convolution of the fundamental spectrum (both spectra are normalized).

1.4.3 Intensity-Dependent Refractive Index

When a light pulse with high intensity propagates through a material with non-zero third order optical susceptibility, the refractive index of the latter changes with the light intensity. This effect is known as an intensity-dependent refractive index.

If we consider the third-order polarization as given by Equation 1.15, then the part of the nonlinear polarization that influences the propagation of a beam with frequency ω is given by [12]:

$$P^{NL}(\omega) = 3\epsilon_0\chi^{(3)}|E(\omega)|^2E(\omega) \quad (1.17)$$

and the total polarization of the beam with frequency ω becomes:

$$P(\omega) = \epsilon_0\chi_{eff}E(\omega) \quad (1.18)$$

where $\chi_{eff} = \chi^{(1)} + 3\chi^{(3)}|E(\omega)|^2$. Since, in general, the refractive index can be written as:

$$n^2 = 1 + \chi_{eff} \quad (1.19)$$

we thus get the intensity-dependent refractive index:

$$n^2 = 1 + \chi^{(1)} + 3\chi^{(3)}|E(\omega)|^2 \quad (1.20)$$

We can rewrite the above equation by making use of the linear refractive index $n_0 = (1 + \chi^{(1)})^{1/2}$, leading to:

$$n = n_0 + n_3|E(\omega)|^2 \quad (1.21)$$

where $n_3 = \frac{3\chi^{(3)}}{2n_0}$. Introducing the light intensity as $I = 2n_0\epsilon_0c|E(\omega)|^2$, we can rewrite the intensity-dependent refractive index as:

$$n = n_0 + \frac{3}{4n_0^2\epsilon_0c}\chi^{(3)}I \quad (1.22)$$

1.5 Ultrashort pulse characterization

With our current technology, we can easily characterize pulses with time duration of the nanosecond or picosecond timescale with detectors with hundreds of picoseconds of response time. However, femtosecond pulses have time durations shorter than the response time of these electronic devices, and therefore cannot be measured that easily. Their characterization is a demanding task, since we need to know both the spectral power and phase in order to retrieve the ultrashort pulse. We can use a traditional spectrometer in order to obtain the spectral power, but the spectral phase is harder to obtain. Autocorrelation [13] allows for an estimate of the pulse's time duration, only if the pulse's temporal shape is well known. However, several methods have been developed in order to overcome this problem, like FROG [14], SPIDER [15], MIIPS [16] and d-scan.

1.5.1 Autocorrelation

The autocorrelation technique uses the pulse to measure itself. A replica of the pulse with a well known time delay is created, and by scanning the time delay between the two pulses, one gains information about the pulse itself. Interferometric setups like a Michelson interferometer (see [Figure 1.5](#)) can be used to measure field autocorrelation, but they contain no phase information about the pulse itself.

To understand this concept, one needs to know the output signal measured by the detector:

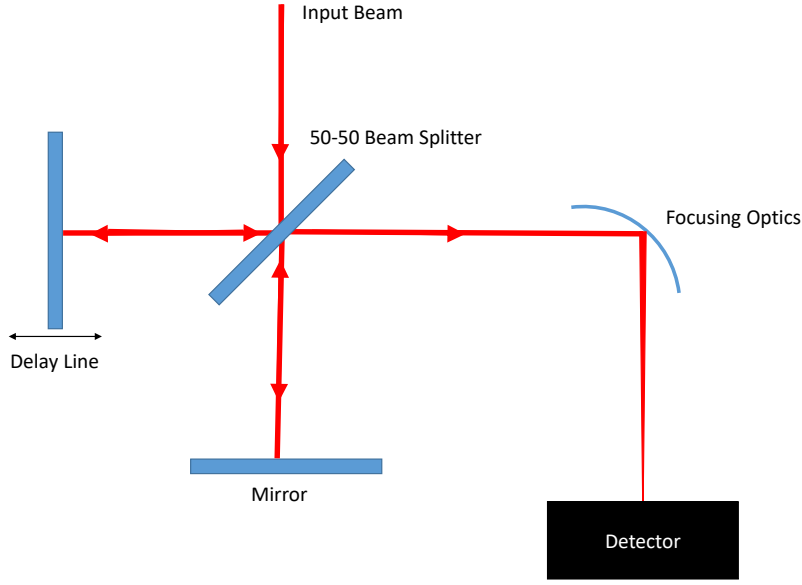


FIGURE 1.5: Michelson interferometer setup.

$$A_F(\tau) = \int_{-\infty}^{+\infty} |E(t) + E(t - \tau)|^2 dt = \int_{-\infty}^{+\infty} |E(t)|^2 + |E(t - \tau)|^2 + 2|E(t)E^*(t - \tau)|^2 dt \quad (1.23)$$

the first two terms contribute to the integral only with a constant term, but the last term is proportional to the magnitude of the Fourier transform of the spectrum $S(\omega)$, from which we cannot obtain information about the spectral phase.

If we use a nonlinear detector (e.g., a nonlinear $\chi^{(2)}$ crystal, a filter and a typical detector) the output signal is proportional to the intensity of the squared sum of the two pulses, which contains more information:

$$A_2(\tau) = \int_{-\infty}^{+\infty} |(E(t) + E(t - \tau))^2|^2 dt \quad (1.24)$$

which contains information about the pulse chirp and, consequently, its bandwidth. However, it cannot provide information about the pulse phase, since two different pulses can have the same autocorrelation, and can only provide good information about the pulse temporal duration if it is perfectly Gaussian or another well-known shape.

1.5.2 Frequency Resolved Optical Gating (FROG)

If we substitute the optical detector with a second harmonic crystal and a spectrometer, we measure the output signal spectrum instead of its intensity. This technique is called second harmonic generation FROG, and allows to measure a spectrogram representation of the pulse (pulse's spectrum as a function of the delay), which allows for a complete phase retrieval. However, SHG-FROG traces are symmetrical with respect to delay, which means that SHG-FROG cannot distinguish a pulse from its time-reversed self (e.g., it cannot distinguish a positively chirped pulse from a negatively chirped pulse). For more information regarding SHG-FROG ambiguities, please see [17].

1.5.3 Spectral phase interferometry for direct electric field reconstruction (SPIDER)

Another way to obtain the spectral phase of an ultrashort pulse is to mix a frequency-shifted replica of the pulse with itself, obtaining an interferogram that also yields information about the spectral phase. To do this, the input beam is generally divided into 3 beams, where two of them are combined (with a known time delay) in order to create two identical pulses. The remaining beam is strongly chirped by propagating through a dispersive material, which leads to an intrapulse delay between higher and lower frequencies. This beam and the other two pulses are combined in a sum-frequency generation crystal. Therefore, the two pulses will interact with different frequencies from the chirped pulse, and the two upconverted output pulses will have different central wavelengths, which is equivalent to a frequency shift between two identical pulses and will result in a spectral interferogram that can be measured in a normal spectrometer.

1.5.4 Multiphoton Intrapulse Interference Phase Scan (MIIPS)

The MIIPS technique introduced a new paradigm in the ultrashort pulse characterization area, and consists in applying different known spectral phases to a pulse and using a nonlinear signal to correct the original phase of the pulse. If we have an ultrashort pulse with spectral phase $\phi(\omega)$, we can apply a known spectral phase $\varphi(\omega)$ by using an active pulse shaper. Since the maximum SHG (as an example) occurs for a flat spectral phase, we can determine experimentally what introduced phase at frequency ω produces the maximum SHG at frequency 2ω , and iteratively, one gets a MIIPS trace that allows a flattening of the pulse spectral phase.

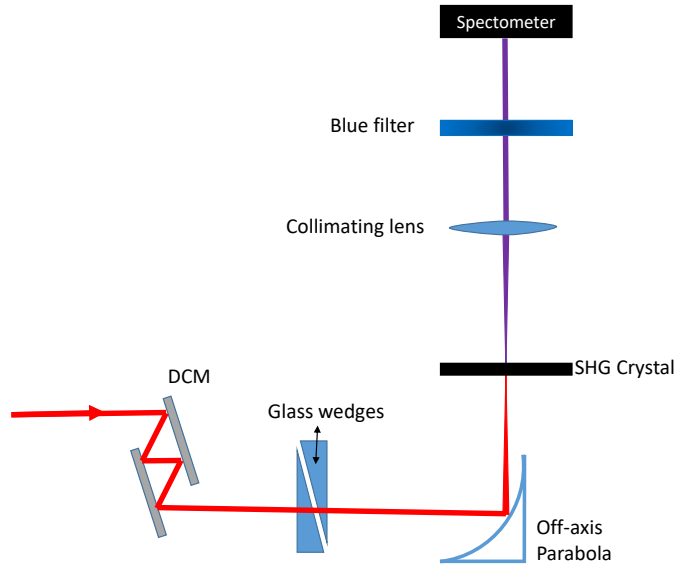


FIGURE 1.6: Typical d-scan setup. DCM: Double Chirped Mirrors.

1.5.5 Dispersion-scan

In 2012, M. Miranda et al. [18] developed a new technique called d-scan (short for dispersion-scan), which enables the characterization of ultrashort light pulses using an unprecedentedly simple and fully inline optical setup. In this method, the spectrum of a nonlinear signal, such as SHG (or, for the purpose of this thesis, THG) is recorded for different amounts of dispersion applied to the light pulse, creating a 2D d-scan trace from which the spectral phase of the pulse can be retrieved and, therefore, by inverse Fourier transform, provides the exact temporal intensity profile of the pulse. A typical d-scan setup is presented in [Figure 1.6](#).

1.5.5.1 Mathematical description

Let us consider an ultrashort pulse, that can be described by its complex spectral amplitude:

$$\tilde{E}(\omega) = |\tilde{E}(\omega)| \exp[i\phi(\omega)] \quad (1.25)$$

When the pulse goes through a piece of glass of thickness z , it gains an additional phase term given by $\exp[izk(\omega)]$, leading to a different complex spectral amplitude:

$$\tilde{E}(\omega) = |\tilde{E}(\omega)| \exp[i\phi(\omega)] \exp[izk(\omega)] \quad (1.26)$$

where $k(\omega) = \frac{\omega}{c} n_{glass}(\omega)$, n_{glass} being given by Sellmeier's equation for glass.

By shining the beam on a material with non-zero third-order nonlinear optical susceptibility (getting, in this case, THG), we get a d-scan trace of the form:

$$S(\omega, z) = \left| \int \left(\int \tilde{E}(\Omega) \exp[izk(\Omega)] \exp[i\Omega t] d\Omega \right)^3 \exp(-i\omega t) dt \right|^2 \quad (1.27)$$

The above equation can be described as follows: after the pulse propagates in glass, we go to the time domain and cube it, thus generating the third harmonic. Then, we go back to frequency domain, and square the result, in order to get the spectral power. To fully retrieve the electric field in the time domain, we first guess a spectral phase and simulate the d-scan arising from that same phase. If the measured and the simulated scan are different, then we re-guess the spectral phase until a good agreement is obtained. For an explanation of different algorithms used for the phase retrieval, see e.g., [19, 20].

An example of a typical d-scan trace with different spectral phases is presented in [Figure 1.7](#).

It is quite impressive that the effects of a quadratic and cubic phase are similar whether we are dealing with SHG d-scan or THG d-scan, i.e., a quadratic phase changes the d-scan trace's optimum dispersion and a cubic phase tilts the d-scan trace.

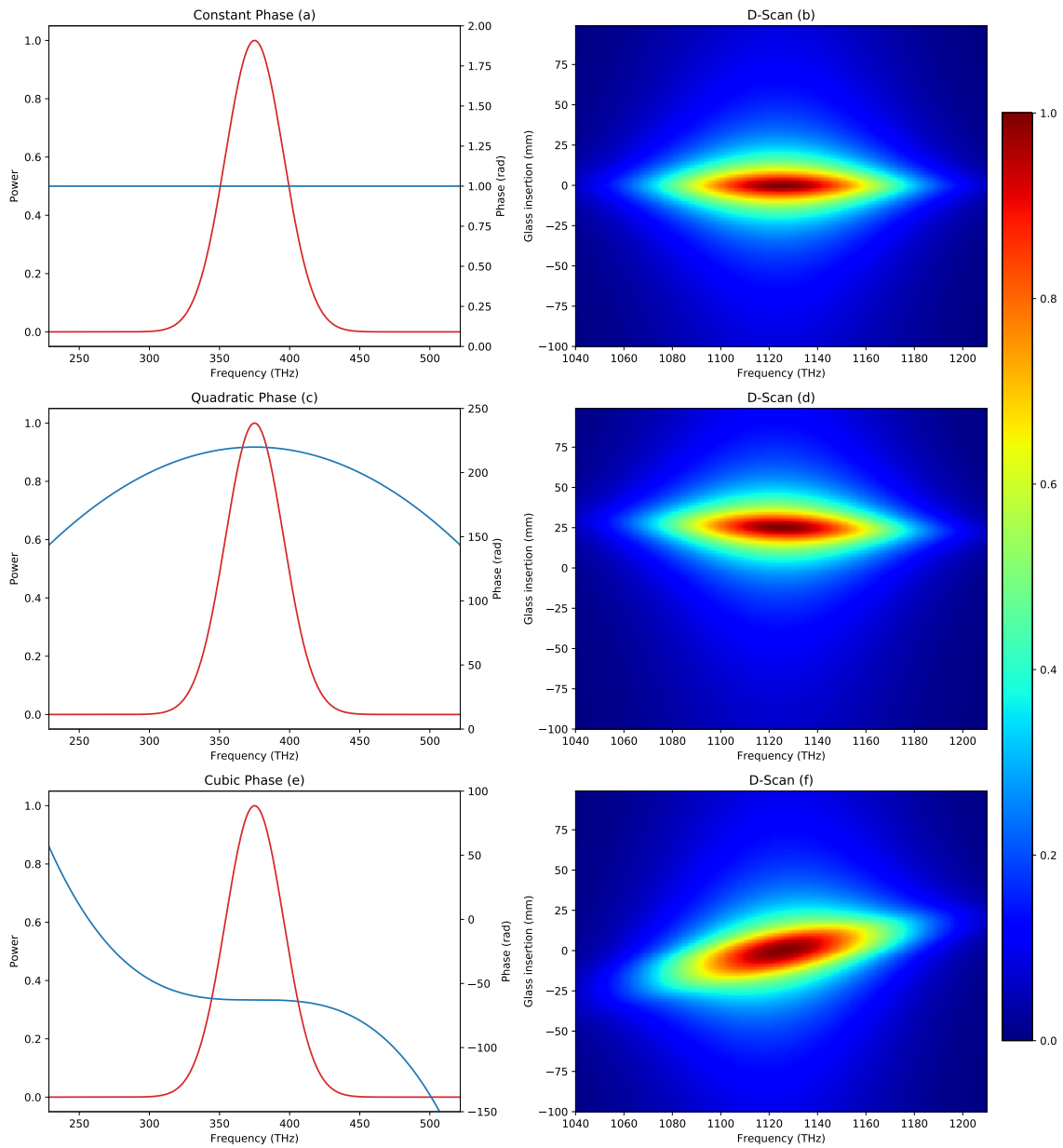


FIGURE 1.7: THG d-scan trace for a constant (a,b), quadratic (c,d) and cubic phase (e,f). One sees that, if the ultrashort pulse has a quadratic phase, its d-scan trace changes the optimum dispersion, and the trace gets slightly tilted, whereas if the phase is cubic, the d-scan trace is strongly tilted.

1.6 Ultrafast time-resolved spectroscopy

One of the major applications of ultrashort pulses is the time-resolved study of ultrafast dynamical processes, either on biological, chemical or solid-state materials [21, 22]. A typical example of these ultrafast dynamical processes is the scattering of photoexcited carriers in a semiconductor material, due to interactions with the lattice or other carriers [see chapter 2 for further details].

Most of these ultrafast spectroscopy schemes can be understood in the frame of the pump-probe approach [4], illustrated in Figure 1.8. In this technique, a laser pulse with high intensity (labelled pump) excites the studied sample in some way. Let's consider that this excitation changes some material property \mathcal{P} in the following way:

$$\mathcal{P}(t) = \mathcal{P}_0 + \Delta\mathcal{P}(t - t_0) \quad (1.28)$$

where \mathcal{P}_0 is the initial value of the property \mathcal{P} and $\Delta\mathcal{P}(t - t_0)$ is the change induced by the pump arriving at time t_0 . Later, a laser pulse, typically with lower intensities (labelled probe), arrives at the sample with a time delay τ . Then, by studying the probe or other effects induced by the interaction between the pump and the probe, one gets information of the material's response at time $t - t_0 = \tau$. By changing the time delay τ between the two pulses, we can extract the time dependence of the material response function $\Delta\mathcal{P}(\tau)$.

If we associate the material response function of the studied parameter with a microscopic model of the physical process under investigation, we can gain insight into the dynamics of these processes. Using pump-probe techniques, we are able to study

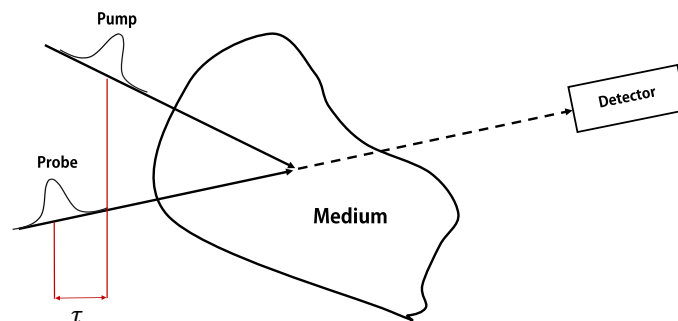


FIGURE 1.8: Typical pump-probe scheme.

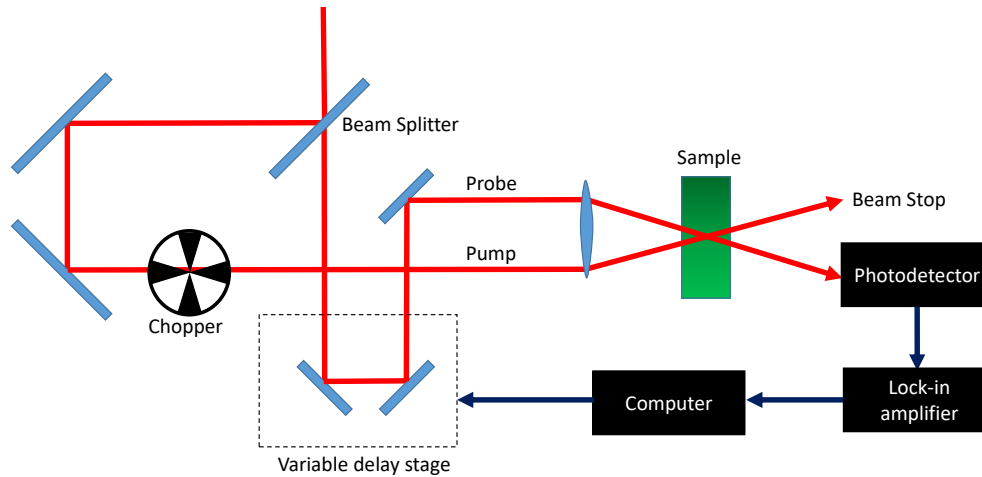


FIGURE 1.9: Typical degenerate pump-probe setup in transmission geometry.

properties like transmission, fluorescence yield, refractive index changes, dichroism and birefringence, etc. [23–25].

The great amount of pump-probe measurements techniques arise from the different modes of detection and the choice of the pump and probe beams. In terms of detection, typically a detector with a slow response time compared to the material's dynamic is used, where the material's response is time-integrated. The time resolution in this case comes from the ability to scan the pump-probe delay precisely.

When choosing the pump and probe beams, there are two main setups. Using the degenerate setup, the pump and probe beams are similar, derived from the same laser and occupy the same spectral band. In the case of the non-degenerate setup, the pump occupies a different spectral band from the probe, the latter being derived from the same laser as the pump, but frequency up-converted by a nonlinear process.

A typical degenerate pump-probe setup is shown in Figure 1.9, where the pump and probe beams are focused into the sample with a controllable and measurable time delay τ . Then, the averaged probe beam power is measured using a time-integrating detector as a function of τ , giving access to the material's response as a function of time. One may use a chopper – used to modulate the frequency of the pump beam - and a lock-in amplifier, in order to measure only the probe power induced by the pump beam.

1.7 Purpose of this thesis

The most common nonlinear signal for d-scan has been SHG, which has been used not only to characterize ultrashort pulses in the time domain [26], but has also been the first experimental technique used to measure ultrashort pulse instabilities at coherence level [27]. However, d-scan has already been used with third-order processes, like THG d-scan [28, 29], XPW (Cross-Polarized Wave) d-scan [30, 31] - which can be particularly useful to measure pulses in the DUV region [32] - SD (Self-Diffraction) d-scan [33] - which is useful to measure two ultrashort pulses simultaneously [34] - and also THIS (Third-Harmonic *In Situ*) d-scan [35], which allows for *in situ*, in-parallel characterization of ultrashort laser pulses in a gas or solid target.

Using SHG d-scan to measure ultrashort pulses, although being the most common d-scan technique, can be a problem when using octave-spanning lasers, due to overlap between the SHG and the fundamental spectra. In these cases, it is helpful to use higher-order nonlinearities, like THG [28]. During the course of this thesis we will present several examples of THG d-scan measurements of broadband few-cycle laser pulses obtained in graphene films produced by different growing methods, which enable characterizing the used ultrashort pulses while providing insight of the electronic dynamics in graphene and its dependence on the synthesis conditions.

Chapter 2

Graphene

Graphene consists in a single layer of carbon atoms arranged in an hexagonal lattice [see [Figure 2.1](#)] and is a very promising material, mainly due to its extremely high broadband nonlinear optical susceptibility [36] and the possibility of occurrence of inter-band transitions at all optical frequencies. It was first studied theoretically by P. R. Wallace in 1947 [37], in a accidental way, due to the fact that Wallace was studying the band theory of graphite, needing the band theory of a single layer of graphite (graphene) for that purpose. Graphene was first produced experimentally in 2004 (surprisingly, using only a scotch tape and a pencil), by Andre Geim and Kostya Novoselov [38], which gave them the Nobel prize in Physics in 2010 [39].

Besides its strong mechanical strength, high optical absorption and high electron mobility, allowing for very unique applications [40–43], its high broadband nonlinear optical susceptibility allows for ultrafast broadband and intense third-harmonic generation (THG), enabling not only to characterize the used ultrashort pulses but also to study the dynamics of the charge carriers in graphene. Additionally, the possibility of obtaining an enhanced nonlinear signal when using multi-layer graphene [44] adds an additional interest to this work.

Even though graphene is, by definition, single layer, it is rather usual to talk about multi-layer graphene. When dealing with a single layer of graphene, we call it Single Layer Graphene (SLG). When dealing with two stacked layers of graphene, we call it Bilayer Graphene. When dealing with more than two layers, it is usually called Multi-Layer Graphene (MLG).

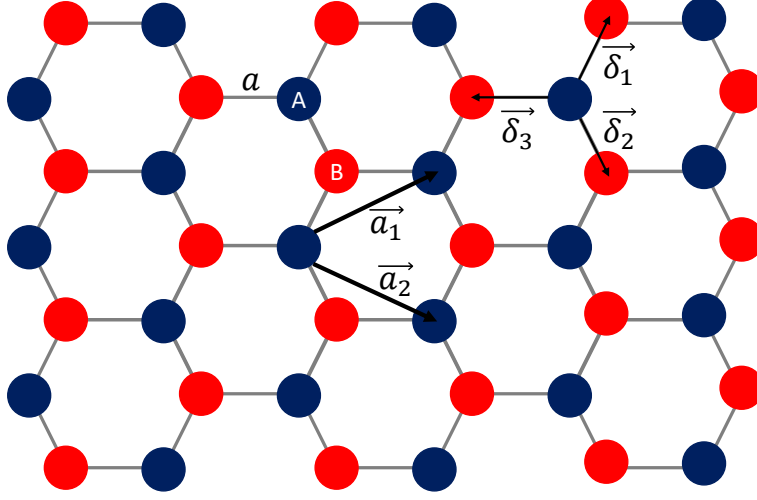


FIGURE 2.1: Graphene honeycomb lattice with 2 triangular sublattices (A and B, represented in red and blue dots, respectively). The distance between a carbon atom and its nearest neighbour is $a = 1.42\text{\AA}$.

2.1 Electronic structure

Graphene structure is not a Bravais lattice, but can be seen as a triangular lattice with a basis of two atoms per cell [45]. The lattice vectors can be written as:

$$\begin{aligned}\vec{a}_1 &= \frac{a}{2} (3\hat{x} + \sqrt{3}\hat{y}) \\ \vec{a}_2 &= \frac{a}{2} (3\hat{x} - \sqrt{3}\hat{y})\end{aligned}\quad (2.1)$$

which implicates that the reciprocal lattice vectors are:

$$\begin{aligned}\vec{k}_x &= \frac{2\pi}{3a} (\hat{x} + \sqrt{3}\hat{y}) \\ \vec{k}_y &= \frac{2\pi}{3a} (\hat{x} - \sqrt{3}\hat{y})\end{aligned}\quad (2.2)$$

The three nearest-neighbours vectors in real space are given by:

$$\vec{\delta}_1 = \frac{a}{2} (\hat{x} + \sqrt{3}\hat{y}), \quad \vec{\delta}_2 = \frac{a}{2} (\hat{x} - \sqrt{3}\hat{y}), \quad \vec{\delta}_3 = -a\hat{x} \quad (2.3)$$

and the next nearest-neighbours are located at: $\vec{\delta}'_1 = \pm\vec{a}_1$, $\vec{\delta}'_2 = \pm\vec{a}_2$ and $\vec{\delta}'_3 = \pm(\vec{a}_2 - \vec{a}_1)$.

The tight-binding Hamiltonian for the electron in graphene, assuming that they can hop to both nearest and next-nearest neighbours, is ($\hbar = 1$):

$$H = -t \sum_{\langle i,j \rangle, \sigma} (a_{\sigma,i}^\dagger b_{\sigma,j} + h.c.) - t' \sum_{\langle\langle i,j \rangle\rangle, \sigma} (a_{\sigma,i}^\dagger a_{\sigma,j} + b_{\sigma,i}^\dagger b_{\sigma,j} + h.c.) \quad (2.4)$$

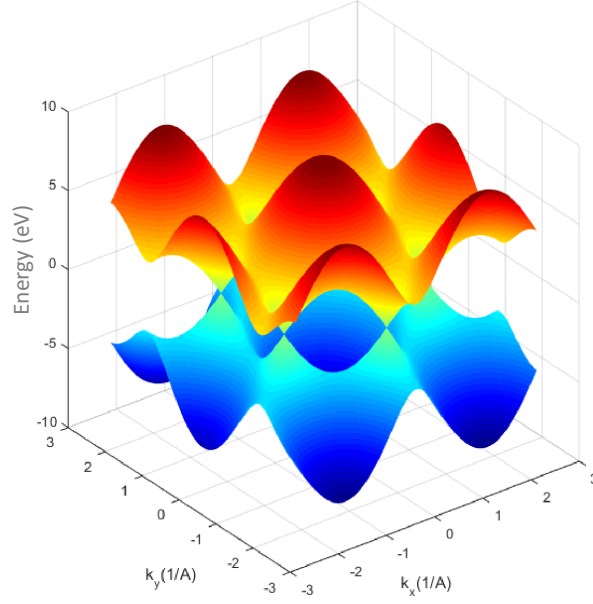


FIGURE 2.2: Graphene energy band structure with $t = 2.7eV$ and $t' = 0 eV$, for the π (yellow) and π^* (blue) bands.

where $a_{\sigma,i}$ ($a_{\sigma,i}^\dagger$) annihilates (creates) an electron with spin $\sigma = \uparrow, \downarrow$, on site \vec{R}_i on sublattice A ($b_{\sigma,i}$ ($b_{\sigma,i}^\dagger$) are analogous for sublattice B). t is the nearest-neighbour energy hopping, while t' is the next nearest-neighbour energy hopping. We can calculate the energy bands for this Hamiltonian, which are given by:

$$E_{\pm}(\vec{k}) = \pm t \sqrt{3 + f(\vec{k})} - t' f(\vec{k}) \quad (2.5)$$

where the plus and minus sign applies to the upper (π) and lower (π^*) band, respectively, and $f(\vec{k})$ is a dimensionless quantity given by:

$$f(\vec{k}) = 2 \cos(\sqrt{3}k_y a) + 4 \cos\left(\frac{\sqrt{3}}{2}k_y a\right) \cos\left(\frac{3}{2}k_x a\right) \quad (2.6)$$

By plotting Equation 2.6 as a function of k_x and k_y in MATLAB, we get the graphene's band structure that can be seen in Figure 2.2

We can see that, if $t' = 0$, the spectrum is symmetric around zero energy. If $t' \neq 0$, then the electron-hole symmetry is broken and the bands π and π^* become asymmetric. If we expand the band structure near the point \vec{K} or \vec{K}' , given by $\vec{K} = \frac{2\pi}{3a} \left(\hat{k}_x + \frac{1}{\sqrt{3}} \hat{k}_y \right)$ and $\vec{K}' = \frac{2\pi}{3a} \left(\hat{k}_x - \frac{1}{\sqrt{3}} \hat{k}_y \right)$ we get the dispersion relation in $\vec{k} = \vec{K} + \vec{q}$:

$$E_{\pm}(\vec{q}) \approx v_F |\vec{q}| + \mathcal{O}((q/K)^2) \quad (2.7)$$

where \vec{K} and \vec{K}' are called the Dirac points, and v_F is the Fermi velocity, given by $v_F = 3ta/2 \simeq 1 \times 10^6 \text{ m.s}^{-1}$. This energy dispersion describes particles that are quantum mechanically described as massless Dirac fermions.

One notices that the main difference between this case and the traditional one is the fact that the Fermi velocity doesn't depend neither on the energy nor the momentum.

2.2 Optical properties

The massless Dirac fermions in graphene provide an universal optical response, expressed in terms of the fine-structure constant [46] $\alpha = e^2/hc \approx 1/137,036$. In the infrared limit, the optical absorption coefficient of a single layer of graphene is equal to $\pi\alpha \approx 2.3\%$ (which makes a single atomic layer of graphene visible to the naked eye!). When dealing with multi-layer graphene, and since the light energy is typically very superior to the graphene's Fermi energy, its optical absorption is given by $N\pi\alpha$, where N is the number of graphene layers.

2.3 Hybridization in graphene

Graphene is an isolated single layer of carbon hexagons consisting of sp^2 hybridized C-C bonding with π -electron clouds [47]. Carbon atoms in the ground state have 2 core electrons and 4 valence electrons, with the electronic structure $(1s)^2 (2s)^2 (2p)^2$, containing 2 unpaired electrons in the $2p$ orbital.

When carbon is in the crystalline phase, one valence electron from the $2s$ orbital is excited to the $2p_z$ orbital, and the electronic configuration is altered to $(1s)^2 (2s)^1 (2p_x)^1 (2p_y)^1 (2p_z)^1$, with an energy cost of 4 eV. However, the formed bonds are much stronger, giving rise to more stability. But why are these bonds stronger? When this excitation occurs, the wave functions of at least two of the valence electrons are mixed (i.e., carbon is hybridized), which creates new orbits, enhancing the binding energy of carbon with its nearest neighbours. The superposition of a $(2s)$ orbital with n $(2p)$ orbitals is named sp^n hybridization.

Graphene is sp^2 hybridized, meaning that one orbital ($2s$) and two orbitals ($2p$) are mixed, creating 3 new orbitals ϕ_i ($i = 1, 2, 3$), which are:

$$|\phi_1\rangle = \frac{1}{\sqrt{3}}|2s\rangle - |2p_y\rangle \quad (2.8)$$

$$|\phi_2\rangle = \frac{1}{\sqrt{3}}|2s\rangle + \sqrt{\frac{2}{3}}\left(\sqrt{\frac{3}{2}}|2p_x\rangle + \frac{1}{2}|2p_y\rangle\right) \quad (2.9)$$

$$|\phi_3\rangle = -\frac{1}{\sqrt{3}}|2s\rangle - \sqrt{\frac{2}{3}}\left(\sqrt{\frac{3}{2}}|2p_x\rangle - \frac{1}{2}|2p_y\rangle\right) \quad (2.10)$$

2.4 Ultrafast dynamics of charge carriers in graphene

Let us consider a semiconductor with an energy bandgap E_g . If the material absorbs a photon of energy $\hbar\omega$, with $\hbar\omega > E_g$, then an electron from the valence band will be promoted to the conduction band, remaining with an excess energy of $\hbar\omega - E_g$, and therefore with a non-zero wave vector determined by the semiconductor band structure. The electron will now lose this excessive energy over time, mainly due to interactions with other carriers and with the crystal lattice. After a time τ , the electron will recombine with a hole in the valence band, and the material returns to its initial state, as can be seen in [Figure 2.3](#). If we replace the semiconductor by a metal, the same process occurs, but the absorption can lead either to an intraband excitation of an electron in the conduction band or the same process described before. We call ultrafast carrier dynamics to the scattering and recombination mechanisms and to the time scale that they occur. In order to study these dynamics, one usually studies the influence of the excited carriers on optical properties of the material, like the refractive index ($\tilde{n} = n' + in''$) and the relative permittivity ($\varepsilon = \varepsilon' + i\varepsilon''$).

In this section, we will do a brief literature review of the study of ultrafast carrier dynamics in graphene.

2.4.1 Literature review

By making femtosecond reflectivity and transmission measurements, Seibert et al. [\[48\]](#) were able to study, with time resolution, the generation, relaxation and recombination of non-equilibrium charge carriers in solid graphite, back in 1990. The experiments were performed with a standard pump-probe method, with a dispersion-compensated mode-locked dye laser supplying optical pulses of 50 fs duration, centered at $\lambda = 620\text{nm}$ at a repetition rate of 100 MHz. The samples used consisted of highly oriented pyrolytic

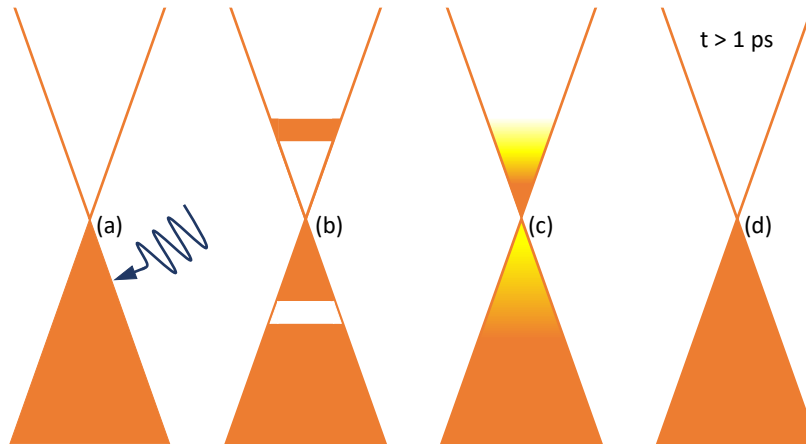


FIGURE 2.3: Ultrafast carrier dynamics in graphene. A photon interacts with the material (a), and is absorbed, causing an electron to be promoted to the conduction band (b). Later, the electron will begin to lose energy due to electron-electron and electron-phonon scattering (c) and will eventually decay to its initial state (d).

graphite (HOPG), with 350 Å thickness. On a sub-picosecond time scale, a strong, initial, broadband absorption saturation was observed, caused by state filling by a hot, dense π -band electron population, which then recovers with a fluence- and probe-wavelength-dependent time constant as the carriers cool and recombine in less than 1 ps.

In 2008, Dawlaty et al. [49], reported on the measurement of carrier relaxation times in epitaxial graphene layers grown on SiC wafers. A Ti:sapphire mode-locked laser with 86 MHz pulse repetition rate, 780 nm center wavelength and approximately 85 fs pulse width was used, delivering pump pulses with energies between 3-15 nJ and weak probe pulses with energies between 30-100 pJ. By using ultrafast optical pump-probe spectroscopy, they were able to find two distinct time scales associated with the relaxation of nonequilibrium photogenerated carriers: an initial fast relaxation in the 70-120 fs range, associated with carrier-carrier intraband scattering, and a slower relaxation in the 0.4-1.7 ps range, associated with carrier-phonon intraband and interband scattering processes. The latter is found to be inversely proportional to the degree of crystalline disorder in the graphene layers, as measured by Raman spectroscopy.

In 2010, Lui et al. [50] managed to observe significant light emission from graphene under excitation by ultrashort laser pulses, although graphene having no band gap. The samples were excited by 30-fs laser pulses with photon energies of 1.5 eV delivered from a 80 MHz repetition rate mode-locked Ti:sapphire oscillator. The light emission exhibits a nonlinear dependence with the laser fluence. In two-pulse correlation measurements, a dominant relaxation time of tens of femtoseconds is observed, and a two-temperature

model describing the interactions between the electrons and the strongly coupled optical phonons is in agreement with the experimental observations.

Oum et al. [51], in 2014, were able to investigate the ultrafast carrier dynamics and phonon relaxation of CVD-grown monolayer and 9-layer graphene on a quartz substrate. A pump-supercontinuum probe (PSCP) technique was used, where a multifilament supercontinuum was generated in a translating 2 mm thick CaF_2 plate from the second harmonic (400 nm, 12 mW) of the fundamental beam of a regeneratively amplified Titanium:sapphire system, which allowed to extend their study deeper into the UV region. The normalized change in optical density was probed over the range 260-640 nm, reaching into the region of graphene's Fano resonance.

As usual, two time constants of 160 fs and 4 ps were found and assigned to carrier-optical phonon scattering and slower phonon relaxation processes, respectively. The carrier distribution at early times was clearly hotter for 400 nm excitation than for 800 nm excitation. A pronounced spectral bleach feature was observed below 300 nm. It immediately formed after photoexcitation and recovered slowly, with a time constant of 35 ps for monolayer and time constants of 120 and 970 ps for 9-layer graphene. The same dynamics were found for weak transient absorption features above 300 nm, which emerged after approximately 0.5 ps. The slow dynamics were assigned to interfacial heat flow from graphene to the quartz substrate. The bleach and absorption features were well described by a simple model assuming a red-shift of the Fano resonance. This red-shift disappeared with progressive cooling of graphene.

The effects of ambient temperature on the properties of monolayer graphene were studied in 2017, by Hafez et al. [52], using terahertz time-domain spectroscopy as well as time-resolved terahertz spectroscopy enabled by an optical-pump/terahertz-probe technique. The THz quasisingle cycle pulses are generated by optical rectification of 800-nm, 40-fs Ti:sapphire laser pulses in a $LiNbO_3$ crystal by employing the pulse-front tilting technique.

The measurements proved that graphene is very sensitive to the ambient environmental conditions, to the sample's preparation technique and to the initial Fermi level.

2.5 Raman Spectroscopy

2.5.1 Raman Scattering

Let us suppose that a photon excites a sample, creating a time-dependent perturbation of the Hamiltonian. Since the photon has a fast changing electric field, only electrons will respond to the perturbation. Therefore, the perturbation induced by a photon of energy $\hbar\omega_L$ increases the total energy to $E_{GS} + \hbar\omega_L$, where E_{GS} is the energy of the ground state. Typically, the total energy now does not correspond to a stationary state, and the system is said to be in a virtual state, and therefore the system will leave this unstable situation, formally emitting a photon and returning to one of its stationary states [53].

When the system returns to its initial state - and, therefore, the emitted photon remains the same as the incident one - the effect is named Rayleigh scattering, or elastic scattering. However, the photon can lose part of its energy in the interaction process *, exiting the sample with a lower energy $\hbar\omega_{Sc}$, which corresponds to the Stokes process. Since the sample has to return to a stationary state, the lost energy must be that of a phonon energy $\hbar\Omega = \hbar\omega_L - \hbar\omega_{Sc}$. This process corresponds to the Raman scattering [54], and is the basis to Raman spectroscopy.

2.5.2 Raman spectrum

If we plot the intensity of the scattered light as a function of the difference between the incident and the scattered photon energy (the Raman shift, typically measured in cm^{-1}), we get the famous Raman spectrum - see [Figure 2.4](#).

This type of spectra can give various information about the studied graphene sample, as the structural and electronic properties, the number of graphene layers, the stacking order and the density of impurities and defects. For graphene and other carbon allotropes, three main peaks arise:

- G peak ($\sim 1580cm^{-1}$), which is a typical indicator for sp^2 carbon materials and is related with high frequency in-plane optical phonons at the center of the FBZ.
- D peak ($\sim 1350cm^{-1}$), which corresponds to a "fingerprint" for disorder and its intensity.

*With a much lower probability

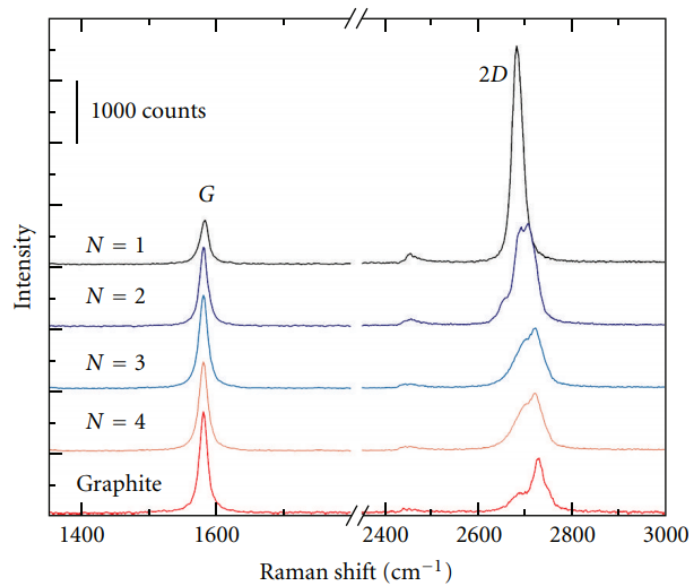


FIGURE 2.4: Raman spectrum of graphene, for different number of layers (1-4) and of bulk graphene (graphite). Reproduced from [55].

- 2D peak ($\sim 2690\text{cm}^{-1}$), whose intensity and dispersion is sensitive to the type of allotrope and, in this particular case, to the number of graphene layers.

2.6 Our graphene samples

All the studied graphene samples were produced at I3N (Institute for Nanostructures, Nanomodelling and Nanofabrication), in the University of Aveiro, within the scope of the project “Ultragraf - Harnessing third-harmonic generation in graphene-coated optics: new devices for ultrafast pulse measurement and frequency upconversion”.

2.6.1 TCVD graphene

First, the copper where graphene will grow is washed with ultrasounds, acetone and isopropanol, 15 minutes in each of the solvents. Then, a 10 minutes and 950°C annealing process begins, with 190 sccm (standard cubic centimeters) of H_2 and 190 sccm of Ar, at a pressure of 276 mbar. Later, the copper samples are oxidized with air, at a flow of 200 sccm and -0.7 mbar during 5 minutes, and then reduced with 50 sccm of H_2 and 0.9 mbar, during 20 minutes.

Now, the conventional growth cycle begins, with a temperature ramp from 950°C to 1090°C , with 190 sccm of H_2 and 190 sccm of Ar, at 276 mbar. The temperature ramp has a slope of $25^\circ\text{C}/\text{min}$. When the maximum temperature is reached, the copper samples

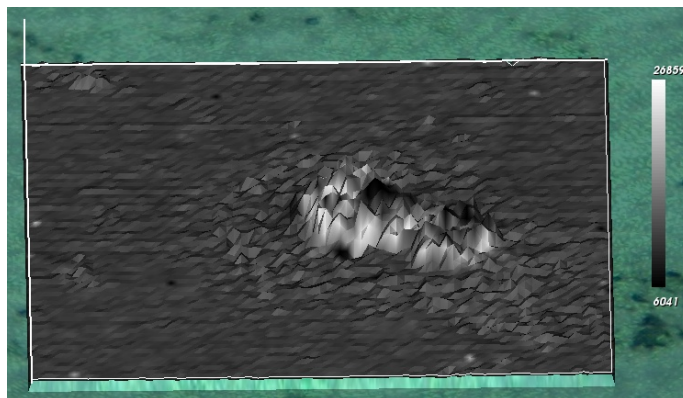


FIGURE 2.5: Topography of an island grown in TCVD-grown graphene. Courtesy of Prof. Dr. Joaquim Agostinho Moreira from IFIMUP/IN - University of Porto.

are maintained at 1090 °C, with the same flow and pressure settings, during 10 minutes. Then, the H_2 flow drops to 35 sccm and the Ar flow increases to 200 sccm, and CH_4 enters the system at 0.15 sccm, during 6 minutes. In the following minute, CH_4 is removed, only to return with a flow of 0.1 sccm, during 40 minutes. Lastly, CH_4 flow is increased to 0.15 sccm during 15 minutes. In the end, the graphene sample is removed from the hot zone in order to cool down. To finish, the growth graphene is then transferred to the used substrate.

During the growth process of TCVD-grown graphene, a significant percentage of graphene is covered with a structure that was not predicted, later named island, after its topography that can be seen in [Figure 2.5*](#). One could think that an island corresponds to an area with a higher number of layers. However the Raman analysis shows that the 2D and the G peak intensities are practically null, which means that the islands do not correspond to multi-layer graphene.

Two sets of TCVD-grown graphene were produced for THG analysis with different percentages of island coverage: a multi-islands set (with approx. 90% of island coverage) and a few-islands set (with approx. 60 % of island coverage). A SEM image for TCVD-grown 5 layers graphene multi-islands and few-islands can be seen in [Figure 2.6](#).

A set of 3 TCVD-grown graphene samples with 1, 2 and 5 layers with no islands was also produced and studied regarding THG.

*The image presented can also be residual PPMA, which is a support polymer used in graphene's transfer. Other tests need to be made to confirm these results.

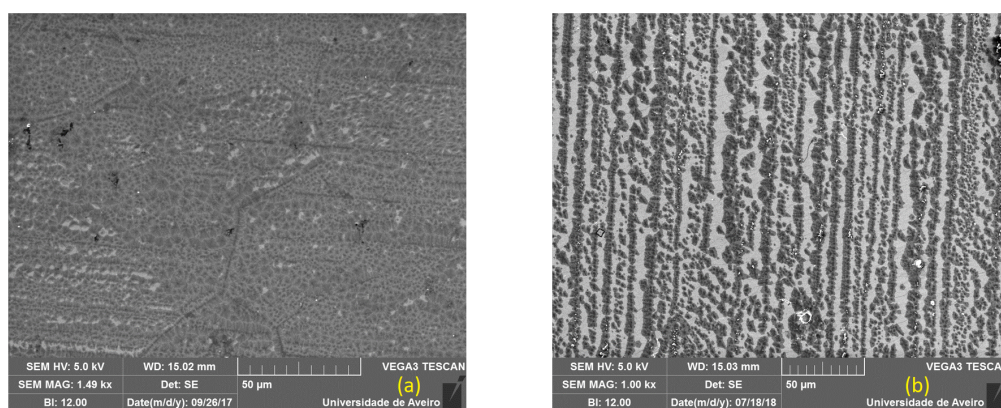


FIGURE 2.6: SEM images of 5 layers TCVD-grown graphene multi-islands (left) and few-islands (right). Courtesy of Bohdan Kulyk from I3N - University of Aveiro.

2.6.2 MPCVD graphene

For the synthesis of MPCVD-grown graphene, circular substrates of 20 mm diameter made from 0.3 mm thick electrolytic copper sheets were used, that were later mechanically polished using a commercial metal cleaner *. Ethanol was used to remove the residues from the metal cleaner, and the circular copper substrates were then loaded into a container filled with acetone and placed in an ultrasonic bath for 15 min. For the substrates where graphene was later transferred, a similar procedure was applied, but instead of acetone, isopropyl was used.

Considering the synthesis process itself, three stages occurred, namely the H_2 plasma treatment of the substrate for 4 minutes, allowing for a cleaner copper surface; the graphene growth with the introduction of CH_4 in the reactor; and the substrate cooling, with a H_2 atmosphere.

In this set of samples, different synthesis conditions were applied in different samples, in order to promote fundamental changes onto the graphene's properties (e.g., an additional H_2 plasma treatment was performed in two samples, after the graphene growth), allowing for a set of 7 samples with different synthesis conditions and, consequently, different absorption curves. Other changed parameters are the duration of the graphene growth and the gas flow of H_2 and CH_4 .

A SEM image for two MPCVD-grown graphene samples - the ones with higher and lower absorption in the DUV region - can be seen in [Figure 2.7](#).

*This process allows to remove native oxide from the copper surface, scratches or wedges, which could potentially serve as a preferential nucleation point during the graphene synthesis.

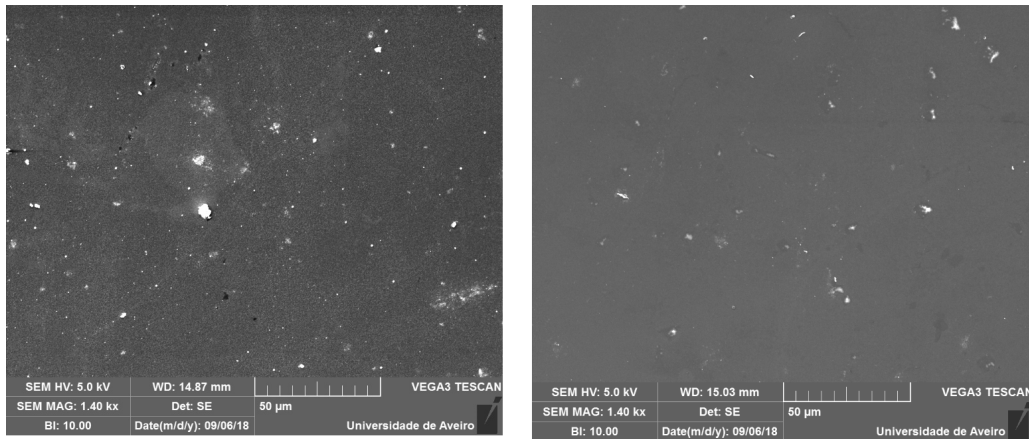


FIGURE 2.7: SEM images for the MPCVD-grown graphene samples with higher (left) and lower (right) absorption in the DUV region. Courtesy of Bohdan Kulyk from I3N - University of Aveiro.

2.7 Functionalization

One of the main purpose of this thesis consists in altering, either chemically or morphologically, graphene's structure, in order to change its nonlinear third order optical susceptibility, namely to enhance the THG efficiency, bandwidth and the sample's resilience to damage.

In the next section, we will describe the functionalization process in the sets of studied graphene samples (for more information about the samples, please see [section 3.2](#)).

All the studied functionalizations were performed at LAQV / REQUIMTE, in the University of Porto, within the scope of the project "Ultragraf - Harnessing third-harmonic generation in graphene-coated optics: new devices for ultrafast pulse measurement and frequency upconversion".

2.7.1 *In situ* diazonium reaction

[Figure 2.8](#) shows the functionalization process occurred for the 5 layers multi-islands TCVD-grown graphene sample, which consisted of adding SO_3H groups via diazonium reaction. The sample was prepared by immersing the material in 75 mL DMF in a purpose-built reactor and degassing with a N_2 stream for 15 minutes. 5 grams of sulfanilic acid were then added to the reactor and heated at 80 °C in an oil bath, and 1.93 mL of isopentyl nitrite (2:1 sulfanilic acid to isopentyl nitrite molar ratio) was added dropwise. The mixture was then left to react for 48 hours, under a N_2 atmosphere. After cooling, the material

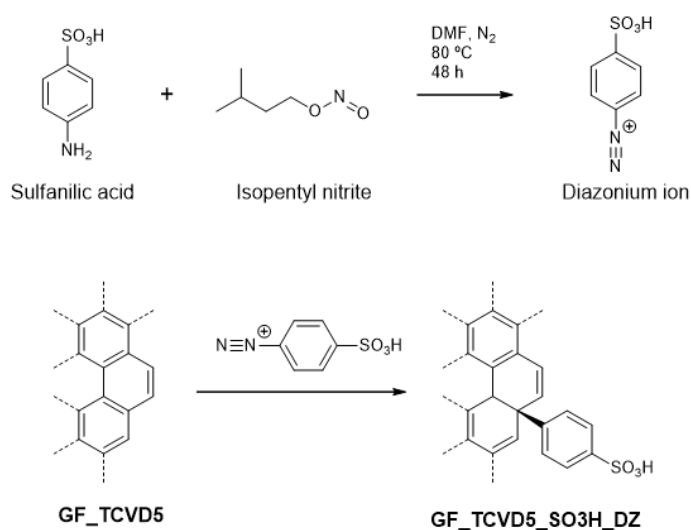


FIGURE 2.8: Preparation of functionalized 5 layers multi-islands TCVD-grown graphene, through *in situ* diazonium reaction. Courtesy of Dr. Bruno Jarrais from LAQV /REQUIMTE - University of Porto.

was washed with 50 mL neat DMF and 100 mL H_2O , and dried overnight in an oven at 80 °C, under vacuum.

2.7.2 Diels-Alder reaction

The functionalization process - consisting in adding NH_2 , SO_3H and $COOH$ groups via Diels-Alder reaction to the 3 layers multi-islands, 3 layers few-islands and 1 layer few-islands TCVD-grown graphene samples, respectively, is shown in Figure 2.9. Each sample was mixed with 50 mL of 0.1 M solutions of propargylamine, dimethyl acetylenecarboxylate, and phenyl vinylsulfonate, respectively, in toluene, under an N_2 atmosphere, and left to react at 100 °C for 48 hours. The materials were then washed by rinsing with 100 mL toluene, followed by 15 min sonication in deionized water, further rinsing with 100 mL acetone, and dried under vacuum at 80 °C overnight.

2.7.3 Photoassisted transfer hydrogenation reaction

Figure 2.10 shows the process used during the functionalization of the 5 layers few-islands TCVD-grown graphene sample through photoassisted transfer hydrogenation reaction with formic acid (the same process was used to functionalize the 5 layers TCVD-grown graphene sample with no islands, but a higher reaction time was used). The sample was placed in a flat bottom flask and then 50 mL of a 1/1 mixture of $HCOOH$ and

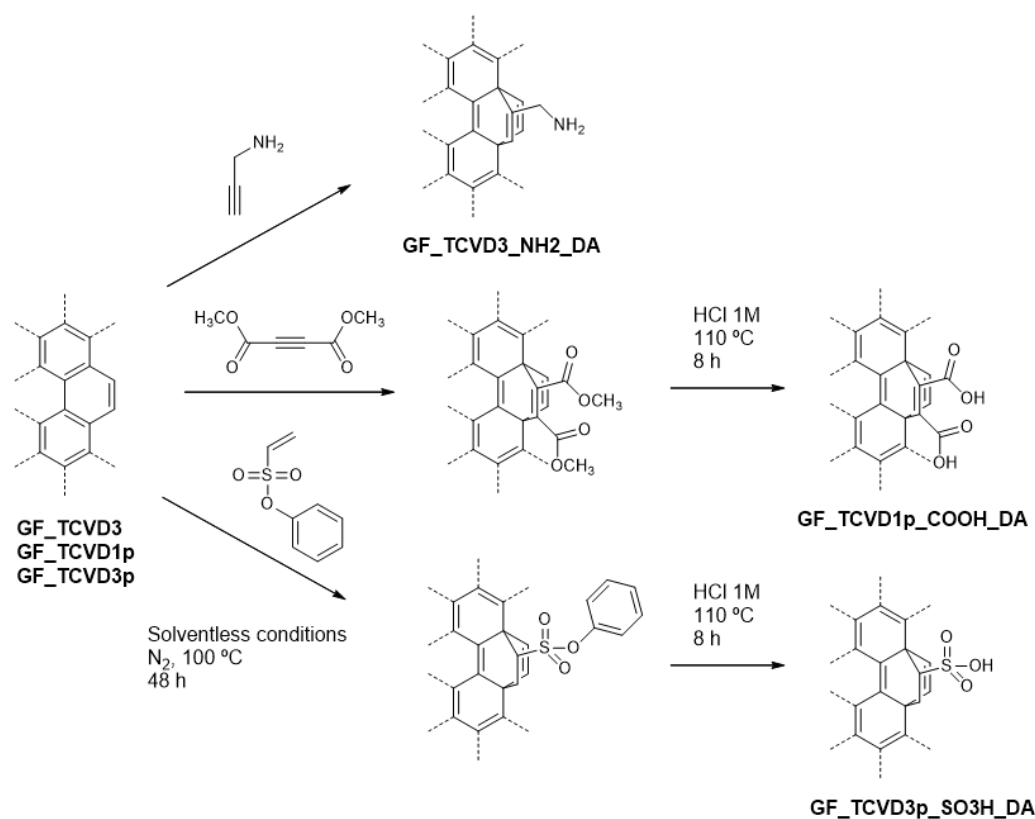


FIGURE 2.9: Preparation of functionalized 3 layers multi-islands 3 and 1 layers few-islands TCVD-grown graphene, through Diels-Alder reaction. Courtesy of Dr. Bruno Jarrais from LAQV/REQUIMTE - University of Porto.

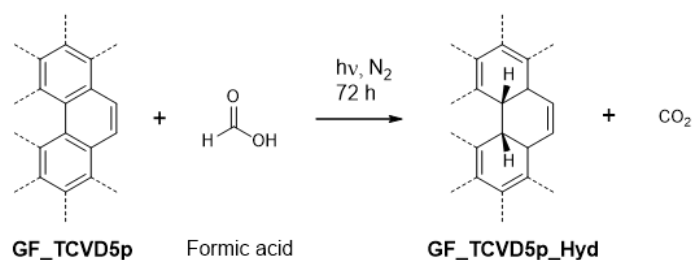


FIGURE 2.10: Preparation of functionalized 5 layers few-islands TCVD-grown graphene, through hydrogenation. Courtesy of Dr. Bruno Jarrais from LAQV/REQUIMTE - University of Porto.

H_2O (v/v) was added. After degassing with a N_2 stream for 15 minutes, the flask was exposed to illumination in QSUN Xe-1 xenon arc chamber fitted with a daylight filter during 48 hours. Afterwards, the substrate was removed from the solution and was thoroughly washed by rinsing with 5×100 mL deionized H_2O , and dried in an oven at 100 °C, under vacuum.

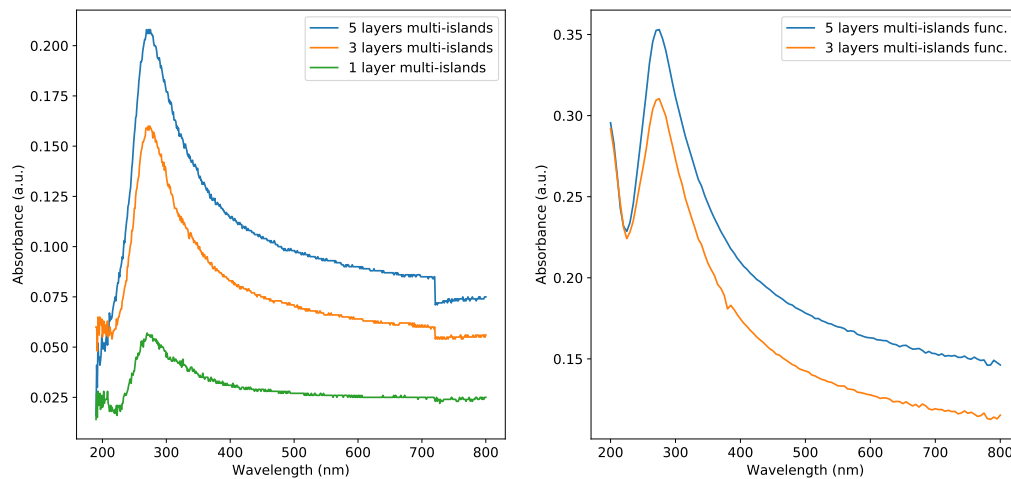


FIGURE 2.11: Absorption spectra for the non-functionalized (left) and the functionalized (right) multi-islands TCVD-grown samples. Courtesy of Dr. Bruno Jarrais from LAQV/REQUIMTE - University of Porto.

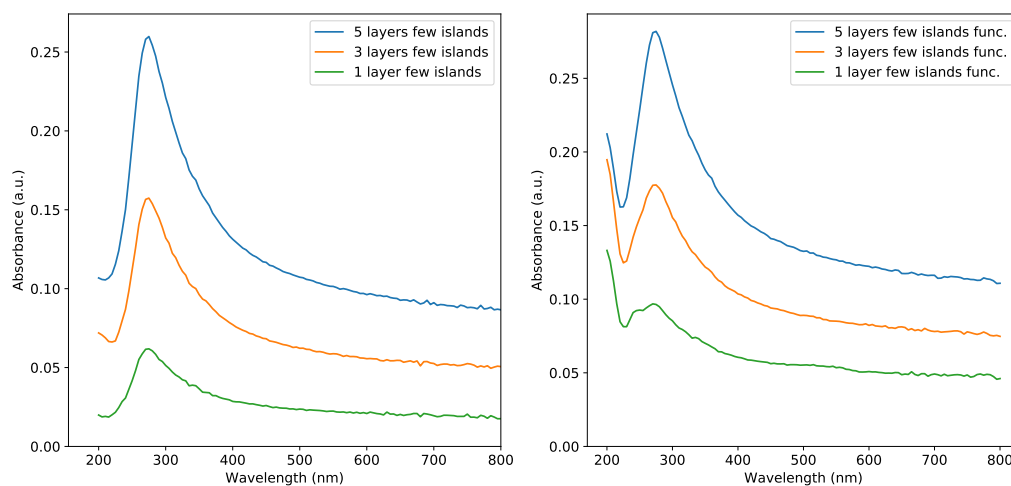


FIGURE 2.12: Absorption spectra for the non-functionalized (left) and the functionalized (right) few-islands TCVD-grown samples. Courtesy of Dr. Bruno Jarrais from LAQV/REQUIMTE - University of Porto.

2.7.4 Absorption spectra

The absorption spectra for both the non-functionalized and the functionalized TCVD-grown graphene samples are presented in [Figure 2.11](#) for the multi-islands samples, and in [Figure 2.12](#) for the few-islands samples. Unfortunately, the 1 layer multi-islands TCVD-grown graphene sample was destroyed in the functionalization process, and therefore was not studied.

For all the non-functionalized samples, it is possible to observe an absorption band near 270 nm, which corresponds precisely to the wavelength region of the THG that is generated with the used Ti:Sa oscillator.

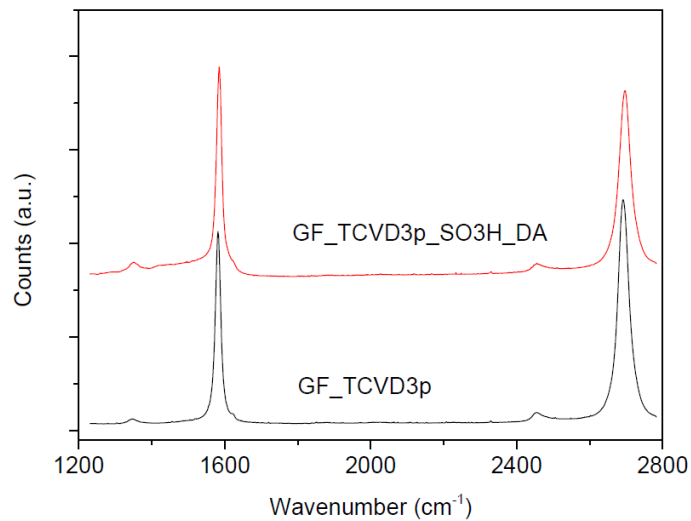


FIGURE 2.13: Raman spectra of the pristine and functionalized CVD graphene materials. Courtesy of Dr. Bruno Jarrais from LAQV/REQUIMTE - University of Porto.

Qualitatively, the functionalization process had the same effect on all samples, leading to a general increase of the absorbance at all wavelengths, and creating an absorbance valley between 200 and 250 nm. For the 1 layer few-islands sample, a shoulder appears at approx. 245 nm, which can be due to $\pi \rightarrow \pi^*$ transitions present in the introduced carbonyl functionalities.

For the 3 layers few-islands sample, a small inflexion is seen at approx. 250 nm, which can be due to blue-shifted $\pi \rightarrow \pi^*$ transitions in the formed sp^3 carbon atoms.

2.7.5 Raman analysis

As a reference, the Raman analysis for the 3 layers few-islands TCVD-grown graphene (Figure 2.13) will be presented.

It is possible to observe an increase in the I_{D}/I_{2D} ratio and an increase of the FWHM of the 2D peak, a strong indication of an increase of the overall disorder of the graphene sample. An increase of the D band (approx. 1350cm^{-1}) can be seen, which means that defects were introduced in the graphitic structure upon functionalization. A blueshift of the D band - confirming the structural changes in the functionalization procedure - can be seen as well.

An optical micrograph from the 3 layers few-islands TCVD-grown graphene sample, before and after functionalization, can be seen in Figure 2.14, confirming the homogeneity of the structural changes upon functionalization over a large area (0.016mm^2).

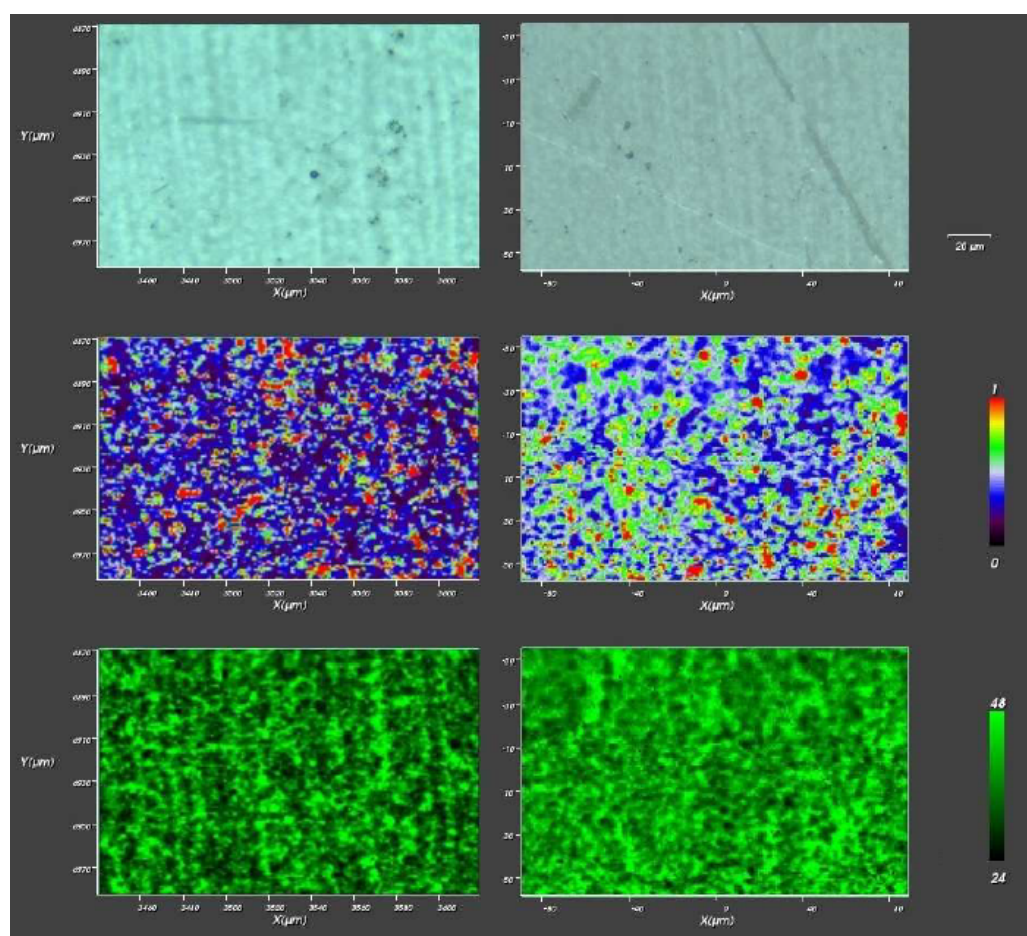


FIGURE 2.14: Optical micrographs (top), Raman IG/I2D (middle) and FWHM(2D) (down) maps of the 3 layers few-islands TCVD-grown graphene non-functionalized (left) and functionalized (right). Courtesy of Dr. Bruno Jarrais from LAQV/REQUIMTE - University of Porto.

Chapter 3

Experimental setup and Results

3.1 Experimental setup

The schematic of the experimental setup is depicted in [Figure 3.1](#). In this experiment, an ultra-broadband Ti:Sa oscillator (Femtolasers Rainbow CEP) was used, with a central frequency of 800 nm, with pulse durations of sub-10 fs and a repetition rate of 80 MHz, delivering ultrashort pulses with 2.5 nJ . The beam underwent 8 bounces in ultra-broadband DCMs (Double Chirped Mirrors) that introduce negative dispersion, propagating then through a pair of glass wedges for variable dispersion adjustment. Then, it passed through a variable filter consisting of fused silica with different transmission indexes, to reduce the power of the pulse. The beam was then focused on the graphene sample using a concave mirror ($f = 5\text{ cm}$), and then collimated using another concave mirror ($f = 5\text{ cm}$). A mirror setup was used instead of a lens setup in order to reduce chromatic aberration. The fundamental and the third harmonic beams then co-propagated through a wavelength separator, consisting of a prism sequence, where the fundamental beam was rejected and the third harmonic signal propagated. The spectra of the third harmonic was then recorded using a fiber coupled spectrometer (Ocean Optics HR4000). One of the glass wedges is attached to a Zaber motor, which is controlled via a LabView program, allowing us to automatically measure the THG signal as a function of the dispersion applied to the pulse.

To align the wavelength separator, a lens setup was devised in order to generate visible THG in a air plasma produced by a sub-30 fs, 1 KHz rep. rate, 800 mJ amplifier (see [Figure 3.2](#)).

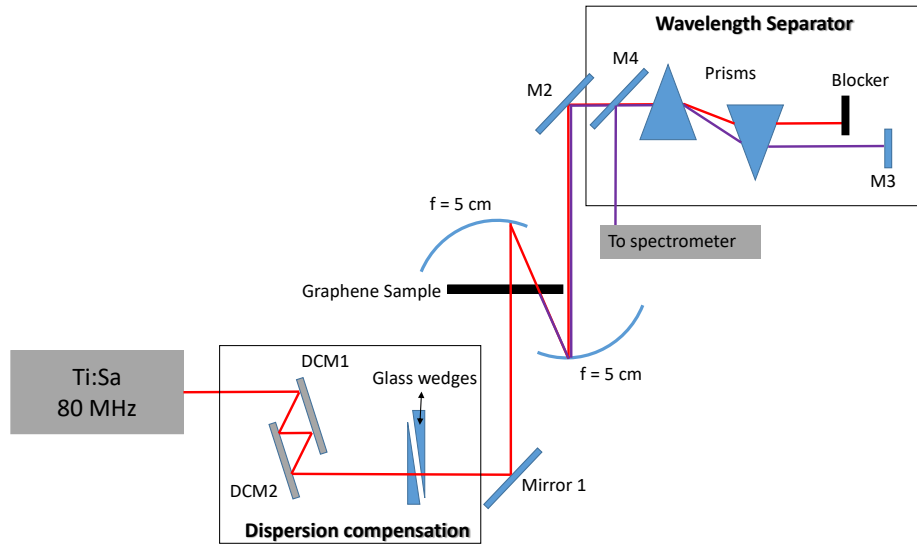


FIGURE 3.1: Experimental setup for THG d-scan. DCM1 and DCM2: Double Chirped Mirrors; M1, M2, M3 and M4: mirrors.

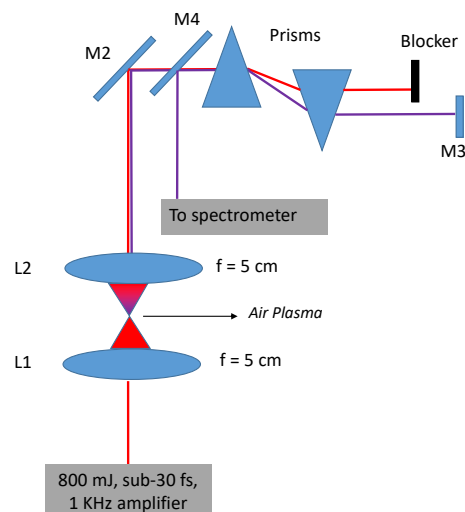


FIGURE 3.2: Experimental setup for the wavelength separator alignment. L1 and L2: Focusing and Collimating Lens; M2, M3 and M4: mirrors.

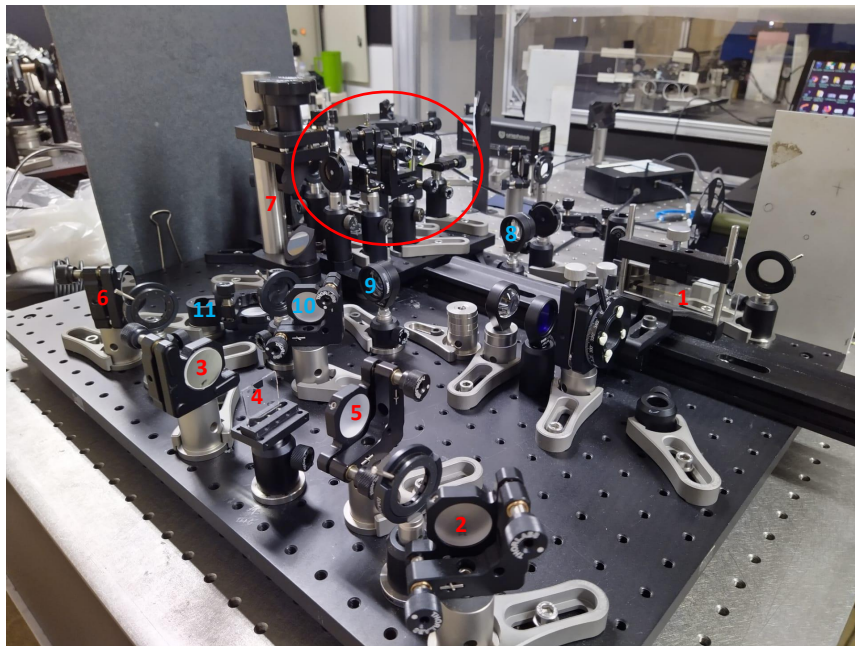


FIGURE 3.3: Experimental setup for THG (red-labeled components) and wavelength separator aligner (blue-labeled components), described in [Figure 3.1](#). 1 - Variable power filter. 2,6,10 - Mirrors. 3,5 - Focusing and collimating concave mirrors, respectively. 4 - Graphene sample. 7 - Periscope. 8,9 - Focusing and collimating lenses for THG in air plasma, respectively. 11 - Flip mirror, to switch between aligning the wavelength separator and measuring THG in graphene. Red circle - Wavelength separator. All the setup is mobile.

The experimental setup can be seen in [Figure 3.3](#), as well as the wavelength separator ([Figure 3.4](#)) and the dispersion compensation setup ([Figure 3.5](#)).

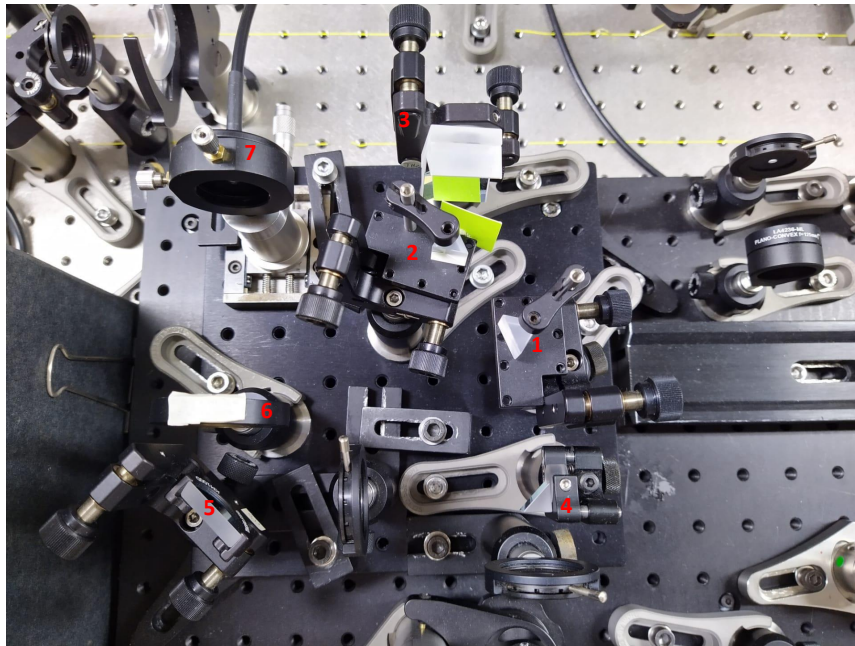


FIGURE 3.4: Experimental setup for the wavelength separator. 1,2 - Set of two prisms to separate the THG from the fundamental beam. The green paper blocks the fundamental beam. 3 - Back-reflecting mirror/periscope. 4,5 - Mirror. 6 - Focusing lens. 7 - Fiber mount.

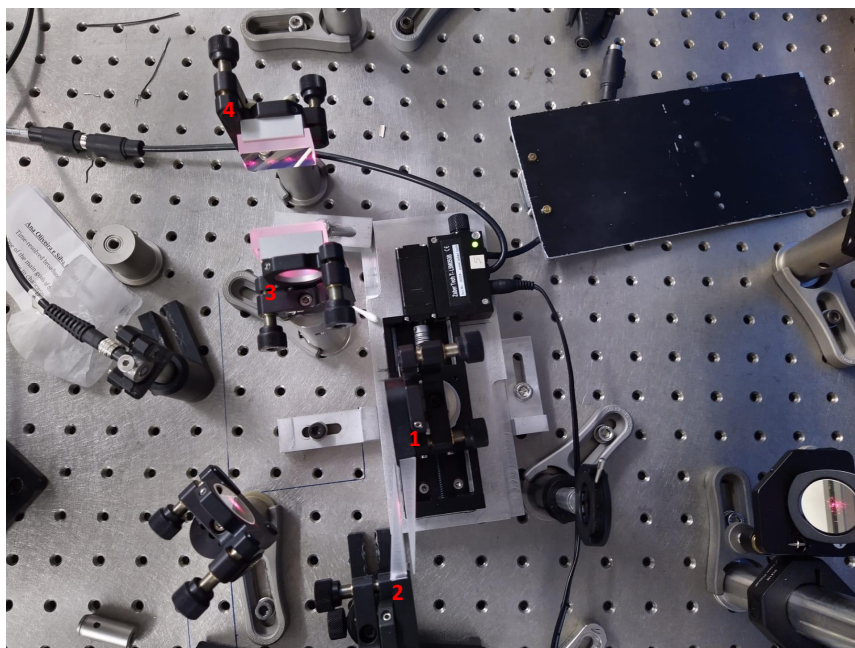


FIGURE 3.5: Dispersion compensation setup. 1,2 - Glass wedges (wedge no. 1 is connected to the Zaber motor). 3,4 - Double Chirped Mirrors.

3.2 Samples

In this work, several graphene samples were studied in terms of THG and its dependence on the number of layers, functionalization and synthesis conditions. Specifically, the samples were divided into different sets, according to their similarities. The sets are as follows (all the substrates are 1mm thick fused silica):

- **Set 1:** MPCVD-grown samples with different absorption curves due to different synthesis conditions;
- **Set 2:** 3 TCVD-grown graphene samples with 1, 2 and 5 layers;
- **Set 3:** 3 TCVD-grown graphene samples with 1, 3 and 5 layers multi-islands (approx. 90% coverage);
- **Set 4:** 3 TCVD-grown graphene samples with 1, 3 and 5 layers with few islands (approx. 60% coverage);

The TCVD-grown 5 layers graphene sample with no islands was functionalized and its THG signal was compared to the non-functionalized one.

Both set 3 and set 4 were also functionalized. However, due to some problems in the lab (namely, a flood that led to the entire rebuilding of our device) it was impossible to compare the THG signal of the non-functionalized and the functionalized samples of this two sets. However, the functionalized results will be shown for completeness.

3.3 MPCVD-grown graphene

3.3.1 Third-Harmonic Generation

A group of six MPCVD-grown graphene samples with different synthesis condition was studied regarding Third-Harmonic Generation. Due to the different synthesis conditions, the transmission curve of each sample is different, as can be seen in [Figure 3.6](#).

The transmission curve is relatively flat in the 600-1200 nm region, which is typical of graphene. There is a very broadband absorption peak in the DUV region, whose peak intensity and wavelength also changes depending on the sample.

In order to study the THG efficiency and the sample's uniformity, a set of 16 THG measurements on different areas of each sample was made, leading to the results shown in [Figure 3.7](#).

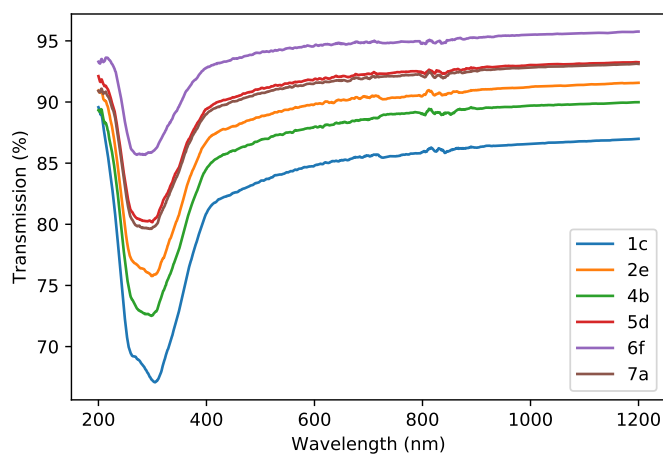


FIGURE 3.6: Transmission curves of the MPCVD-grown graphene samples . Courtesy of Bohdan Kulyk from I3N - University of Aveiro.

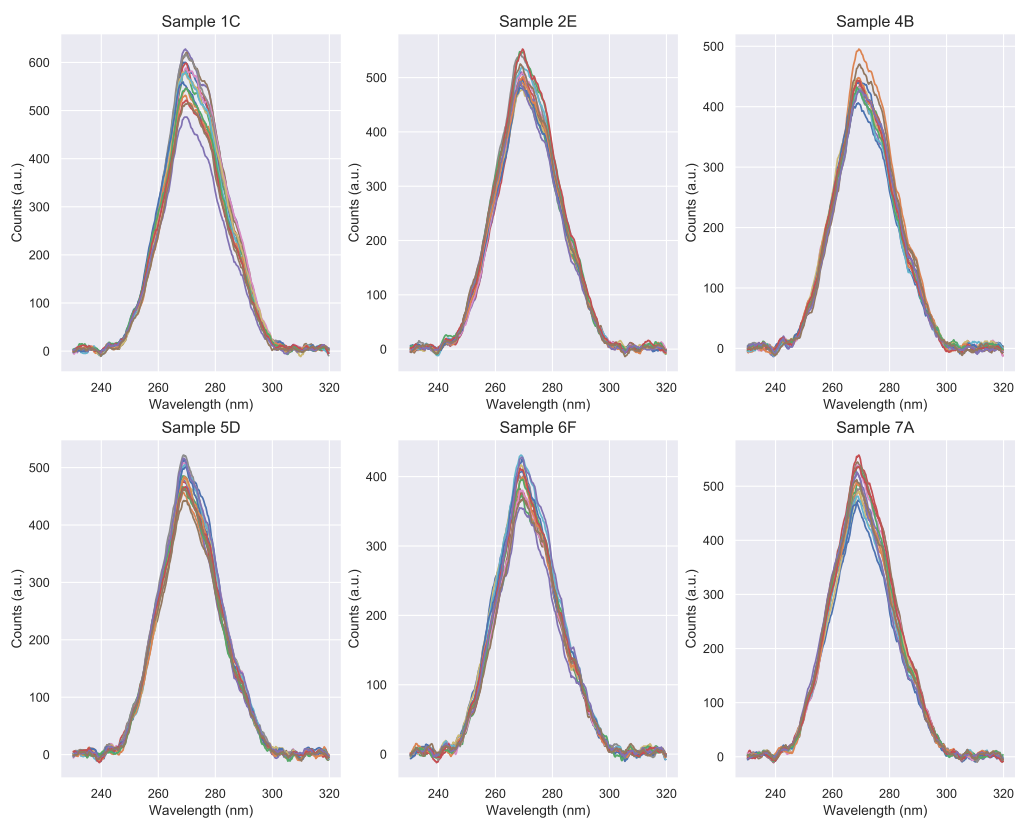


FIGURE 3.7: MPCVD-grown graphene sample's uniformity regarding THG

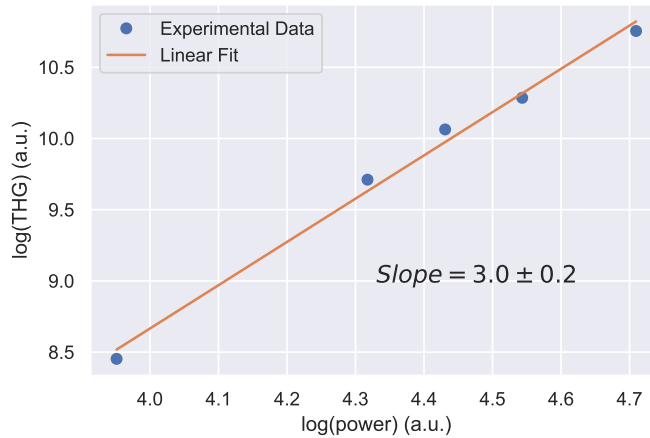


FIGURE 3.8: THG signal as a function of the laser’s input average power.

It is clear that we obtained intense and broadband THG, and that all samples seem to have a similar THG spectra in terms of bandwidth and peak wavelength. Regarding each sample’s uniformity, all samples seem to be rather uniform, as all the measurements for each sample have a similar intensity. The intensity differences can be explained by human error, since the graphene sample is placed on the beam focus by hand and a small deviation leads to a very different laser intensity, due to the small Rayleigh length. However, percentually, the differences in intensity are still small.

By studying the influence of the laser’s average power in the THG intensity for the 1C sample, we get the results from [Figure 3.8](#). By performing a linear fit on the data, we obtain a slope of 3.0 ± 0.2 , which confirms that the measured signal is indeed third-harmonic (since it depends on the cubic power of the incident intensity).

We can now study the influence of the peak absorption on the THG efficiency, by integrating each measurement in wavelength and performing a statistical analysis of the obtained results (see [Figure 3.9](#)).

The THG signal seems to increase with the peak absorption, which in non linear optics is a common result named resonantly enhanced THG, that was already studied experimentally in different materials by Mogner et al. [29] and in graphene by Soavi et al. [56]. However, the possibility of the THG signal enhancement being from an increase of the number of graphene layers cannot be ruled out, since we were not able to measured the number of graphene layers of each sample. In fact, by having a second look at [Figure 3.6](#), the absorption peak changes between each sample may be a good indicative that the samples do not have the same number of layers, since the presence of multiple layers opens a

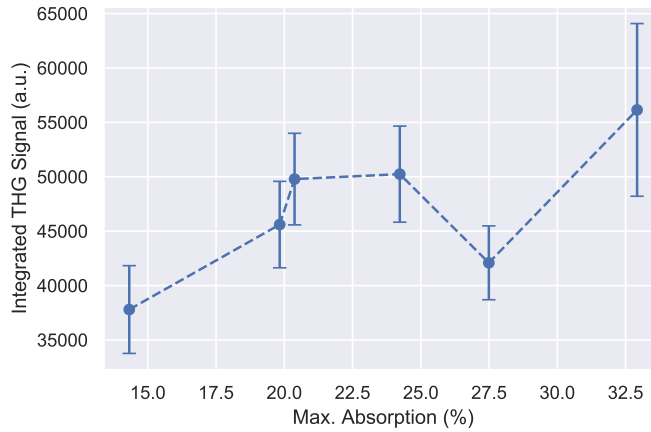
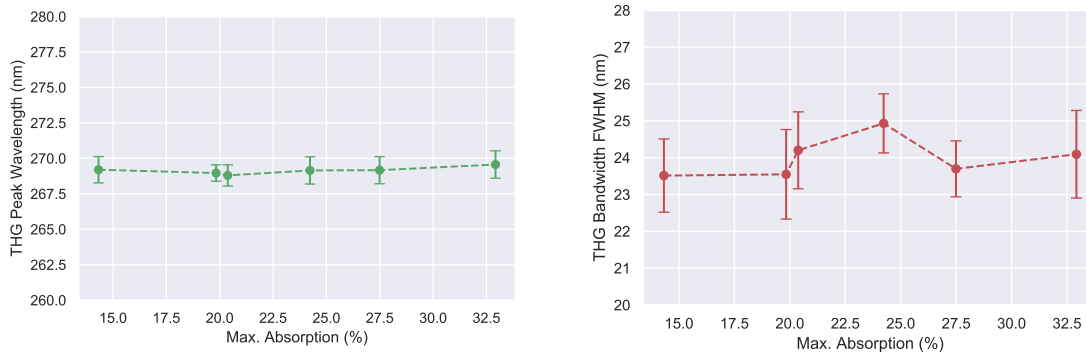


FIGURE 3.9: THG signal vs. peak absorption for the MPCVD-grown graphene samples



(A) THG peak wavelength vs peak absorption for the MPCVD-grown graphene samples.

(B) THG bandwidth (FWHM) vs peak absorption for the MPCVD-grown graphene samples.

FIGURE 3.10: THG shape study vs peak absorption for the MPCVD-grown graphene samples.

bandgap on graphene's band structure, changing its absorption curve by an amount that may depend on the number of graphene layers [57].

Figure 3.10 shows that neither the THG's peak wavelength nor its bandwidth depend on the peak absorption of the samples, which shows that the absorption curve only influences the maximum THG signal obtained with these graphene samples, and not its shape.

To confirm these results, we can measure the THG signal as a function of the dispersion applied to the pulses (i.e., a d-scan - see Figure 3.11). As can be seen, all the traces seem very similar to each other. A residual THG signal for negative dispersion can be seen around 285 nm, possibly due to some kind of resonance. All the traces have a strong tilt, due to residual third order dispersion. A weak, but visible linear signal is seen in all samples (with higher or lower SNR depending on the sample), from 250 to 270 nm regarding

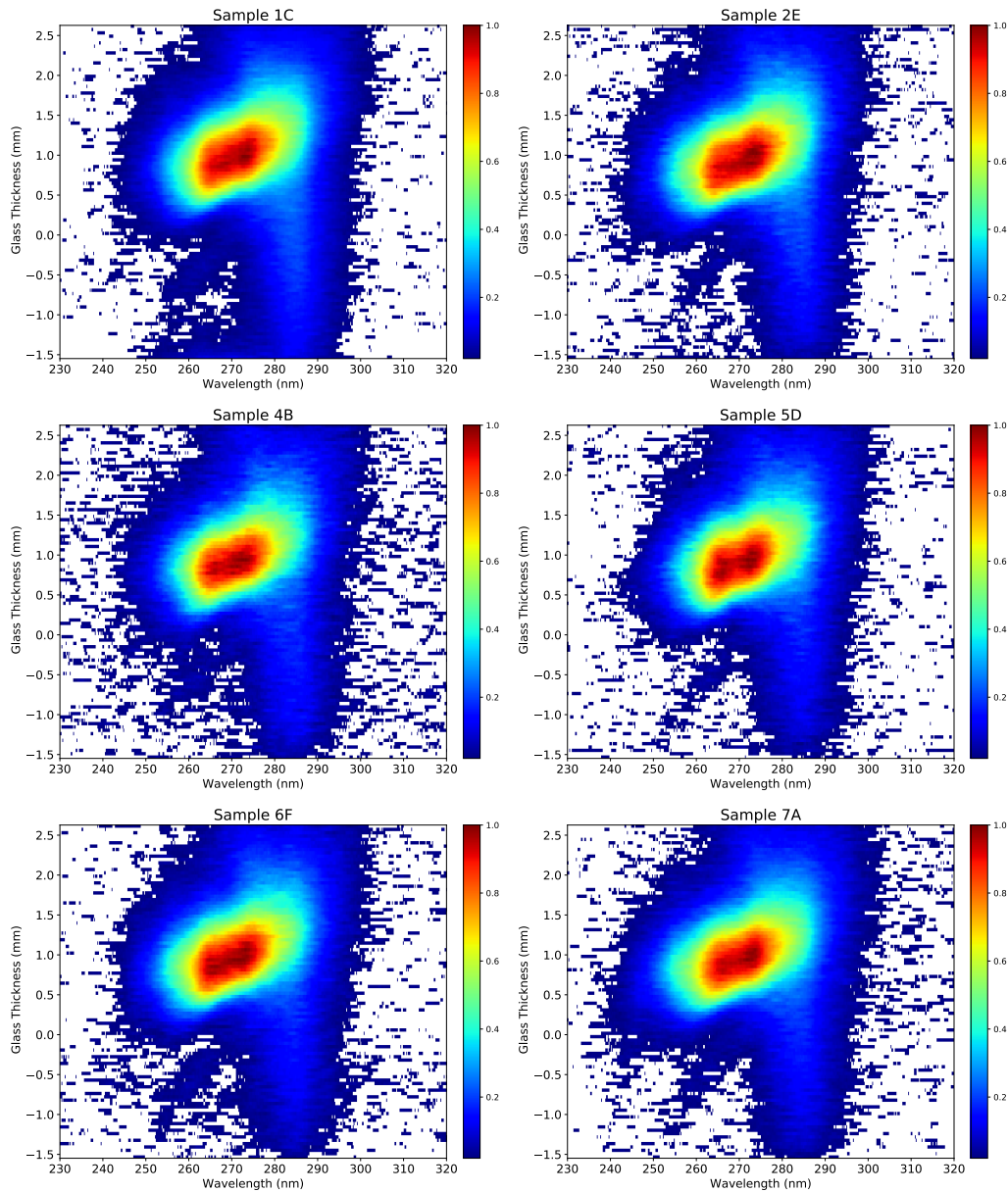


FIGURE 3.11: THG d-scan for each MPCVD-grown graphene sample.

wavelengths and from -1.0 to 0.0 mm regarding glass thickness.

3.3.2 Retrievals

A retrieval algorithm was used to retrieve the spectral phase of each measured d-scan. A set of 10 retrievals (and therefore, of 10 different spectral phases) was made for each sample, in order to achieve statistical significance. A temporal profile was determined for the average spectral phase and for the average spectral phase affected by the standard deviation of the 10 measurements, in order to determine the FWHM's uncertainty.

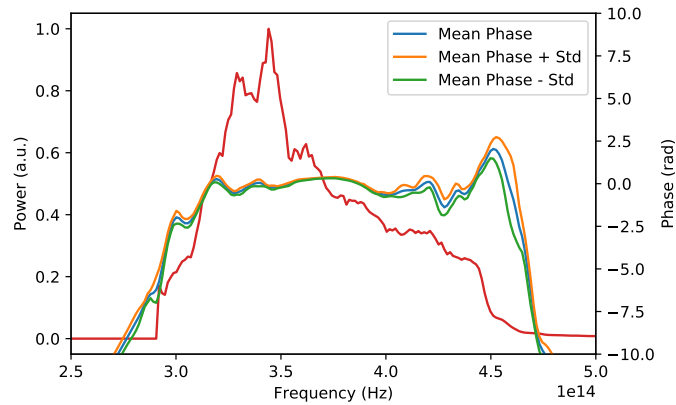


FIGURE 3.12: Phase retrieval for the MPCVD-grown 1C graphene sample.

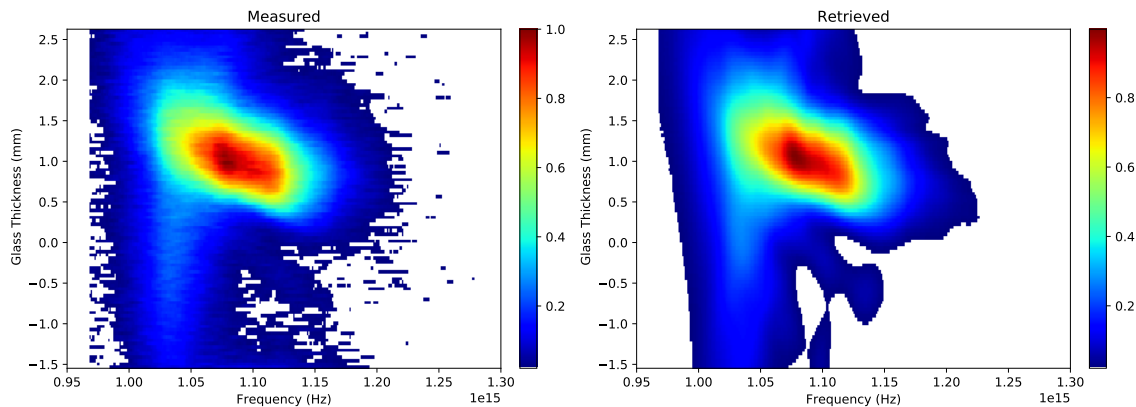


FIGURE 3.13: Measured and retrieved THG d-scan for the MPCVD-grown 1C graphene sample, by using one of the 10 retrieved phases.

As a representative example, [Figure 3.12](#) shows the measured spectral intensity and the average retrieved spectral phase for the MPCVD-grown 1C graphene sample.

As an example, [Figure 3.13](#) shows the measured and retrieved THG d-scan for the MPCVD-grown 1C graphene sample, by using one of the 10 retrieved phases.

By calculating the inverse Fourier transform of the fundamental spectrum affected by the spectral phase, one can determine the temporal profile of the ultrashort pulse, which can be seen for each MPCVD-grown graphene sample in [Figure 3.14](#).

In all retrievals, the main pulse is followed by a post-pulse, which is indicative of residual TOD that was already noticed due to the d-scans' tilt. The similarity between all the determined temporal profiles is quite noticeable. By calculating the FWHM of all the temporal profiles, we get the results from [Table 3.1](#).

It is clear that the d-scans produced by each sample led to ultrashort pulse retrievals with similar FWHM - varying from 7.4 to 7.9 fs - and relatively low uncertainty. These

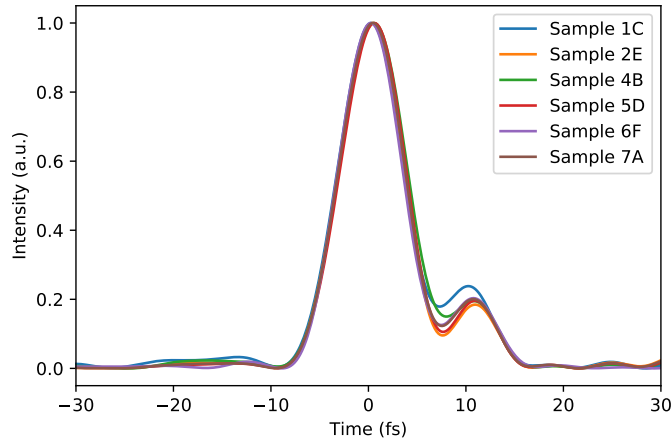


FIGURE 3.14: Retrieved temporal profile of the ultrashort pulses used for THG d-scan for each MPCVD-grown graphene sample.

Sample	1C	2E	4B	5D	6F	7A
FWHM (fs)	7.75	7.56	7.9	7.56	7.4	7.56
σ (fs)	0.09	0.09	0.2	0.09	0.2	0.09

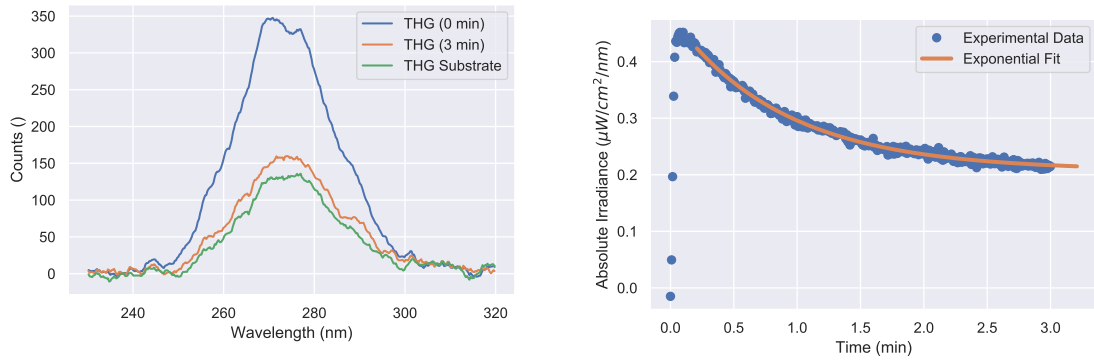
TABLE 3.1: Retrieved FWHM for the THG d-scan with the MPCVD-grown graphene samples.

results are in good agreement with the ones obtained in [18] using the same ultrashort pulses.

3.3.3 Durability

Due to the high average power of the laser, when we shine the beam on the graphene, the THG signal decays over time, which means that the graphene is being damaged over time. A good explanation of this effects takes into account the transfer of heat to the lattice which causes its degradation over the course of time. Several studies have already been made regarding the graphene's damage threshold, stating that above a certain laser intensity, a single laser pulse cleanly ablates graphene, leaving microscopically defined edges [58, 59]. Localized heating is created by using low pulse fluences, leading to melting, vaporization and/or sublimation, whereas with higher pulse fluences a large, non-equilibrium electron temperature is created and, by picosecond electron-phonon coupling times, a rapid energy transfer capable of ejecting material is provided [60].

By using a 7 fs laser pulse with 80 MHz of Repetition Rate, and average power of 100 mW, we have a pulse energy of 1.25 nJ, which leads to a peak power of 1.79×10^5 W. Since we are using a 5 cm focal length mirror, and estimating the beam diameter of 1 cm, we



(A) THG in the MPCVD-grown 1C graphene sample at the beginning of the experiment, after 3 minutes, and THG in the substrate. (B) Integrated THG signal over time from the MPCVD 1C sample.

FIGURE 3.15: THG decay rate study for the MPCVD-grown 1C graphene sample.

have a beam radius at the focus of $2.55 \mu\text{m}$, leading to a peak intensity of $876,2 \text{ GW}\cdot\text{cm}^{-2}$ and a peak fluence of $6.13 \text{ mJ}\cdot\text{cm}^{-2}$, which is a relatively low peak fluence and is mainly due to the long focal distance used.

By measuring the integrated THG signal as a function of time (e.g., with the MPCVD 1C graphene sample), it is possible to visualize, indirectly, the graphene's degradation in the course of time, as seen in [Figure 3.15](#).

The THG signal appears to decay exponentially, which is confirmed by the good agreement obtained with the presented exponential fit *, with $R^2 = 0.993$. In this case, we have obtained a decay rate of 0.019s^{-1} .

Since the decay is exponential and not instantaneous, we can assume that we are on the low fluence regime, and that the graphene's degradation is caused by a thermal effect.

By performing a statistical analysis of the decay rate for all the MPCVD samples, we get the results shown in [Figure 3.16](#).

It appears that the higher the absorption peak in the DUV, the higher the damage resistance, which is a crucial result. However, the possibility of the resilience to damage being increased due to the higher number of layers, which increases the damage resistance [61], once again cannot be ruled out.

This result shows that, by changing the synthesis conditions of the MPCVD-grown graphene, one can change both the THG efficiency and the damage resistance of the samples, which proves to be an important result.

*All the exponential fits were obtained using the Python function `curve_fit`, from the `scipy` module, which uses a nonlinear least squares method. The general exponential function used for the fit was $f(t) = a + be^{-ct}$.

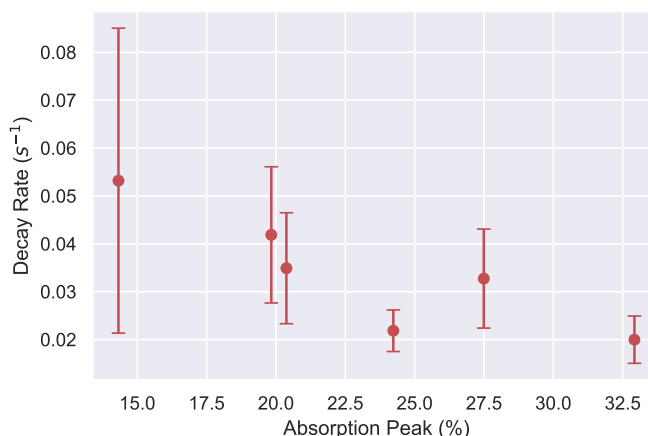


FIGURE 3.16: THG decay rate for the MPCVD-grown graphene samples.

3.4 TCVD-grown graphene

3.4.1 Third-Harmonic Generation

Third-Harmonic Generation was also studied in a set of three TCVD-grown graphene samples with 1, 2 and 5 layers. The THG spectra for all samples, as well as a THG spectrum for the substrate for comparison, is shown in [Figure 3.17](#).

It is clear that the number of layers influences the THG efficiency, since the THG signal increases with the number of layers. The shape of the THG does not change from the 5 layers to the 2 layers TCVD-grown graphene. However, it seems that we were not able to measure THG in a single layer graphene, since its spectrum is very similar to the one obtained in the substrate. It is important to note that the peak wavelength and shape for

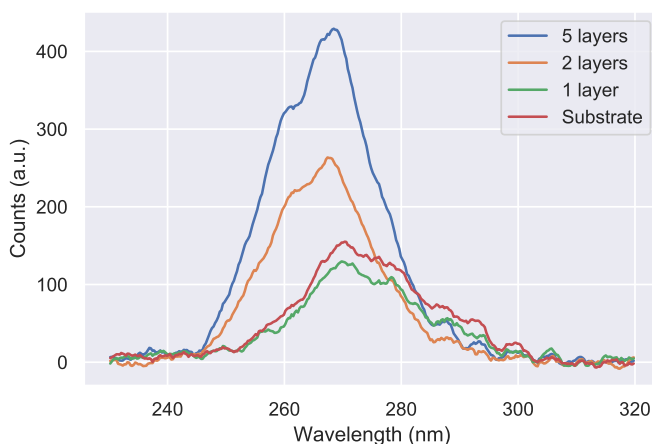


FIGURE 3.17: THG spectra for the TCVD-grown graphene samples with no islands and the substrate.

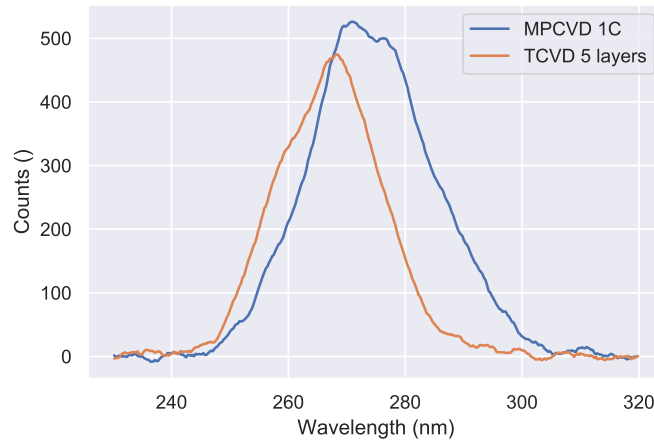


FIGURE 3.18: THG spectra for the 5 layers TVCD-grown graphene with no islands and the MPCVD-grown 1C graphene.

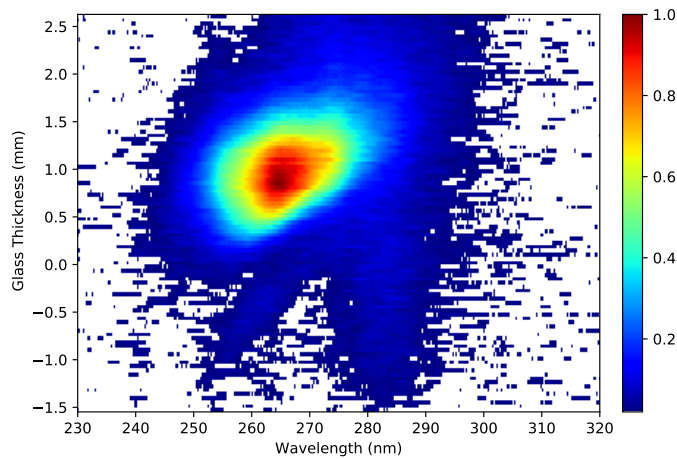


FIGURE 3.19: THG d-scan for 5 layers TCVD-grown graphene with no islands.

the THG in the substrate is clearly different from the THG in 5 and 2 layers graphene, which is a good marker to tell if the third harmonic was generated in graphene or in the substrate.

We can also compare the THG signal obtained with 5 layers TCVD-grown graphene with the one obtained with the MPCVD-grown 1C graphene. By analysing the results of [Figure 3.18](#), we can see that the TCVD-grown graphene presents a smaller bandwidth compared to the MPCVD-grown graphene, and there is a clear blue-shift of the THG peak wavelength. The shape of the spectrum is also different.

If we now measure, once again, the THG intensity as a function of the dispersion applied to the pulse, we get a d-scan trace as the one presented in [Figure 3.19](#).

The first thing we notice is the big difference comparing to the THG d-scans obtained



FIGURE 3.20: Decay rate for the MPCVD-grown 1C and the 5 layers TCVD-grown graphene sample

with the MPCVD-grown graphene samples, since the latter has a higher SNR in the 280-300 nm region. However, the presented d-scan also has a residual THG signal for negative dispersion centered at 285 nm, and the other residual THG signal with a tilt is also visible. The overall d-scan also presents a tilt, resulting from residual third order dispersion.

We were not able to measure a d-scan for the 2 layers TCVD-grown graphene, since it gets destroyed before the full measurement is made. We are therefore led to believe that the thermal effects are stronger in 2 layers TCVD-grown graphene, which could be consistent with the fact that a higher number of graphene layers leads to a higher resilience to damage [61].

3.4.2 Durability

As well as the MPCVD-grown graphene samples, the THG signal decays over time when using the TCVD-grown graphene samples. Once again, we were able to perform a statistical study regarding the THG decay rate and, comparing it with the decay rate from the MPCVD-grown graphene - sample 1C, since it's the one that has a similar THG intensity to the 5 layers TCVD-grown graphene - we obtain the results presented in [Figure 3.20](#).

These results show that the MPCVD-grown graphene has a higher damage resistance than the TCVD-grown graphene, for a similar initial THG signal.

3.5 Graphene functionalization

During the course of this thesis, we were able to study the effect of graphene functionalization on the THG process. In this particular case, the 5 layers TCVD-grown graphene

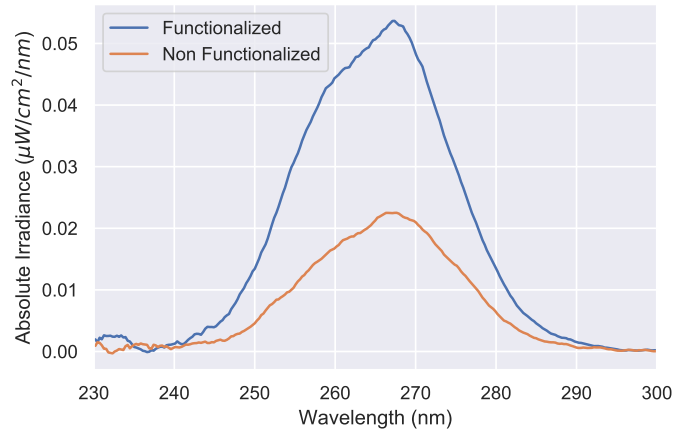


FIGURE 3.21: THG spectra for the non-functionalized and the functionalized 5 layers TCVD-grown graphene sample with no islands.

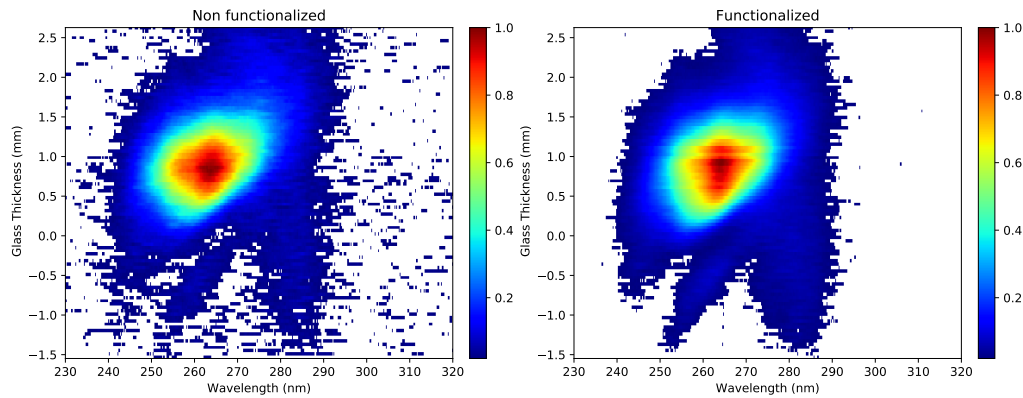


FIGURE 3.22: THG d-scan for the non-functionalized (left) and the functionalized (right) TCVD-grown 5 layers graphene sample with no islands.

was functionalized through photoassisted transfer hydrogenation reaction with formic acid.

The THG spectra for both the functionalized and the non-functionalized 5 layers TCVD-grown graphene is presented in [Figure 3.21](#).

It is clear that the functionalization process led to an increase in the THG efficiency, since the THG signal suffered an increase of almost 2.5x compared to the signal obtained with the non-functionalized graphene sample. For lower wavelengths, the THG signal seems to have increased its SNR, corresponding to an increase in the FWHM.

By performing a THG d-scan with the functionalized TCVD-grown 5 layers graphene sample, and comparing it with the one obtained with the non-functionalized sample, we get the results from [Figure 3.22](#), showing that the SNR increased due to the functionalization process.

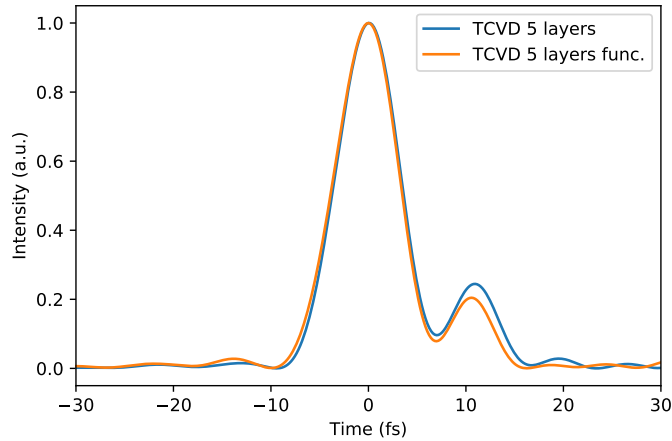


FIGURE 3.23: Temporal profile of the ultrashort pulses used to perform THG in TCVD-grown graphene with 5 layers (functionalized and non-functionalized).

3.5.1 Retrievals

By performing a phase retrieval of the d-scans obtained with the non-functionalized and the functionalized graphene samples - using the same technique used with the MPCVD-grown graphene samples - we get the temporal profiles represented in [Figure 3.23](#), which shows that the functionalization does not prevent the d-scan algorithm from completely retrieving the spectral phase and, therefore, the temporal profile of the used ultrashort pulses.

It is clear that the determined temporal profiles are qualitatively equal to the ones obtained with the MPCVD-grown graphene samples, regarding the main pulse's shape and the post-pulse resulting from residual TOD.

The calculated FWHM for each temporal profile is equal to $(7.4 \pm 0.2) fs$ for both samples, which is a similar value to the ones obtained with the MPCVD-grown graphene samples. This is an important result and shows that the d-scan retrieval algorithm (and the d-scan process itself) is strong enough to retrieve the temporal profile of ultrashort pulses even with different THG spectral curves created by different synthesis conditions [\[29\]](#).

3.5.2 Durability

We can now study the influence of the functionalization process in the graphene's resilience to damage. The THG signal overtime for the 5 layers TCVD-grown functionalized graphene can be seen in [Figure 3.24](#).

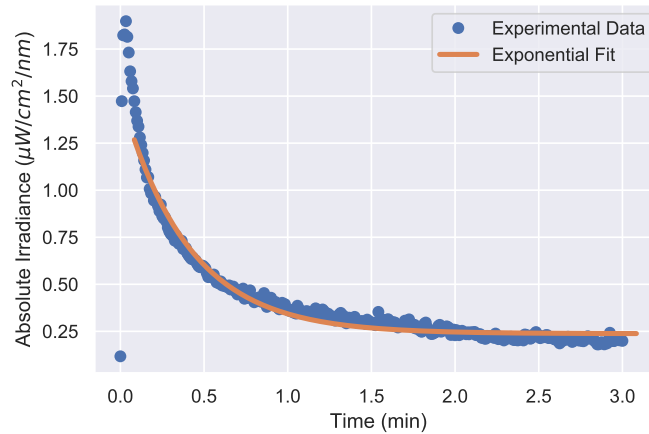


FIGURE 3.24: THG signal overtime for the 5 layers TCVD-grown functionalized graphene sample with no islands.

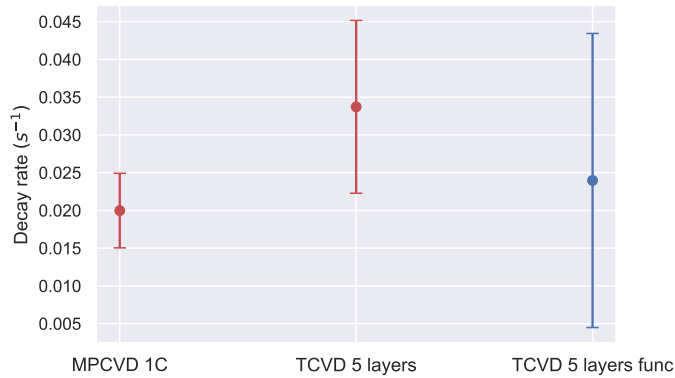


FIGURE 3.25: THG decay rate for the MPCVD-grown 1C, 5 layers TCVD-grown and 5 layers TCVD-grown functionalized graphene sample.

In this case, the higher THG signal leads to a higher decay rate of 0.041s^{-1} . One could think that the functionalization process failed in terms of durability. However, since graphene has a high absorption in the DUV region, the higher the THG signal, the higher the absorption, which can lead to thermal processes that degrade graphene's structure. Therefore, it is only viable to compare the samples' resilience to damage in similar conditions, i.e., with a similar initial THG signal, which can be achieved by putting the sample slightly out of the focus. By doing so, and comparing the decay rate to the other samples, we get the results from [Figure 3.25](#).

In this case, it is clear that the functionalization was successful in terms of resilience to damage, since we were able to lower the THG decay rate for the 5 layers TCVD-grown functionalized graphene sample. The decay rate measured for the functionalized

graphene sample has a high variance, that may be explained by the functionalization process: as seen in [Figure 2.14](#), one can clearly see that the sample is not completely uniform, and therefore, some graphene areas can be more functionalized than others. In this case, some areas may have a higher density of sp^3 carbons than others, leading to a higher resilience to damage.

3.6 TCVD-grown graphene with islands

3.6.1 Clarification

Graphene functionalization could in principle improve the THG signal, both in terms of intensity and bandwidth, as well as graphene's resistance (as seen before). However, due to technical problems in FEMTOLAB (a flood), the entire THG measurement setup had to be rebuilt, which led to the impossibility of comparing the nonlinear signal from non-functionalized and the functionalized graphene samples with islands. We will still present these results for completeness.

Due to some problems in the functionalization process, the 1 layer multi-islands TCVD-grown graphene sample was destroyed, and therefore could not be functionalized.

3.6.2 Comparison

A THG spectrum for all functionalized samples can be seen in [Figure 3.26](#). In general terms, the THG signal is stronger for multi-islands graphene rather than few-islands graphene, which can mean that the presence of islands enhances the THG. We can clearly see that the THG signal increases with the number of layers, as expected [36]. We can also see that the bandwidth seems to increase with the THG intensity. All the THG spectra have the same shape, except the one provided by the 1 layer few-islands TCVD-grown graphene, whose signal is strongly comparable with the one from the substrate (1mm of fused silica).

3.6.3 d-scans

A d-scan measurement was made for each sample. The measured and retrieved scans for each sample can be seen from [Figure 3.27](#) to [Figure 3.31](#). In these cases, a full retrieval was performed, where not only the pulse's spectral phase was retrieved, but also its spectral intensity.

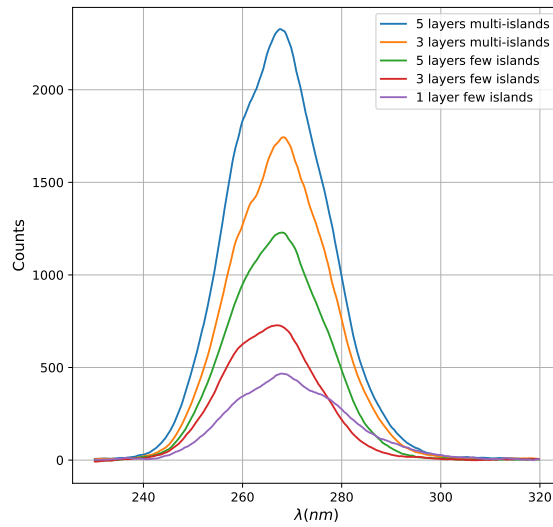


FIGURE 3.26: Third Harmonic Generation in functionalized TCVD-grown graphene - multi-islands and few-islands.

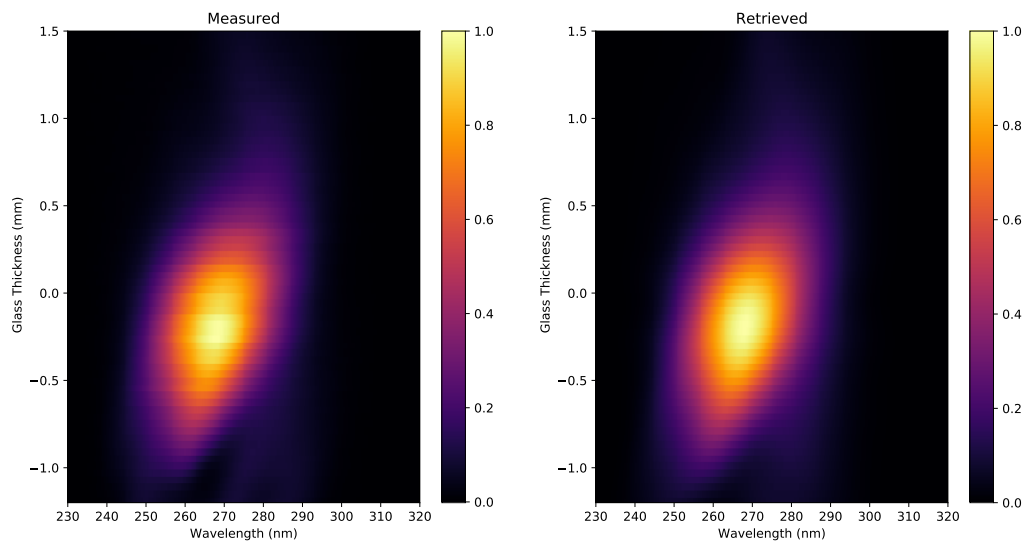


FIGURE 3.27: Measured (left) and retrieved (right) d-scans for 5 layers multi-islands TCVD-grown functionalized graphene.

At first sight, every scan seems to be well retrieved. The optimum dispersion point seems to change slightly depending on the sample.

The retrieved spectral intensity and temporal profile of the scan from each sample can be seen in [Figure 3.32](#).

In all the pulse's temporal profile retrieval, a post-pulse can be seen, a strong indicative of a residual TOD which can also be seen on the strong tilt on the trace's shape. The FWHM of all retrievals is similar and varies from 7,2 to 7,8 fs (see [Table 3.2](#)), leading to an average value of $(7.6 \pm 0.2) fs$.

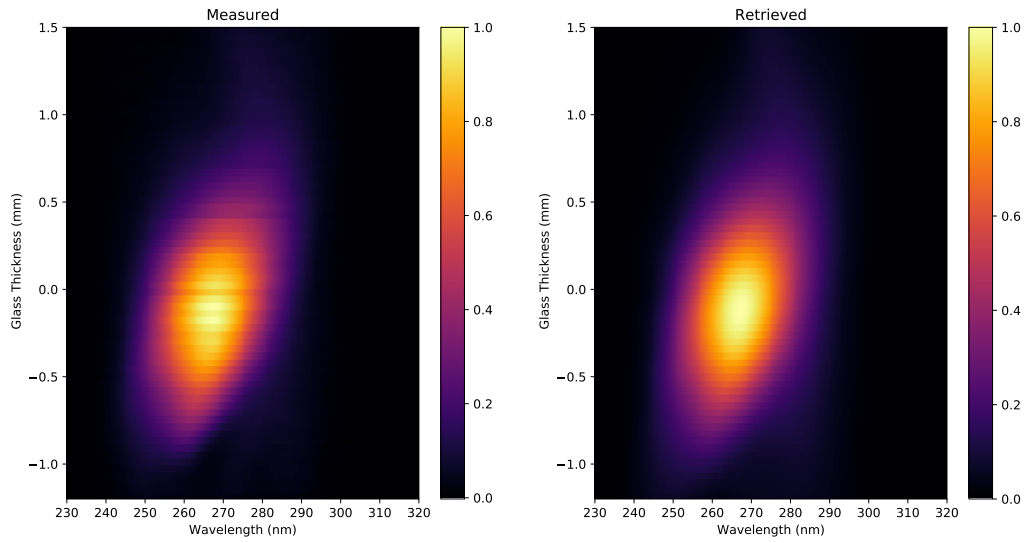


FIGURE 3.28: Measured (left) and retrieved (right) d-scans for 3 layers multi-islands TCVD-grown functionalized graphene.

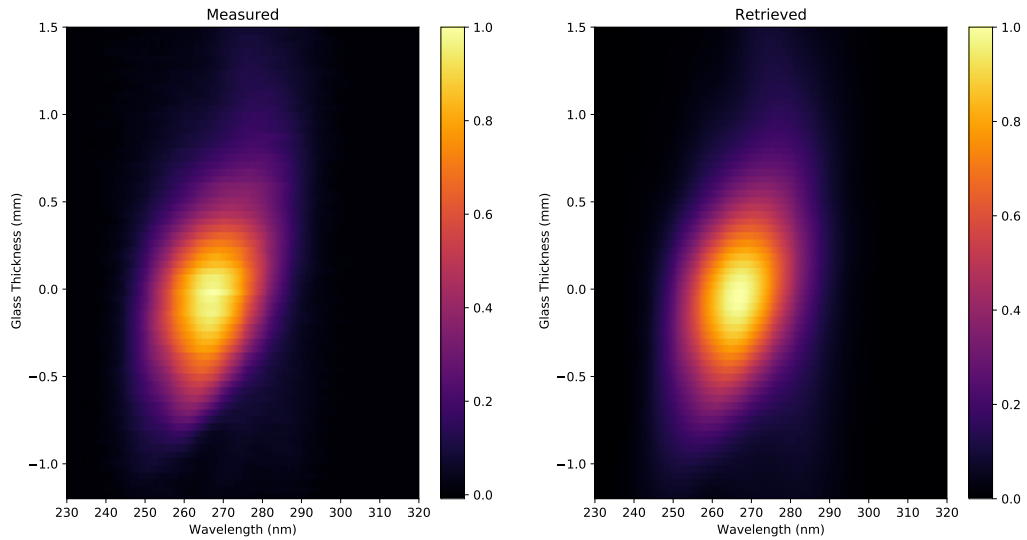


FIGURE 3.29: Measured (left) and retrieved (right) d-scans for 5 layers few-islands TCVD-grown functionalized graphene.

FWHM (fs)	5 layers	3 layers	1 layer
multi-islands	7.83	7.83	-
few-islands	7.62	7.42	7.21

TABLE 3.2: Retrieved FWHM for the THG d-scan with TCVD-grown functionalized graphene samples with islands.

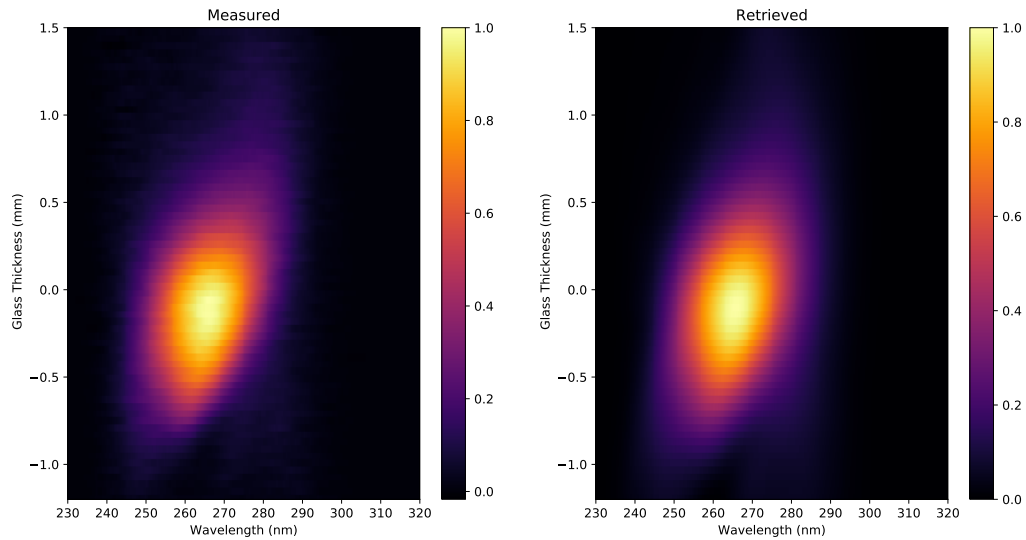


FIGURE 3.30: Measured (left) and retrieved (right) d-scans for 3 layers few-islands TCVD-grown functionalized graphene.

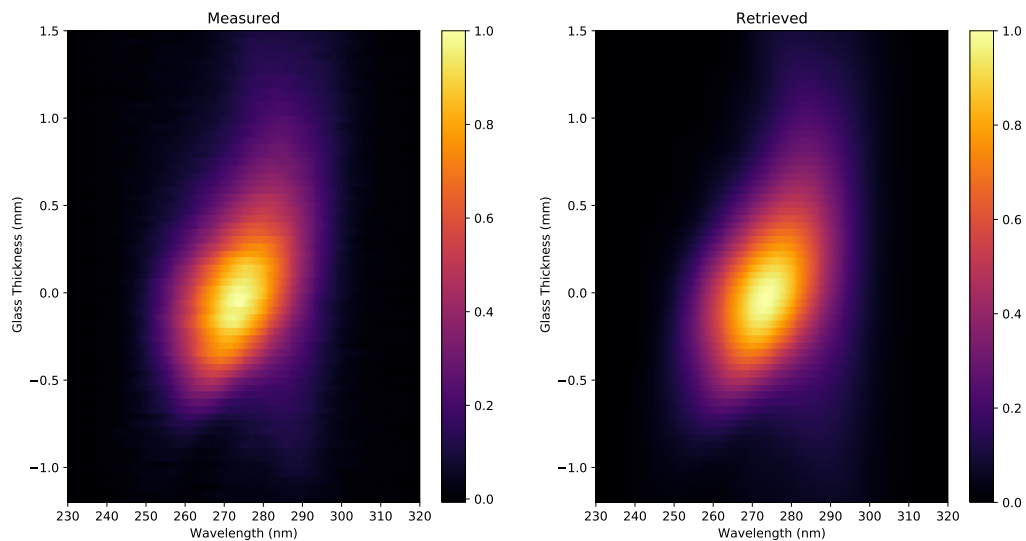
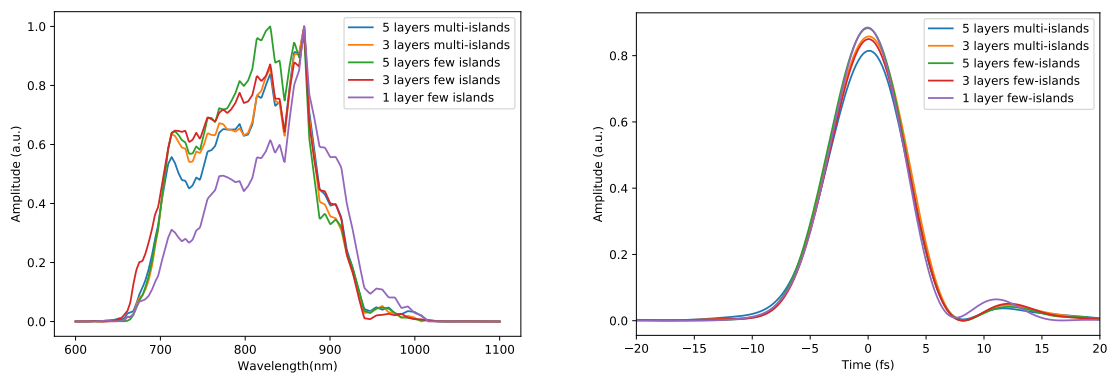


FIGURE 3.31: Measured (left) and retrieved (right) d-scans for 1 layer few-islands TCVD-grown functionalized graphene.

Considering the spectral retrieval, we can clearly see that they are very similar to each other, except for the case of 1 layer few-islands TCVD-grown graphene, which has a weaker contribute from 650 to 800 nm. For the other spectrum retrievals, the spectrum seems to be approximately flat in that region. If we compare the retrieved spectrum with the measured spectrum, we obtain the results shown in [Figure 3.33](#).

By calculating the RMS error between the measured and retrieved spectra for each sample, we can see that the retrieved spectrum that is closer to the measured one corresponds to the one obtained with 1 layer few-islands TCVD-grown graphene. There is,



(A) Retrieved spectral intensity for functionalized TCVD-grown graphene with islands. (B) Retrieved ultrashort pulse in the time domain for functionalized TCVD-grown graphene with islands.

FIGURE 3.32: Full retrieval for THG d-scan with functionalized TCVD-grown graphene with islands.

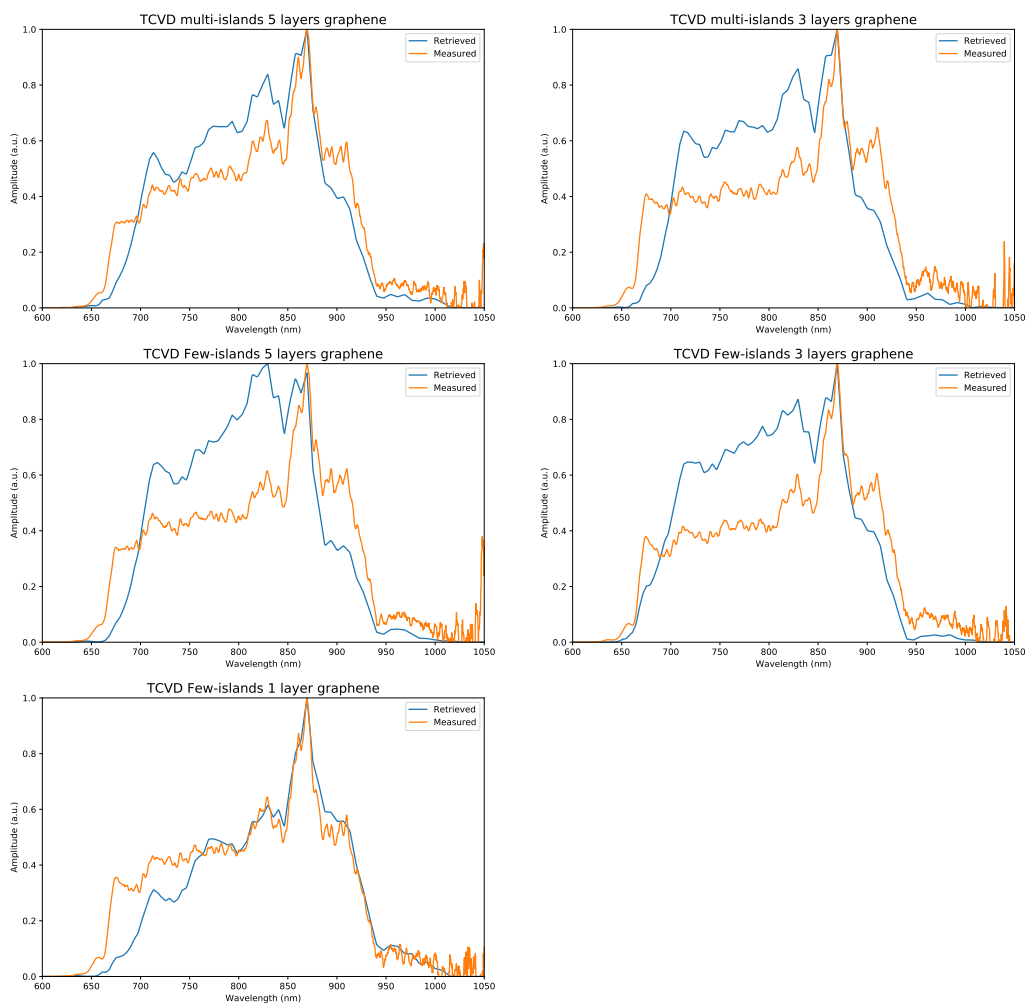


FIGURE 3.33: Comparison of the measured (orange) and retrieved (blue) spectra for THG d-scan with TCVD-grown functionalized graphene.

however, a simple explanation to the discrepancies between the measured and the retrieved fundamental spectra.

In a full retrieval d-scan, the retrieved fundamental spectrum is the one right at the focus. Therefore, there are chromatic aberrations that may lead to differences between the actual fundamental spectrum and the spectrum at the focus used for THG (which is the retrieved spectrum).

3.7 Simulation

A good way to *visualize* the third-order nonlinear response of the studied samples is to simulate a THG spectrum with a fundamental spectrum, assuming a flat frequency response *, and comparing it with the measured spectra for all the graphene samples. The results are presented in [Figure 3.34](#).

By looking at the simulated THG spectrum, we can see that it resembles a Gaussian curve, but with a positive skew. The smoothness of the THG spectrum can be explained by the fact that, since the THG is a third-order process, in the spectral domain, it consists of a double auto-convolution, leading to an overall smoothing. The THG spectra is skewed since the fundamental spectrum is not symmetric.

It is clear that the TCVD-grown graphene (whether with or without islands) has a peak blue shift compared to the simulated THG. Regarding the TCVD-grown 5 layers graphene with no islands, a blue peak shift of 1.04% can be seen, a result which was already shown

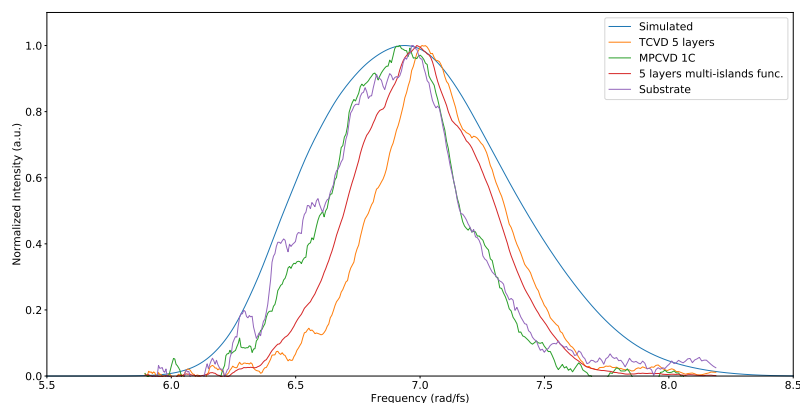


FIGURE 3.34: Simulated THG spectrum vs measured THG spectra for the representative graphene samples.

*which is equivalent to assuming an instantaneous temporal response

by Baudisch *et al.* [62]. The THG in MPCVD-grown graphene does not show a visible peak shift compared to the simulated one, as well as the one generated in the substrate.

Chapter 4

Final remarks and future work

During the course of this thesis, we have fully built and tested a third-harmonic generation and measurement setup, which was used to study the third-order nonlinear response of several graphene samples. The setup is fully mobile and is very well aligned, allowing for THG measurement with low integration times and high SNR.

Regarding MPCVD-grown graphene, we have seen resonant-enhanced THG, regarding the peak absorption in the DUV region, without changing the THG spectral profile.

Considering the TCVD-grown graphene with no islands, we have established that the THG signal increases with the number of layers, and presents a peak shift compared to the third-harmonic generated in MPCVD-grown graphene. The photoassisted hydrogenation of the 5 layers TCVD-grown graphene proved to be successful, as we have increased the SNR of the THG, as well as the sample's resilience to damage.

While dealing with TCVD-grown graphene with islands, we have proven that the presence of islands - yet to be studied - enhances the THG. All the d-scans were useful to retrieve the electric field of the ultrashort pulses, with very little differences from each other.

By simulating the third-harmonic obtained with the fundamental spectrum and a flat frequency response, we have shown that TCVD-grown graphene presents a blue peak shift of approx. 1%, whereas the THG generated with MPCVD-grown graphene does not have a shift.

It is important to mention that all the d-scan retrievals led to ultrashort pulses with similar FWHM, meaning that the d-scan is a powerful technique to determine the complete electrical field of an ultrashort pulse, independently of the sample used to generate THG and of its spectral response.

The developed work has been presented in two posters in two international conferences. Both posters - as well as a poster developed and presented while being a junior researcher at IFIMUP/IN - are presented in [Appendix A](#).

For the next steps, a functionalization in a MPCVD-grown graphene sample for further resilience to damage and higher SNR is a strong hypothesis.

A theoretical model is already being developed by CFP (Centro de Física do Porto), which will allow to calculate the graphene's band structure with and without functionalization. The experimental results will then be compared to the predicted by the theoretical model.

This work was supported by Fundação para a Ciência e Tecnologia (FCT), through a junior research fellowship within the grant 'UltraGraf - Harnessing third-harmonic generation in graphene-coated optics - new devices for ultrafast pulse measurement and frequency up-conversion' (M-ERA-NET2/0002/2016), and through the plurianual funding of IFIMUP - Institute of Physics for Advanced Materials, Nanotechnology and Photonics (UIDB/04968/2020).

Chapter 5

Related work and publications

5.1 Poster presentations

-Tiago Gomes, Miguel Canhota, Miguel Miranda, Helder Crespo, “ Third-harmonic generation in multilayer graphene for ultra-broadband femtosecond pulse characterization”, ELI Summer School 2018, Szeged, Hungary, August 27th-31th 2018.

-Tiago Gomes, Miguel Canhota, Bohdan Kulyk, Alexandre Carvalho, Guilherme Gaspar, Antonio Jose Fernandes, Florinda Costa, Helder Crespo, “Broadband third-harmonic generation in multilayer graphene for the characterization of near single-cycle ultrashort light pulses”, CA17126, Porto, Portugal, March 4th 2019.

-Tiago Gomes, Miguel Canhota, Bohdan Kulyk, Alexandre Carvalho, Guilherme Gaspar, Antonio Jose Fernandes, Florinda Costa, Helder Crespo, “Broadband third-harmonic generation in multilayer graphene for the characterization of near single-cycle ultrashort light pulses”, Condensed Matter Physics National Conference, Porto, Portugal, May 8th-10th 2019.

-Tiago Gomes, Miguel Canhota, Helder Crespo, Miguel Miranda, Cristina Freire, Bruno Jarrais, Bohdan Kulyk, Fernanda Costa, Alexandre Fernandes, Antonio Carvalho, “Broadband few-cycle pulse characterization by third-harmonic dispersion-scan in multilayer and optically improved functionalized graphene coatings”, UFO (Ultrafast Optics) 2019, Bol, Croatia, October 6th-11th 2019.

-Tiago Gomes, Miguel Canhota, Helder Crespo, Miguel Miranda, Cristina Freire, Bruno Jarrais, Bohdan Kulyk, Fernanda Costa, Alexandre Fernandes, Antonio Carvalho, "Temporal measurement of few-cycle laser pulses by third-harmonic dispersion-scan with optically improved graphene coatings", Graphene Industrial Forum & 2DM, Online Conference, May 27th 2020.

5.2 Oral presentations

"Ultrafast Third-Harmonic Generation in Graphene", in CFP - Centro de Física do Porto, Faculdade de Ciências da Universidade do Porto, 2018

Appendix A

Publications

During the course of this thesis, two posters were presented in international conferences, as well as a poster developed while being a junior researcher at IFIMUP/IN, which was presented at two conferences. All the posters are reproduced in this appendix.



Broadband few-cycle pulse characterization by third-harmonic dispersion-scan in multilayer and optically improved functionalized graphene coatings

Tiago Gomes¹, Miguel Canhota¹, Alexandre Carvalho², Bohdan Kulyk², Miguel Miranda³, Bruno Jarrais⁴, António José Fernandes², Cristina Freire⁴, Florinda Costa², Helder Crespo¹

¹IFIMUP-IN and Dept. of Physics and Astronomy, Faculty of Sciences, University of Porto, Portugal

²3N-Aveiro, Dept. of Physics, University of Aveiro, Portugal

³Sphere Ultrafast Photonics, S.A., Rua do Campo Alegre, 1021, Edifício FC6, 4169-007 Porto

⁴REQUIMTE/LAQV, Dept. of Chemistry and Biochemistry, Faculty of Sciences, University of Porto, Portugal

up201504587@fc.up.pt

Summary

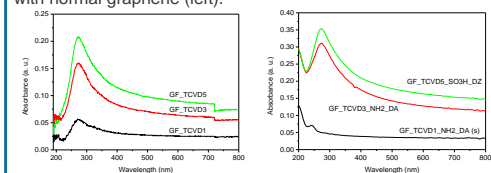
We present recent results on broadband third-harmonic generation (THG) of few-cycle laser pulses in graphene coatings with different synthesis and functionalization conditions. By measuring this nonlinear signal as a function of the dispersion applied to the pulses (THG dispersion scan), we can fully reconstruct the temporal profile of pulses from a few-cycle Ti:Sapphire laser oscillator.

Introduction

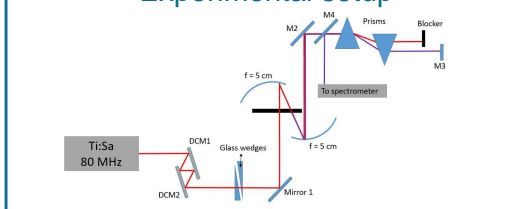
Graphene is a very promising optical material, mainly due to its extremely high broadband nonlinear optical susceptibility¹ and the possibility of occurrence of inter-band transitions at all optical frequencies. Ultrafast third-harmonic generation (THG) in graphene allows not only to characterize ultrashort pulses but also to study charge carrier dynamics in graphene. Additionally, the possibility of obtaining an enhanced nonlinear signal when using multi-layer graphene² is also very appealing. The new technique of dispersion scan (d-scan) developed by Miranda et al.³ enables characterizing ultrashort light pulses using an unprecedentedly simple and fully inline optical setup. In this method, the spectrum of a nonlinear signal (in this case, THG) is recorded for different amounts of dispersion applied to a light pulse, creating a 2D d-scan trace from which the spectral phase of the pulse can be retrieved and, therefore, the exact temporal intensity profile and temporal phase of the pulse can be obtained by inverse Fourier transform.

Graphene functionalization

THG was performed on TCVD-grown graphene⁴ (5, 3 and 1 layers) and on the same graphene coatings after functionalization. The spectra below show the change in the functionalized graphene linear absorption (right) in comparison with normal graphene (left).



Experimental setup



References:

- [1] E. Hendry et al., Phys. Rev. Lett., 105, 97401 (2009)
- [2] S.A. Mikhailov, Physica E, 44 (2012)
- [3] M. Miranda et al., Opt. Express, 20 (2012)
- [4] Bohdan Kulyk et al., in 6th Dresden Nanosynthesis Symposium, "Materials challenges for automotive industry – Micro- and nanoscale characterization", Dresden, Germany, 31 August 2018.

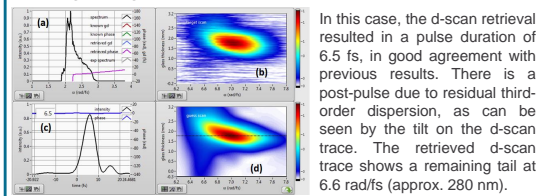
Acknowledgements:

Fundação para a Ciência e a Tecnologia (FCT), through grants NECL - NORTE-01-0145-FEDER-022096, UID/NAN/50024/2019, M-ERA-NET2/0002/2016, PTDC/FIS-MAC/28887/2017.



Pulse Characterization

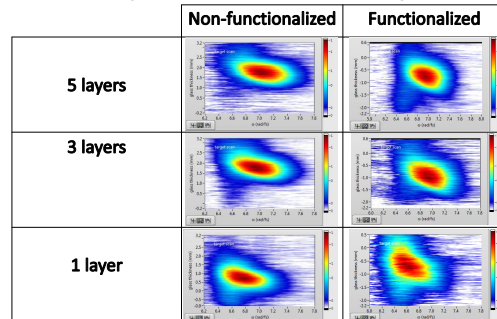
A pulse reconstruction is shown for 5-layer non-functionalized TCVD grown-graphene, deposited on 1mm of fused silica.



In this case, the d-scan retrieval resulted in a pulse duration of 6.5 fs, in good agreement with previous results. There is a post-pulse due to residual third-order dispersion, as can be seen by the tilt on the d-scan trace. The retrieved d-scan trace shows a remaining tail at 6.6 rad/fs (approx. 280 nm).

Results and discussion

The comparison between the non-functionalized and the functionalized graphene is shown in the next figure.




Pulse reconstruction from THG d-scan traces in functionalized graphene with 5 and 3 layers led to pulse durations of 7.1 fs


Conclusions

- ▶ We were able to fully characterize the ultrashort pulses using the non-functionalized and the functionalized graphene.
- ▶ THG traces using 5- and 3-layer functionalized graphene show narrower bandwidths compared to pristine graphene (under investigation)
- ▶ There is a shift in the peak of the THG signal for the 5-layer functionalized graphene (also under investigation)

FIGURE A.1: Poster presented at Ultrafast Optics (UFO 2019) in Bol, Croatia, from 6th-11th October 2019.



MAY 27, 2020
CONFERENCE
ONLINE



TEMPORAL MEASUREMENT OF FEW-CYCLE LASER PULSES BY THIRD-HARMONIC DISPERSION-SCAN WITH OPTICALLY IMPROVED GRAPHENE COATINGS

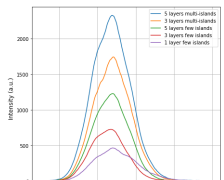
Tiago GOMES¹, Miguel CANHOTA¹, Alexandre CARVALHO², Bohdan KULYK², Miguel MIRANDA³, Bruno JARRAIS⁴, António José FERNANDES², Cristina FREIRE⁴, Florinda COSTA², Helder CRESPO¹

¹IFIMUP and Departamento de Física e Astronomia, Faculdade de Ciências, Universidade do Porto, Rua do Campo Alegre s/n, 4169-007 Porto, Portugal
²3N-Aveiro, Dept. of Physics, University of Aveiro, Aveiro, Portugal
³Sphere Ultrafast Photonics, S.A., Rua do Campo Alegre, 1021, Edifício FC6, 4169-007 Porto, Portugal
⁴REQUIMTE/LAQV, Dept. of Chemistry and Biochemistry, Faculty of Sciences, University of Porto, Porto, Portugal

Graphene in ultrafast photonics

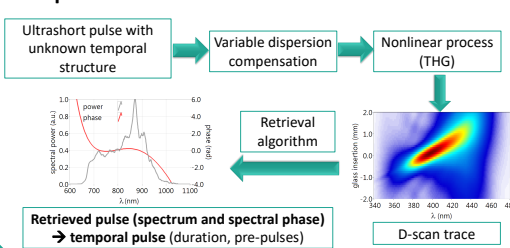
Graphene consists of a single layer of carbon atoms arranged in an hexagonal lattice and is a very promising material in photonics, mainly due to its extremely high and broadband nonlinear optical susceptibility^{1,2} and the possibility of occurrence of interband transitions at all optical frequencies. It allows broadband ultrafast third-harmonic generation (THG), enabling not only to characterize the used ultrashort pulses³ but also to study the dynamics of the charge carriers in graphene. The possibility of obtaining an enhanced nonlinear signal and increased damage threshold in multi-layer² and functionalized graphene coatings are two key points in this work.

THG in functionalized graphene



- In average, "multi-islands" have a higher coverage of domains with varying number of layers, and therefore are less uniform compared to "few-islands" graphene.
- Signal increases with number of layers
- Similar THG spectrum for all samples, except for 1-layer few-islands (signal comparable to substrate – 1mm thick fused silica)
- Extremely broadband THG, from 240-300 nm (~25 nm FWHM)

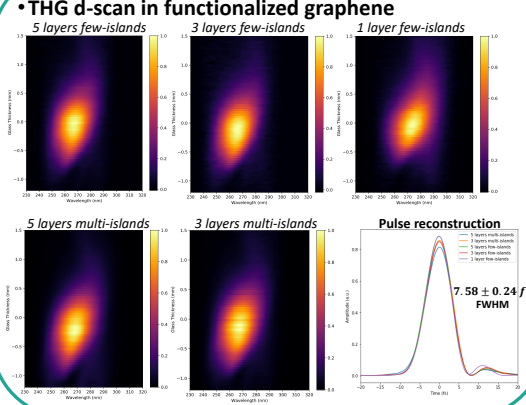
Dispersion-scan⁴



Retrieved pulse (spectrum and spectral phase) → temporal pulse (duration, pre-pulses)

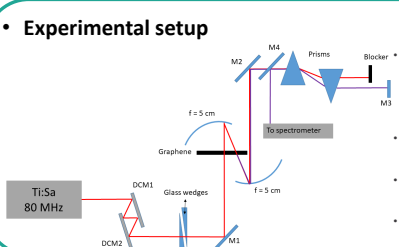
D-scan trace

THG d-scan in functionalized graphene



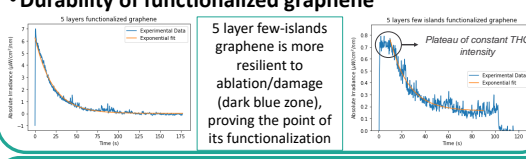
Pulse reconstruction: 7.58 ± 0.24 fs FWHM

Experimental setup



- DCM's (Double Chirped Mirrors) and glass wedges: dispersion compensation
- M1, M2, M3, M4: Mirrors
- Energy per pulse: ~1,25 nJ
- Pulse duration: sub-10 fs

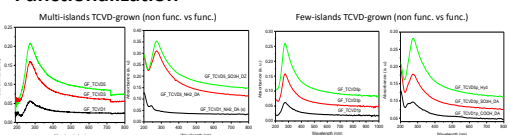
Durability of functionalized graphene



5 layer few islands graphene is more resilient to ablation/damage (dark blue zone), proving the point of its functionalization

Plateau of constant THG intensity

Functionalization




Conclusions

- We obtained broadband third-harmonic generation in single and multi-layer functionalized graphene.
- We were able to fully retrieve the temporal profile of our laser pulses from a Ti:Sapphire 80 MHz Rep. Rate oscillator, with very similar temporal structures for all samples (FWHM = 7.58 ± 0.24 fs).
- The hydration functionalization for the 5-layer few-islands graphene was successful, as a plateau of constant THG intensity over exposure time can be obtained.

CONTACT PERSON

Tiago Gomes
up201504587@fc.up.pt



REFERENCES

- [1] E. Hendry et al., Phys. Rev. Lett., 105, 97401 (2009)
- [2] S. A. Mikhailov, Physica E 44, 924-927 (2012)
- [3] F. Silva et al., in Conference on Lasers and Electro Optics (CLEO) (OSA, 2013), paper CW1H.5
- [4] M. Miranda et al., Opt. Express 20, 688-697 (2012)

ACKNOWLEDGEMENTS

The authors acknowledge funding from the Foundation for Science and Technology (FCT) through grants UID/04968/2020, M-ERA-NET2/0002/2016,




FIGURE A.2: Poster presented at the online conference Graphene Industrial Forum & 2DM 2020, presented in May 27th 2020.

Broadband third-harmonic generation in multilayer graphene for the characterization of near single-cycle ultrashort light pulses



U.PORTO

Tiago dos Santos Gomes¹, Miguel Canhota¹, Bohdan Kulyk², Alexandre Carvalho², Guilherme Gaspar², António José Fernandes², Florinda Costa², Helder Crespo¹

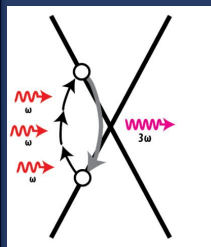
¹IFIMUP-IN and Dept. of Physics and Astronomy, Faculty of Science, University of Porto, 4169-007 Porto, Portugal.

²I3N-Aveiro, Dep. Physics of the University of Aveiro, Portugal

Email: up201504587@fc.up.pt

We present results on broadband third-harmonic generation (THG) obtained in multi-layer graphene films using few-cycle ultra-broadband laser pulses. The use of graphene films produced by different growing methods allows us to fully characterize the used light pulses using the d-scan technique and to study the quantum dynamics of charge carriers in graphene.

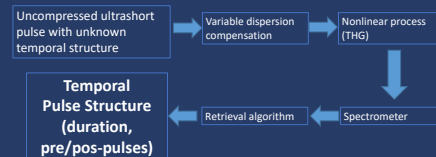
THG in Graphene



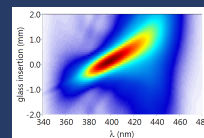
- Single layer of carbon atoms (2D)
- Very high nonlinear optical susceptibility [1]
- Inter-band transitions at all optical frequencies
- THG signal enhancement when using multilayer graphene [2]

Further analysis of the nonlinear response of graphene grown in different conditions should provide information on the quantum dynamics of the charge carrier in graphene.

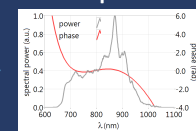
THG d-scan [3]



d-scan trace



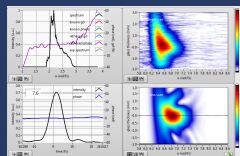
Spectral intensity and phase



Results obtained

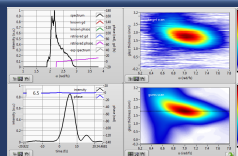
TCVD-grown graphene

MPCVD-grown graphene With incrusted nanodiamonds

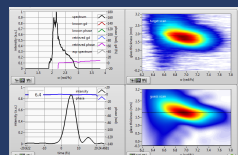


- Peak shift to approx. 280 nm, possibly due to a resonance
- Different spectrum – residual TOD not visible
- Not possible to reconstruct the laser pulse (yet)

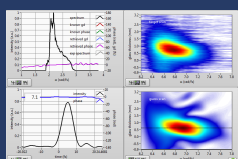
5 layers



3 layers



1 layer



Discussion

- In all the d-scans it is possible to simultaneously compress and fully characterize the used laser pulse, with FWHM of 6.5 (5 layers), 6.4 (3 layers) and 7.1 fs (1 layer).
- The existence of residual third-order dispersion (TOD) leads to the existence of a post-pulse.
- It is possible to see a remaining tail arising at 280 nm, possibly due to an intrinsic resonance of the graphene films.
- All the reconstructed pulses are similar in the time domain.

Conclusions

Graphene is a promising material for measuring ultrashort pulses over a broad spectral range, and we have successfully measured pulses from a few-cycle laser oscillator, where the d-scan trace enabled measuring pulses down to 6.4 fs. The THG band is significantly large (~50 nm @ 266 nm), thus enabling the full characterization of the light pulse and furthermore the study of the quantum dynamics of the graphene carriers.

References

- [1] E. Hendry et al, Phys. Rev. Lett. 105 (2009) 97401
- [2] S.A. Mikhailov, Physica E 44 (2012) 924
- [3] M. Miranda et al, Opt. Express 20, 688-697 (2012)

Acknowledgments:

Fundação para a Ciência e a Tecnologia (FCT), Portugal (Grants 'UltraGraf' M-ERA-NET2/0002/2016, UID/ NAN/50024/2013, NORTE-01- 0145-FEDER-022096 and the Network of Extreme Conditions Laboratories - NECL)
Fundação para a Ciência e a Tecnologia, Projecto UID/NAN/50024/2019



FIGURE A.3: Poster presented at the COST Action CA17126, at University of Porto, presented in March, 4th 2019, and at the Condensed Matter Physics National Conference, at University of Porto, presented from May 8th-10th 2019.

Bibliography

- [1] T. H. Maiman, "Stimulated optical radiation in ruby masers," *Nature*, vol. 187, no. 493, 1960.
- [2] F. J. McClung and R. W. Hellwarth, "Giant optical pulsations from ruby," *Appl. Opt.*, vol. 1, pp. 103–105, 1962.
- [3] L. E. Hargrove, R. L. Fork, and M. A. Pollack, "Locking of HeNe laser modes induced by synchronous intracavity modulation," *Appl. Phys. Lett.*, vol. 5, pp. 4–5, 1964.
- [4] A. M. Weiner, *Ultrafast Optics*. John Wiley and Sons, Inc., 2009.
- [5] I. Chowdhury, A. Wu, X. Xu, and A. Weiner, "Ultra-fast laser absorption and ablation dynamics in wide-band-gap dielectrics," *Appl. Phys. A*, vol. 81, pp. 1627–1632, 2005.
- [6] K. Gaffney and H. Chapman, "Imaging atomic structure and dynamics with ultrafast x-ray scattering," *Science*, vol. 316, no. 5830, pp. 1444–1448, 2007.
- [7] O. Wada, "Femtosecond all-optical devices for ultrafast communication and signal processing," *New J. Phys.*, vol. 6, no. 183, 2004.
- [8] P. Maine, D. Strickland, P. Bado, M. Pessot, and G. Mourou, "Generation of ultra-high peak power pulses by chirped pulse amplification," *IEEE Journal of Quantum Electronics*, vol. 24, no. 2, pp. 398–403, 1988.
- [9] The nobel prize in physics 2018. [Online]. Available: <https://www.nobelprize.org/prizes/physics/2018/summary/>
- [10] J.-C. Diels and W. Rudolph, *Ultrashort Laser Pulse Phenomena*. Elsevier Inc., 2006.
- [11] R. Szipöcs, K. Ferencz, C. Spielmann, and F. Krausz, "Chirped multilayer coatings for broadband dispersion control in femtosecond lasers," *Optics Letters*, vol. 19, no. 3, 1994.

- [12] R. W. Boyd, *Nonlinear optics*. Academic Press, Inc., 2008.
- [13] J. C. M. Diels, J. J. Fontaine, I. C. McMichael, and F. Simoni, "Control and measurement of ultrashort pulse shapes (in amplitude and phase) with femtosecond accuracy," *Appl. Opt.*, vol. 24, no. 9, pp. 1270–1282, 1985.
- [14] D. J. Kane and R. Trebino, "Characterization of arbitrary femtosecond pulses using frequency-resolved optical gating," *IEEE J. Quantum Electron.*, vol. 29, no. 2, pp. 571–579, 1993.
- [15] C. Iaconis and I. A. Walmsley, "Spectral phase interferometry for direct electric-field reconstruction of ultrashort optical pulses," *Opt. Lett.*, vol. 23, no. 10, pp. 792–794, 1998.
- [16] V. Lozovoy, I. Pastirk, and M. Dantus, "Multiphoton intrapulse interference. iv. ultrashort laser pulse spectral phase characterization and compensation," *Optics Letters*, vol. 29, no. 7, 2004.
- [17] B. Seifert, H. Stolz, and M. Tasche, "Nontrivial ambiguities for blind frequency-resolved optical gating and the problem of uniqueness," *J. Opt. Soc. Am. B*, vol. 21, no. 5, pp. 1089–1097, 2004.
- [18] M. Miranda, T. Fordell, C. Arnold, A. L'Huillier, and H. Crespo, "Simultaneous compression and characterization of ultrashort laser pulses using chirped mirrors and glass wedges," *Optical Society of America*, vol. 20, no. 1, 2012.
- [19] M. Miranda, C. L. Arnold, T. Fordell, F. Silva, B. Alonso, R. Weigand, A. L'Huillier, and H. Crespo, "Characterization of broadband few-cycle laser pulses with the d-scan technique," *Optics Express*, vol. 20, no. 17, 2012.
- [20] M. Miranda, J. Penedones, C. Guo, A. Harth, M. Louisy, L. Neoričić, A. L'Huillier, and C. L. Arnold, "Fast iterative retrieval algorithm for ultrashort pulse characterization using dispersion scans," *Journal of the Optical Society of America B*, vol. 34, no. 1, 2017.
- [21] G. R. Fleming, *Chemical Applications of Ultrafast Spectroscopy (Volume 13)*. NY, Oxford University Press, 1985.
- [22] J. Shah, *Ultrafast Spectroscopy of Semiconductors and Semiconductor Nanostructures*. Springer-Verlag, NY, 1999.

- [23] M. Zervos, A. Othonos, M. Sergides, T. Pavloudis, and J. Kioseoglou, "Observation of the direct energy band gaps of defect-tolerant Cu_3N by ultrafast pump-probe spectroscopy," *J. Phys. Chem. C*, vol. 124, no. 6, pp. 3459–3469, 2020.
- [24] H. Jani and L. Duan, "Time-frequency spectroscopy of gas transient dispersion using few-cycle pump-probe reflectometry," *Phys. Rev. Applied*, vol. 13, no. 054010, 2020.
- [25] A. Ueda, K. Matsuda, T. Tayagaki, and Y. Kanemitsu, "Carrier multiplication in carbon nanotubes studied by femtosecond pump-probe spectroscopy," *Appl. Phys. Lett.*, vol. 92, no. 233105, 2008.
- [26] I. Sytceвич, C. Guo, S. Mikaelsson, J. Vogelsang, A.-L. Viotti, B. Alonso, R. Romero, P. T. Guerreiro, A. L'Huillier, H. Crespo, M. Miranda, and C. L. Arnold, "Characterizing ultrashort laser pulses with second harmonic dispersion scans," *Submitted to arXiv*, 2020.
- [27] B. Alonso, S. Torres-Peiró, R. Romero, P. T. Guerreiro, A. Almagro-Ruiz, H. Muñoz-Marco, P. Pérez-Millán, and H. Crespo, "Detection and elimination of pulse train instabilities in broadband fibre lasers using dispersion scan," *Sci. Rep.*, vol. 10, no. 7242, 2020.
- [28] F. Silva, M. Miranda, S. Teichmann, M. Baudisch, M. Massicotte, F. Koppens, J. Biegert, and H. Crespo, "Pulse measurement from near to mid-ir using third harmonic generation dispersion scan in multilayer graphene." 2013 Conference on Lasers and Electro-Optics - International Quantum Electronics Conference, 2013, p. CFIE₃₅.
- [29] M. Hoffmann, T. Nagy, T. Willemsen, M. Jupé, D. Ristau, and U. Morgner, "Pulse characterization by the d-scan in absorbing nonlinear media," *Optics Express*, vol. 22, no. 5, 2014.
- [30] A. Tajalli, B. Chanteau, M. Kretschmar, H. Kurz, D. Zuber, M. Kovačev, U. Morgner, and T. Nagy, "Few-cycle optical pulse characterization via cross-polarized wave generation dispersion scan technique," *Opt. Lett.*, vol. 41, no. 22, pp. 5246–5249, 2016.
- [31] A. Tajalli, M. Ouillé, A. Vernier, F. Böhle, E. Escoto, S. Kleinert, R. Romero, J. Csontos, U. Morgner, G. Steinmeyer, H. M. Crespo, R. L. Martens, and T. Nagy, "Propagation

- effects in the characterization of 1.5-cycle pulses by xpw dispersion scan," *IEEE Journal of Selected Topics in Quantum Electronics*, vol. 25, no. 4, pp. 1–7, 2019.
- [32] A. Tajalli, T. K. Kalousdian, M. Kretschmar, S. Kleinert, U. Morgner, and T. Nagy, "Full characterization of 8 fs deep uv pulses via a dispersion scan," *Opt. Lett.*, vol. 44, no. 10, pp. 2498–2501, 2019.
- [33] M. Canhota, F. Silva, R. Weigand, and H. M. Crespo, "Inline self-diffraction dispersion-scan of over octave-spanning pulses in the single-cycle regime," *Opt. Lett.*, vol. 42, no. 15, pp. 3048–3051, 2017.
- [34] M. Canhota, R. Weigand, and H. M. Crespo, "Simultaneous measurement of two ultrashort near-ultraviolet pulses produced by a multiplate continuum using dual self-diffraction dispersion-scan," *Opt. Lett.*, vol. 44, no. 4, pp. 1015–1018, 2019.
- [35] H. M. Crespo, T. Witting, M. Canhota, M. Miranda, and J. W. G. Tisch, "In situ temporal measurement of ultrashort laser pulses at full power during high-intensity laser–matter interactions," *Optica*, vol. 7, no. 8, pp. 995–1002, 2020.
- [36] E. Hendry, P. J. Hale, J. Moger, A. K. Savchenko, and S. A. Mikhailov, "Coherent nonlinear optical response of graphene," *Phys. Review Letters*, vol. 105, no. 097401, 2010.
- [37] P. Wallace, "The band theory of graphite," *Phys. Rev.*, vol. 71, no. 622, 1947.
- [38] K. Novoselov, A. Geim, S. Morozov, D. Jiang, Y. Zhang, S. Dubonos, I. Grigorieva, and A. Firsov, "Electric field effect in atomically thin carbon films," *Science*, vol. 306, no. 5696, pp. 666–669, 2004.
- [39] The nobel prize in physics 2010. [Online]. Available: <https://www.nobelprize.org/prizes/physics/2010/summary/>
- [40] Y.-M. Lin, K. A. Jenkins, A. Valdes-Garcia, J. P. Small, D. B. Farmer, and P. Avouris, "Operation of graphene transistors at gigahertz frequencies," *Nano Letters*, vol. 9, no. 1, pp. 422–426, 2009.
- [41] A. Yu, I. Roes, A. Davies, and Z. Chen, "Ultrathin, transparent, and flexible graphene films for supercapacitor application," *Applied Physics Letters*, vol. 96, no. 25, p. 253105, 2010.
- [42] S. Alwarappan, A. Erdem, C. Liu, and C.-Z. Li, "Probing the electrochemical properties of graphene nanosheets for biosensing applications," *The Journal of Physical Chemistry C*, vol. 113, no. 20, pp. 8853–8857, 2009.

- [43] F. Wang, Y. Zahng, C. Tian, C. Girit, A. Zettl, M. Crommie, and Y. Shen, "Gate-variable optical transitions in graphene," *Science*, vol. 320, no. 5873, pp. 206–209, 2008.
- [44] S. A. Mikhailov, "Theory of the nonlinear optical frequency mixing effect in graphene," *Physica E*, vol. 44, pp. 924–927, 2012.
- [45] A. H. C. Neto, F. Guinea, N. M. R. Peres, K. S. Novoselov, and A. K. Geim, "The electronic properties of graphene," *Rev. Mod. Phys.*, vol. 81, no. 109, 2009.
- [46] Z. Xu, *Graphene - Fabrication, Characterizations, Properties and Applications*. Academic Press, 2018.
- [47] M. Inagaki, F. Kang, M. Toyoda, and H. Konno, *Advanced Materials Science and Engineering of Carbon*. Butterworth-Heinemann, 2014.
- [48] K. Seibert, G. C. Cho, W. Kütt, H. Kurz, D. H. Reitze, J. I. Dadap, H. Ahn, M. C. Downer, and A. M. Malvezzi, "Femtosecond carrier dynamics in graphite," *Phys. Rev. B*, vol. 42, 1990.
- [49] J. M. Dawlaty, S. Shivaraman, M. Chandrashekhar, F. Rana, and M. G. Spencer, "Measurement of ultrafast carrier dynamics in epitaxial graphene," *Appl. Phys. Lett.*, vol. 92, no. 042116, 2008.
- [50] C. H. Lui, K. F. Mak, J. Shan, and T. F. Heinz, "Ultrafast photoluminescence from graphene," *Phys. Rev. Lett.*, vol. 105, no. 127404, 2010.
- [51] K. Oum, T. Lenzer, M. Scholz, D. Y. Jung, O. Sul, B. J. Cho, J. Lange, and A. Muller, "Observation of ultrafast carrier dynamics and phonon relaxation of graphene from the deep-ultraviolet to the visible region," *J. Phys. Chem. C*, vol. 118, no. 12, 2014.
- [52] H. A. Hafez, X. Chai, Y. Sekine, M. Takamura, I. Oguri, K. Al-Naib, M. M. Dignam, H. Hibino, and T. Ozakir, "Effects of environmental conditions on the ultrafast carrier dynamics in graphene revealed by terahertz spectroscopy," *Phys. Rev. B*, vol. 95, no. 165428, 2017.
- [53] A. Ferrari and D. Basko, "Raman spectroscopy as a versatile tool for studying the properties of graphene," *Nature Nanotech*, vol. 8, pp. 235–246, 2013.
- [54] C. V. Raman and K. S. Krishnan, "A new type of secondary radiation," *Nature*, vol. 121, pp. 501–502, 1928.

- [55] D. Cooper *et al.*, "Experimental review of graphene." *ISRN Condensed Matter Physics*, vol. 56, 2012.
- [56] G. Soavi, G. Wang, H. Rostami, D. Purdie, D. De Fazio, T. Ma, B. Luo, J. Wang, A. Ott, D. Yoon, S. Bourelle, J. Muench, I. Goykhman, S. Dal Conte, M. Celebrano, A. Tomadin, M. Polini, G. Cerullo, and A. Ferrari, "Broadband, electrically tunable third-harmonic generation in graphene," *Nature Nanotechnology*, vol. 13, pp. 583–588, 2018.
- [57] J. M. B. Lopes dos Santos, N. M. R. Peres, and A. H. Castro Neto, "Graphene bilayer with a twist: Electronic structure," *Phys. Rev. Lett.*, vol. 99, pp. 256 802–256 805, 2007.
- [58] M. Currie, J. Caldwell, F. Bezares, J. Robinson, T. Anderson, H. Chun, and M. Tadjer, "Quantifying pulsed laser induced damage to graphene," *Applied Physics Letters*, vol. 99, pp. 211 909 – 211 909, 2011.
- [59] A. Roberts, D. Cormode, C. Reynolds, T. Newhouse-Illige, B. LeRoy, and A. Sandhu, "Response of graphene to femtosecond high-intensity laser irradiation," *Applied Physics Letters*, vol. 99, no. 051912, 2011.
- [60] X. Liu, D. Du, and G. Mourou, "Laser ablation and micromachining with ultrashort laser pulses," *IEEE Journal of Quantum Electronics*, vol. 33, no. 10, pp. 1706–1716, 1997.
- [61] A. M. Beltaos, A. Matkovic, A. Kovačević, and U. Ralevic, "Damage effects on multi-layer graphene from femtosecond laser interaction," *Phys. Scr.*, no. 014015, 2014.
- [62] M. Baudisch, A. Marini, J. Cox, T. Zhu, F. Silva, S. Teichmann, M. Massicotte, F. Koppens, L. Levitov, F. Abajo, and J. Biegert, "Ultrafast nonlinear optical response of dirac fermions in graphene," *Nature Comm.*, vol. 9, no. 1018, 2018.